Editorial corner – a personal view
Polymer-based sensors: A high potential to be further developed

*P. Krawczak**

Department of Polymers and Composites Technology & Mechanical Engineering, Ecole des Mines de Douai, 941 rue Charles Bourseul, BP 10838, 59508 Douai, France

Inorganic materials are frequently used to manufacture sensors. However intensive research efforts have been produced in order to develop the large potential of polymers in the field of sensing and monitoring.

The chemical diversity of plastics, their 'tunability' and their ability to be industrially processed using economically viable technologies with high productivity can actually be profitable to produce sensing devices or active elements of sensors exploiting a wide range of functional properties (e.g. electrical, dielectric, piezoelectric, pyroelectric or optical properties; weight or dimensions variations, etc). The final products obtained that way may then compete with more traditional components based on metals or ceramics, which are often brittle, require very constraining processing conditions (high temperatures, clean rooms…) and are compatible with a limited number of substrates only. Moreover, they may show functionalities difficult to reach by other ways.

Specialty polymers are used for this kind of applications. They are generally quite different from the commodity and engineering plastics usually used in the plastics industry and may require adapted processing techniques (such as microstructuring for instance).

These organic materials seem to be very promising for a broad range of practical applications: detection of chemical components, solvents, aromas, moisture, contacts, leakage; measurement of force, deformation, temperature, pH, etc.

Well known examples are fluorinated polymers (polyvinylidene fluoride, polytrifluorethylene) used for their piezoelectric and/or pyroelectric properties in force and/or heat sensors, intrinsic (polypyrrole, polyaniline) or extrinsic (addition of conducting particles such as carbon black, carbon nanotubes, metals or metal oxides) conducting polymers used in the electronic noses (detection of volatile organic components). Another example is the detection of moisture by means of polymers such as poly(ethylene glycol), poly(methyl methacrylate), polyimides, polypyridine or various derivatives of cellulose.

Other developments for more specific applications are also going on, such as biosensors/biochemical sensors, using polymers on which enzymes are chemically linked or polymers whose degradation is catalysed by some enzymes, which can result in a capacity variation.

Polymer-based sensors undoubtedly represent both a fertile ground of further scientific developments and an interesting high added-value outlet for the plastics industry.

Prof. Dr. Patricia Krawczak
Member of International Advisory Board

---

*Corresponding author, e-mail: krawczak@ensm-douai.fr

Synthesis and property of polymer nanospheres with Pd/P4VP shells via surface RAFT polymerization

S. P. Shi, L. F. Zhang, J. Zhu, W. Zhang, Z. P. Cheng, X. L. Zhu*

Key Lab. of Organic Synthesis of Jiangsu Province, College of Chemistry, Chemical Engineering and Materials Science, Soochow (Suzhou) University, 199 Renai Road, Suzhou 215123, China

Abstract. A reversible addition-fragmentation chain transfer (RAFT) agent with carbazole as Z-group was immobilized on the surfaces of the cross-linked poly (4-vinylbenzyl chloride-*co*-styrene) (PVBCS) nanospheres with a diameter of about 70 nm by the reaction of benzyl chloride groups in the PVBCS between carbazole and carbon sulfide. Then surface RAFT polymerization of 4-vinylpyridine (4VP) was used to modify the nanospheres to produce a well-defined and covalently tethered P4VP shell. By surface activation in a PdCl$_2$ solution and then reduction by hydrazine hydrate (N$_2$H$_4$·H$_2$O), the P4VP composite shells were obtained containing densely palladium metal nanoparticles. The chemical composition of the nanosphere surfaces at various stages of the surface modification was characterized by X-ray photoelectron spectroscopy (XPS). Transmission electron microscopy (TEM) was used to characterize the morphology of the hybrid nanospheres. The Pd/P4VP shell nanospheres were also applied to the catalytic reaction and proved to be efficient and reusable for the Heck reaction.

Keywords: polymer composites, RAFT polymerization, palladium catalyst

1. Introduction

Organic/inorganic hybrid nanoparticles have attracted much attention due to their fascinating optical, electronic, magnetic, photoelectric, bio-compatible, and catalytic properties [1–3]. Among the hybrid materials, core-shell nanospheres usually consist of polymer shells and inorganic cores. The organic polymer shell mainly determines the chemical properties of nanoparticles, while the physical properties of nanoparticles are governed by both the size and shape of inorganic cores. There have been a number of methods to prepare core-shell nanospheres with different sizes, structures and compositions, such as sol-gel process [4], layer-by-layer assembly [5], encapsulation of different nanoparticles in cross-linked shell [6] and so on [7, 8]. Recently, rapid progress in the field of

controlled/living radical polymerizations [9–11] has paved the way to prepare well-defined core-shell nanospheres by grafting the polymer chains to the solid nanoparticles [12–14]. Among the major controlled polymerization strategies developed, reversible addition-fragmentation chain transfer (RAFT) [11] polymerization has become one of the most promising techniques to prepare polymer grafted solid supports because this technique can adapt to a wide range of reaction conditions, provides a procedure for the simple preparation of various of block copolymers, and has the compatibility with a wide range of functional monomers [15–17]. Until now, RAFT polymerization has been successfully utilized to graft various polymeric chains onto solid supports to form core-shell systems such as functionalized silica particles [18], gold nano-

---

particles [19], CdSe nonaparticles [20], carbon nanotubes [21], Merrifield resins [22] and silica wafers [23]. Recent progress in this field also involves the preparation of hybrid nanoparticles coated with functional polymer brushes [24–26]. For example, Nishi and Kobatake prepared gold nanoparticles covered with photochromic diarylethene polymer that expressed a bright red color via RAFT polymerization [25]. However, there have been few reports on procedures to graft functional polymer chains onto solid supports and the properties, such as catalytic properties, of the shell modified materials.

Palladium is a highly active and selective catalyst in C–C bond formation reactions [27–30]. However, the problem that concerns many researchers is to combine high efficiency of the catalyst with the possibility of its easy separation from the reaction products. To the best of our knowledge, the synthesis of palladium (Pd)/polymer nanospheres with core-shell structure via RAFT technique and the investigation of their catalytic properties have not been reported till now. In this work, hybrid nanospheres with a well-dispersed Pd/poly (4-vinylpyridine) (P4VP) composite shell and a cross-linked poly (4-vinylbenzyl chloride-*co*-styrene) (PVBCS) core were prepared via the surface-RAFT technique. Cross-linked PVBCS nanospheres were synthesized by emulsion copolymerization of 4-vinylbenzyl chloride (VBC) and styrene in the presence of a cross-linking agent, p-divinylbenzene (DVB). The PVBCS nanosphere surfaces were then converted into polymer-supporting RAFT agents by the reaction of the benzyl chloride groups in the PVBCS with carbazole and carbon sulfide. The surface RAFT polymerization of 4VP produced a well-defined and covalently tethered P4VP shell on the surface of the nanospheres. The Pd/P4VP composite shells were obtained by activating P4VP shells in a $PdCl_2$ solution and then reducing Pd^{2+} by hydrazine hydrate ($N_2H4·H_2O$). The nanospheres with the Pd/P4VP shells were used as catalysts for the Heck reaction between iodobenzene and methyl acrylate; and the results demonstrated that the catalysts were efficient and reusable for the Heck reaction.

2. Experimental
2.1. Materials
4-Vinylbenzyl chloride (VBC, 90%), p-divinylbenzene (DVB, 80%), iodobenzene (98%) were supplied by Acros. Styrene (St) and methyl acrylate (MA, analytical reagent, Shanghai Chemical Reagent Co., Ltd, China) were distilled before use. 4-Vinylpyridine (4VP, 95%) was obtained from Acros, distilled under reduced pressure and then stored at –15°C. Azobisisobutyronitrile (AIBN, 99%, Shanghai Chemical Reagent Co., Ltd, China) was recrystallized twice from ethanol. Benzyl bromide (98%), 2-propanol (analytical reagent), palladium(II) chloride ($PdCl_2$, analytical reagent), sodium dodecyl sulfate (SDS, analytical reagent), potassium persulfate (KPS, analytical reagent), triethylamine (Et_3N, analytical reagent), carbazole (analytical reagent), carbon disulfide (CS_2, analytical reagent), hydrazine hydrate ($N_2H_4·H_2O$, 50%) and dimethyl sulphoxide (DMSO, analytical reagent) were purchased from Shanghai Chemical Reagent Co., Ltd, China. 2-Propanol was dried with activated molecular sieve (4 Å). All other reagents were analytical quality reagents and used as received without further purification.

2.2. Preparation of cross-linked PVBCS nanosphere

The cross-linked PVBCS nanospheres were prepared by emulsion copolymerization of VBC, St and DVB at 65°C, using KPS as an initiator and SDS as a surfactant. About 150 mg of SDS was dissolved in 75 ml of deionized water. The monomers, VBC (1.5 ml, 9.6 mmol), St (4.0 ml, 34.8 mmol) and DVB (1.5 ml, 9.0 mmol) were well-mixed and dropped into the SDS solution under stirring, to give rise to a milky emulsion. Then the emulsion was kept in an ultrasonic bath for 10 min. The above emulsion was then placed in a three-necked round-bottom flask and purged with argon for 30 min. After KPS (50 mg, 0.18 mmol) was added at room temperature, the reaction mixture was kept under an argon atmosphere in an oil bath at 65°C for 12 h. After polymerization, the PVBCS nanospheres were purified by subjecting them to successive centrifugation/redispersion cycles in deionized water, ethanol, and finally tetrahydrofuran (THF). The obtained nanospheres were dispersed and stored in THF.

2.3. Synthesis of chain transfer agent (CTA): benzyl 9H-carbazole-9-carbodithioate (BCBD)

A suspension of KOH (0.24 g, 4.2 mmol) in DMSO (20 ml) was prepared, and carbazole (0.71 g, 4.2 mmol) was added under vigorous stirring. The solution was stirred for 2 h at room temperature and then carbon sulfide (0.38 g, 5.0 mmol) was added dropwise. The resultant reddish red solution was stirred for 5 h at room temperature, and then benzyl bromide (0.86 g, 5.0 mmol) was added. After the mixture was stirred overnight, the mixture was precipitated in a large amount of water, and a yellow solid was obtained. After being recrystallized twice from alcohol, yellow crystals of benzyl 9H-carbazole-9-carbodithioate (BCBD) were obtained. BCBD: Yield: 75%. ^{1}H NMR (CDCl$_3$): δ 4.73 (s, 2H), 7.32–7.47 (m, 9H), 8.00, 7.98 (d, 2H), 8.44, 8.46 (d, 2H). E$_{LEM}$. A$_{NAL}$. Calcd: C 72.03%, H 4.53%, N 4.20%, S 19.23%; found: C 72.15%, H 4.53%, N 4.18%, S 19.14%.

2.4. Synthesis of PVBCS supporting chain transfer agent (CTA): PBCBD

A suspension of potassium hydroxide (0.24 g, 4.2 mmol) in DMSO (20 ml) was prepared, and carbazole (0.71 g, 4.2 mmol) was added under vigorous stirring. The solution was stirred for 2 h at room temperature and then carbon sulfide (0.38 g, 5.0 mmol) was added dropwise. The resultant reddish solution was stirred for 5 h at room temperature, and then the suspension of the PVBCS nanospheres (2.0 g) in THF (50 ml) was added. After stirring at room temperature for 36 h, the nanospheres were isolated by centrifugation at 7200 rpm, and purified by subjecting them to successive centrifugation/redispersion cycles in THF and finally in 2-propanol. The obtained yellow product, PVBCS supporting RAFT agents (PBCBD), was dispersed and stored in 2-propanol. Elemental analysis: S, 2.41% (CTA loading: 0.376 mmol/g PBCBD nanospheres).

2.5. Synthesis of PVBCS-*g*-P4VP nanosphere (PVBCS-1)

In a 25 ml glass tube, 4VP (3 ml, 26 mmol), AIBN (2 mg, 0.012 mmol), 2-propanol (10 ml, containing 0.2 g PBCBD, 0.074 mmol CTA), and free BCBD (0.024 g, 0.074 mmol) were added. The suspension was dispersed by ultrasonic and then purged with argon for 15 min. Polymerization was carried out under vigorous stirring for a predetermined time at 50°C. At the end of the polymerization, the surface modified PVBCS-1 nanospheres were purified by subjecting them to successive centrifugation/redispersion cycles in 2-propanol. The final product, PVBCS-*g*-P4VP nanosphere (PVBCS-1), was dispersed and stored in 2-propanol.

2.6. Preparation of Pd/P4VP shell nanosphere (PVBCS-2)

30 ml of aqueous solution containing 0.1 wt% PdCl$_2$ and 5 ml of 2-propanol suspension containing 0.1 g PVBCS-1 were added to a 50 ml glass tube. After stirring for 30 min, the nanospheres were purified by subjecting them to successive centrifugation/redispersion cycles in deionized water. The purified nanospheres were finally dispersed in 20 ml of deionized water. After adjusting pH to 14 with 1 M NaOH, excess N$_2$H$_4$·H$_2$O was added to the above suspension. The reaction was carried out at 50°C for 1 h to enable the Pd(II) to be converted entirely into palladium metal nanoparticles. The nanospheres were purified by subjecting them to successive centrifugation/redispersion cycles in deionized water. The final black product, Pd/P4VP shell nanosphere (PVBCS-2), was dried under reduced pressure at room temperature.

2.7. Heck reaction

Iodobenzene (5.0 mmol), methyl acrylate (7.5 mmol), triethylamine (Et$_3$N, 7.5 mmol), *N,N*-dimethylformamide (DMF, 20 ml), and the PVBCS-2 (15 mg) were added into a Schleck flask equipped with a constant temperature oil bath, and the mixture was stirred for 8 h at 90°C. After cooling to ambient temperature, the suspension was separated and the precipitate was washed by DMF and diethyl ether. To check its reusability, the precipitate was dried and reused in the next experiment. The filtrate was poured in water (30 ml) and extracted with CH$_2$Cl$_2$ (3×20 ml). The combined organic phases were dried over MgSO$_4$, filtered and evaporated in vacuum. The products were purified by column chromatography on silica gel using petroleum ether/ethyl acetate = 10:1 (v:v) as eluent.

^{1}H NMR (CDCl$_3$): δ 3.81 (s, 3H), 6.43, 6.47 (d, 1H), 7.39 (m, 3H), 7.53 (m, 2H), 7.68, 7.72 (d, 1H). E$_{LEM}$. A$_{NAL}$. Calcd: C 74.06% H 6.21%; found: C 73.23%, 5.97%.

2.8. Characterizations

Elemental analysis of C, H, N and S were measured with an EA1110 instrument. Surface compositions were measured by X-ray photoelectron spectroscopy (XPS). XPS was collected on an XSAM800 spectrometer at a pressure of about $2 \cdot 10^{-8}$ torr using Mg K$_\alpha$ radiation as the exciting source, which was operated at 12 kV and 11 mA. All binding energies (BEs) were referenced to the C 1s hydrocarbon peak at 284.6 eV. In peak synthesis, the line width (full width at half maximum) of the Gaussian peaks was maintained constant for all components in a particular spectrum. Transmission electron microscopy (TEM) images were recorded on FEI TecnaiG220 transmission electron microscopy at 200 kV. The sample was prepared by mounting a drop of the nanosphere dispersion on a carbon-coated Cu grid, and allowing the sample to dry in air. The atomic absorption spectroscopy (AAS) (Varian Duo-220) was used to determine the percentage of palladium in PVBCS-1 nanospheres. The sample was prepared by removing organic substance in a muffle furnace at 700°C and then dissolving in aqua regia. ^{1}H NMR was recorded on an Inova 400 MHz nuclear magnetic resonance instrument with CDCl$_3$ as the solvent and tetramethylsilane (TMS) as the internal standard.

3. Results and discussion

### 3.1. Synthesis of PVBCS nanosphere with Pd nanoparticle/P4VP composite shells

Figure 1 shows the synthetic pathway for the preparation of core-crosslinked PVBCS nanospheres with Pd nanoparticle/P4VP composite shells. The process involves (i) preparation of cross-linked PVBCS nanospheres by emulsion copolymerization of VBC and St in the presence of DVB [31], (ii) immobilization of CTA, PBCBD, on the surface of PVBCS nanospheres via reaction of benzyl chloride group in PVBCS nanospheres with carbazole and carbon sulfide [32], (iii) synthesis of PVBCS-*g*-P4VP nanosphere (PVBCS-1) via RAFT polymerization of 4VP, and (iv) preparation of Pd/P4VP shell nanosphere (PVBCS-2) via activation with PdCl$_2$ solution and then reduction with N$_2$H4·H$_2$O.

Crosslinked PVBCS nanospheres with an average diameter of about 70 nm were obtained by this method (see later). Subsequently, the key step of this work is to attach RAFT agent to the PVBCS surfaces. In general, the attachment of the RAFT agent to the surfaces of nanoparticles can be accomplished through either the Z or the R group [33, 34]. However, in the R-group approach, where the solid support is a part of the leaving R groups, higher molecular weight of grafted polymers and grafting density can be achieved [34]. These advantages inspired us to design RAFT agents anchored onto PVBCS nanosphere surfaces through the method of R group moiety. In this work, the benzyl chloride groups on the PVBCS nanosphere surfaces were further reacted with carbazole and carbon sul-
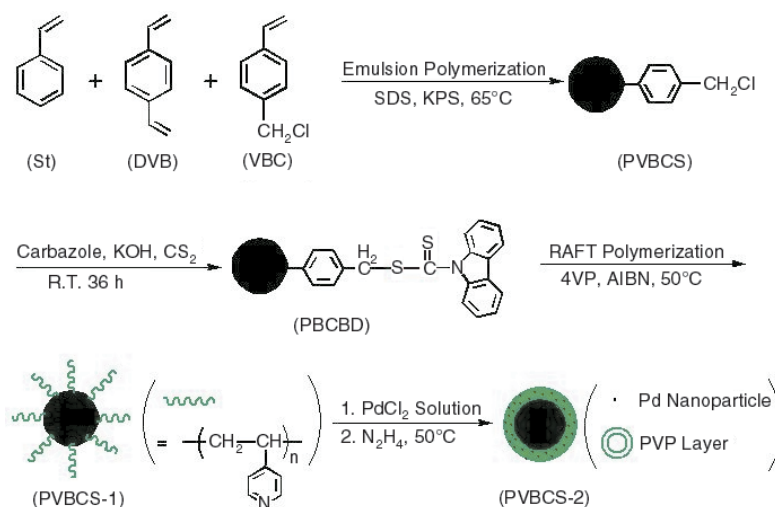
Figure 1. Schematic diagram illustrating the process for the preparation of polymer nanospheres with palladium nanoparticle/P4VP composite shells

fide, leading to the polymer-supporting chain trans-fer agent (PBCBD). Elemental analysis of the poly-mer-supporting PBCBD shows that it contains 2.41% of S element (CTA loading: 0.376 mmol/g). The PBCBD was then used as a macro-RAFT agent to mediate RAFT polymerization of 4VP to pro-duce P4VP brushes on the PVBCS nanosphere sur-faces. The polymerizations ([4VP]:[PBCBD]: [BCBD]:[AIBN] = 2000:6:6:1) were conducted in the presence of a free RAFT agent BCBD in 2-propanol at 50°C for different reaction times. The thickness of P4VP brushes grafted onto PVBCS nanosphere surfaces can be controlled by the poly-merization time, as shown in Table 1. It can be seen from the table, an increase in thickness of grafted P4VP shells from 0 to 3.5 nm is observed when the polymerization time increases from 0 to 24 h, which indicates that the polymerization of 4VP can be well controlled under the present polymerization conditions. At the same time, the content of Pd on different thickness P4VP shells are also increased, which indicates that we can also control the content of Pd loading (from 0–10.1 wt%) in the nanos-pheres by adjusting the polymerization time.

The chemical composition of the nanosphere sur-faces at various stages was determined by XPS. Figure 2(a–c) shows the XPS wide scan, C 1s, and Cl 2p spectra of the PVBCS nanosphere surfaces. The peak components in C 1s at the BEs of about 284.6 and 286.3 eV are attributable to the $\underline{C}$–C/$\underline{C}$–H and $\underline{C}$–Cl species [35, 36], respectively. The Cl 2p
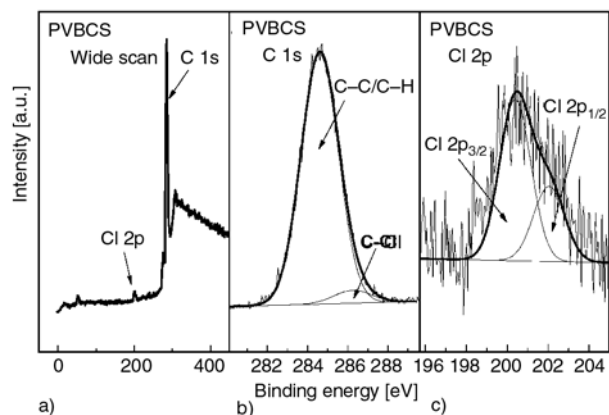
Figure 2. XPS a) wide scan, b) C 1s, and c) Cl 2p core-level spectra of the PVBCS nanosphere surface

core-level spectrum consists of Cl $2p_{3/2}$ and Cl $2p_{1/2}$ doublet at the BEs of about 200.4 and 202.0 eV, respectively [35], attributable to the covalently bonded chlorine (C–$\underline{Cl}$) species.

Figure 3(a–c) shows the XPS wide scan, C 1s and S 2p spectra of the PBCBD nanosphere surfaces after surface modification of PVBCS. The XPS wide scan spectrum shows four peak component at the BEs of about 163, 200, 284 and 400 eV, attrib-utable to S 2p, Cl 2p, C 1s and N 1s species of the PBCBD nanospheres, respectively. The peak com-ponents in C 1s core-level spectrum at the BEs of about 284.6, 284.9 and 286.6 eV are attributable to the $\underline{C}$–C/$\underline{C}$–H, $\underline{C}$–S/$\underline{C}$=S, and $\underline{C}$–Cl species [33, 34], respectively. The S 2p core-level spectrum can be curve-fitted with two peak component with BEs at about 162.9 and 164.2 eV, attributable to the

Table 1. Chemical composition, diameter, and layer thickness of the PVBCS-1 nanospheres

Entry	Polymerization time[a] [h]	N[b] [wt%]	Diameter (D)[c] [nm]	Shell thickness[d] [nm]	Content of Pd[e] [wt %]
1	0	0.00	70	0.0	0.0
2	12	2.20	74	2.0	8.9
3	15	2.44	75	2.5	9.9
4	24	2.90	76	3.0	10.0
5	36	3.43	77	3.5	10.1

[a]Polymerization conditions: 4VP (3 ml), 2-propanol (10 ml, containing 0.2 g PBCBD), AIBN (2 mg), BCBD (0.074 mmol), [M]:[PBCBD]:[BCBD]:[AIBN] = 2000:6:6:1, temperature = 50°C
[b]Percentage of nitrogen of PVBCS-1 nanospheres, deduced from elemental analysis
[c]Diameter of the PVBCS-1, calculated from bulk nitrogen composition and according to Equation (1):

$$D = \left[\frac{\left(\frac{D_0}{2}\right)^3 \cdot 13.32\%}{13.32\% - \%N} \right]^{\frac{1}{3}} \cdot 2 \tag{1}$$

where D_0 is the diameter of the PVBCS (70 nm); 13.32% is the theoretical wt% of nitrogen in P4VP; $\%N$ is the nitrogen composition in the sample.
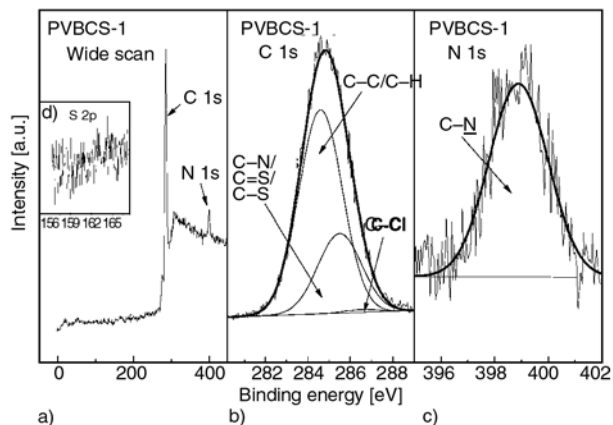[d]Thickness of the P4VP shell in PVBCS-1
[e]Percentage of palladium in PVBCS-1 nanospheres, deduced from the atomic absorption spectroscopy (AAS)
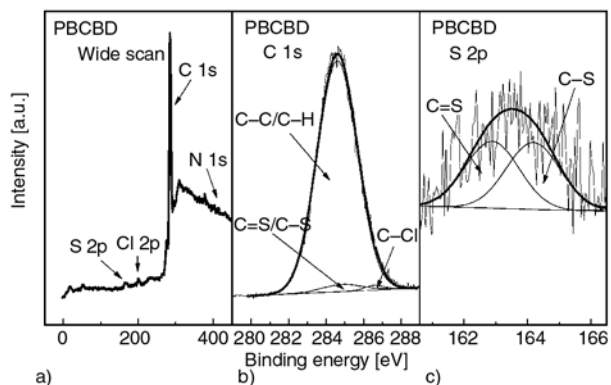
Figure 3. XPS a) wide scan, b) C 1s, and c) S 2p core-level spectra of the PBCBD nanosphere surface

Figure 4. XPS a) wide scan, b) C 1s, c) N 1s, and d) S 2p core-level spectra of the P4VP-grafted PVBCS or PVBCS-1 nanosphere surface from 24 h of surface RAFT polymerization

C=$\underline{S}$ and C–$\underline{S}$ species [23, 36], respectively. It is a key step that the immobilization of RAFT agent on the surfaces of PVBCS nanospheres for this work. Generally, the reaction of benzyl chloride group with carbazole and carbon sulfide is very active and the substitution efficiency of chlorine atoms was reported to be close to 100% [37, 38]. However, the chloride signal can still be discernible in the XPS wide scan spectrum, indicating that there are chlorine atoms in the range of the XPS probing. It is well known that the probing depth of the XPS technique is about 8 nm in an organic matrix [39]. In addition, the XPS-derived surface [Cl]/[C] ratio of 1/100 (after reaction) in PBCBD nanospheres is much lower than that of 1/20 (before reaction) in PVBCS nanospheres, indicating that the most of the benzyl chloride groups have been transferred into the dithioester groups; at the same time, the thickness of CTA layer immobilized on the surfaces of PVBCS nanosphere should be less than 8 nm. All these results demonstrated that the RAFT agent BCBD was successfully anchored onto the PVBCS nanosphere surfaces.

Figure 4(a–c) shows the XPS wide scan, C 1s, and N 1s spectra of the surfaces of PVBCS-1 nanospheres obtained by the surface RAFT polymerization of 4VP for 24 h (as shown in entry 4 of Table 1). The XPS wide scan spectrum shows two dominant peak component at the BEs of about 284 and 400 eV, attributable to C 1s, and N 1s species of the PVBCS-1 nanospheres, respectively. In addition, a sulfur signal is also discernable though it is weaker, as shown in Figure 4d. The C 1s core-level spectrum of the PVBCS-1 surface can be curve-fitted into three peak components with BEs at 284.6,

285.5, and 286.5 eV, attributable to the $\underline{C}$–C/$\underline{C}$–H, $\underline{C}$–N/$\underline{C}$=S/$\underline{C}$–S, and $\underline{C}$–Cl species, respectively. The N 1s core-level spectrum shows a predominantly peak component at BEs of 398.9 eV, attributable to the imine moiety (–N=) of the pyridine rings [40]. The results indicate that the P4VP shells were successfully immobilized onto the PVBCS nanosphere surfaces.

Poly(vinylpyridine) is the most used polymer for nanoparticle stabilization because it fulfils ligand requirements [41]. In this work, the PVBCS-1 nanospheres were activated in the PdCl₂ solution, and then hydrazine hydrate was used as the reducing agent for the PdCl₂-activated nanospheres. The nanospheres gradually turned from light-yellow to black, indicating the formation of palladium metal nanoparticles in the P4VP shell (PVBCS-2). Figure 5(a–d) shows the XPS wide scan, C 1s, N 1s, and Pd 3d spectra of the PVBCS-2 nanosphere surfaces. The XPS wide scan shows five peak components at the BEs of about 162, 200, 284, 335, and 398 eV, attributable to S 2p, Cl 2p, C 1s, Pd 3d, and N 1s species, respectively. The C 1s core-level spectrum of the PVBCS-2 surface can be curve-fitted into three peak components with BEs at about 284.6, 285.5, and 286.5 eV, attributable to the $\underline{C}$–C/$\underline{C}$–H, $\underline{C}$–N/$\underline{C}$–S/$\underline{C}$=S, and $\underline{C}$–Cl species, respectively. The peak component at the BEs of 398.9 eV in the N 1s core-level spectrum is attributable to the imine moiety (–N=) of the pyridine rings. The XPS spectrum of Pd 3d can be curve-fitted into two spin-orbit-split doublets, as illustrated in Figure 5d. The two peak components at the BEs
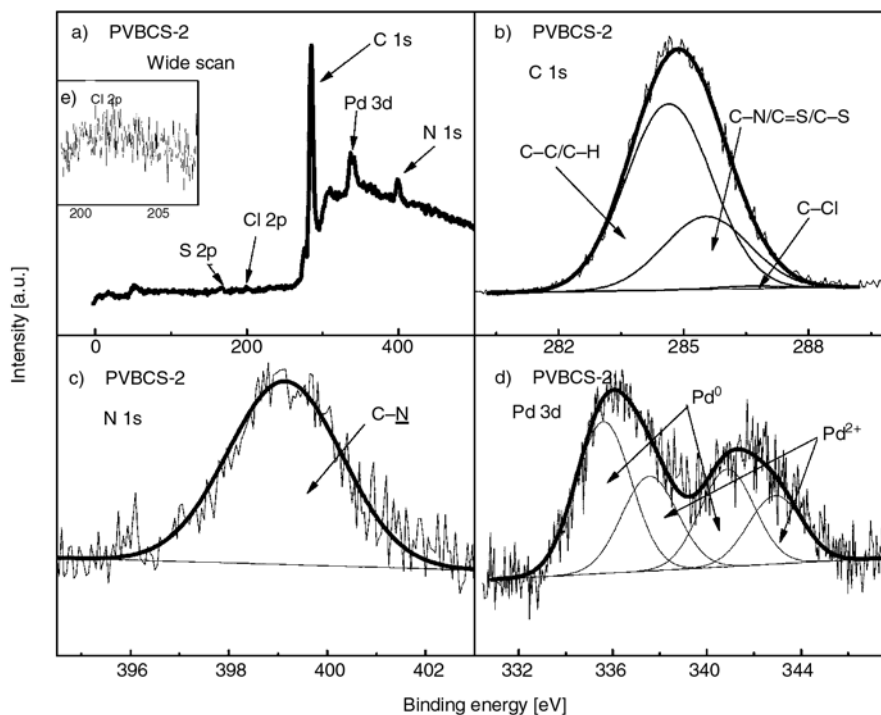
Figure 5. XPS a) wide scan, b) C 1s, c) N 1s, d) Pd 3d, and e) Cl 2p core-level of the Pd/P4VP composite shell nanos-phere (PVBCS-2 nanosphere) surface

of about 335.4 and 340.7 eV are attributable to the Pd $3d_{5/2}$ and Pd $3d_{3/2}$ species, which can be indexed to the Pd (0) state [36, 42]. The other set of peaks at 337.7 eV (Pd $3d_{5/2}$) and 342.9 eV (Pd $3d_{3/2}$) is ascribed to the Pd^{2+} [38, 43]. Calculating the integration areas of these two doublets using XPS-PEAK software, it can be estimated that the atomic ratio of Pd^0/Pd^{2+} was about 59:41. The oxidation form of Pd is possibly palladium oxide, which may result from the surface oxidation of palladium nanoparticles when they are exposed to air. A similar phenomenon was also reported by others [42, 43].

3.2. Activity for the heck reaction of the PVBCS-2 nanospheres

It is well-known that Pd is effective in catalyzing C–C bond formation reactions [27–30]. Among palladium-catalyzed couplings, the Suzuki-Miyaura [29], Sonogashira [27] and Heck [28] reactions are the most widely used. In this work, the catalytic activity of the PVBCS-2 nanospheres for Heck reaction was investigated using the model reaction of iodobenzene and methyl acrylate (Figure 6). The reaction of iodobenzene (1.0 equiv) and methyl acrylate (1.5 equiv) with 15 mg of PVBCS-2 nanos-
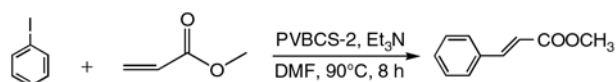
Figure 6. Schematic diagram illustrating Heck reaction using iodobenzene and methyl acrylate as the model reagents

pheres was performed at 90°C in DMF containing triethylamine (1.5 equiv). The results are listed in Table 2.

The freshly synthesized PVBCS-2 nanospheres exhibit a higher activity. Although the activity of the catalyst gradually decreases somewhat after subsequent recycling, the catalyst still shows a good activity even if it was used three times. XPS spectroscopy technique was also used to check the chemical composition of the recycled catalyst (PVBCS-2A) surfaces after being used four times. Figure 7(a–d) shows the XPS wide scan, C 1s,
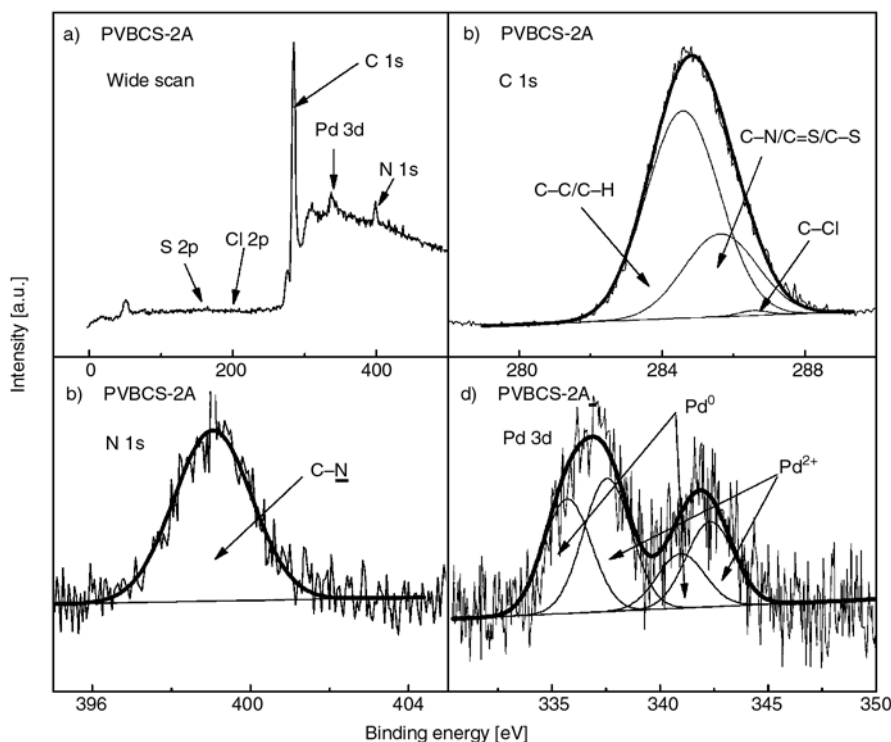
Table 2. Results of Heck reaction catalyzed by PVBCS-2 nanosphere

Run[a]	1	2	3	4
Isolated yield [%][b]	97	95	94	94

[a]Reaction performed with 5.0 mmol of idobenzene, 7.5 mmol of methyl acrylate, 7.5 mmol of triethylamine, 20 ml of DMF, PVBCS-2 (15 mg, Pd% = 8.9 wt%)
[b]Isolated yield after filtration of crude reaction mixture on silica gel

Figure 7. XPS a) Wide scan, b) C 1s, c) N 1s, and d) Pd 3d core-level spectra of the recycled PVBCS-2 nanophere (PVBCS-2A nanosphere) surface

N 1s, and Pd 3d spectra of the PVBCS-2A nanosphere surfaces. The XPS wide scan, C 1s, and N 1s spectra of the PVBCS-2A nanosphere surfaces have no significant changes as compared with the PVBCS-2 nanosphere surfaces. The XPS wide scan shows five peak components at the BEs of about 162, 200, 284, 335, and 398 eV, attributable to S 2p, Cl 2p, C 1s, Pd 3d, and N 1s species, respectively. The C 1s core-level spectrum of the PVBCS-2 surface can be curve-fitted into three peak components with BEs at about 284.6, 285.5, and 286.5 eV, attributable to the $\underline{C}$–C/$\underline{C}$–H, $\underline{C}$–N/$\underline{C}$–S/$\underline{C}$=S, and $\underline{C}$–Cl species, respectively. The peak component at the BEs of 398.9 eV in the N 1s core-level spectrum is attributable to the imine moiety (–N=) of the pyridine rings. As illustrated in Figure 7d, the doublet with a binding energy at 335.4 eV (Pd $3d_{5/2}$) and 340.7 eV (Pd $3d_{3/2}$) can be indexed to the Pd^0. The other set of peaks at 337.6 eV (Pd $3d_{5/2}$) and 342.3 eV (Pd $3d_{3/2}$) is ascribed to the Pd^{2+}. Different from the result of original PVBCS-2 nanospheres, the atomic ratio of Pd^0/Pd^{2+} is about 33:67 by calculating the integration areas of these two doublets using XPSPEAK software after fours times catalytic cycles, being lower than the ratio (59:41) of the initial catalyst.

The increased oxidation form of Pd possibly results from the surface oxidation of palladium nanoparticles during the Heck reaction [42, 43].

3.3. Morphology of the PVBCS nanospheres

The morphologies of the PVBCS nanospheres at different stages of surface functionalization were observed by TEM. PVBCS nanospheres with an average diameter of about 70 nm, as determined by TEM (Figure 8(a, b)), were obtained. After surface functionalization, the PVBCS-supporting chain transfer agent (PBCBD) was obtained, and the size and morphology of the nanospheres are almost identical to these of the PVBCS nanospheres (Figure 8c). Figure 8d shows the TEM image of the P4VP grafted PVBCS nanospheres (PVBCS-1) with a 76 nm of diameter after RAFT polymerization for 24 h. Figure 8e shows the TEM images of the Pd/P4VP shell nanospheres (PVBCS-2). The small dark spots representing the palladium metal nanoparticles are dispersed throughout the surface of the PVBCS-2 nanospheres in the P4VP shell. The surface of the nanoparticles becomes a little rough after being recycled four times, as shown in Figure 8f. During the reaction process, most of the
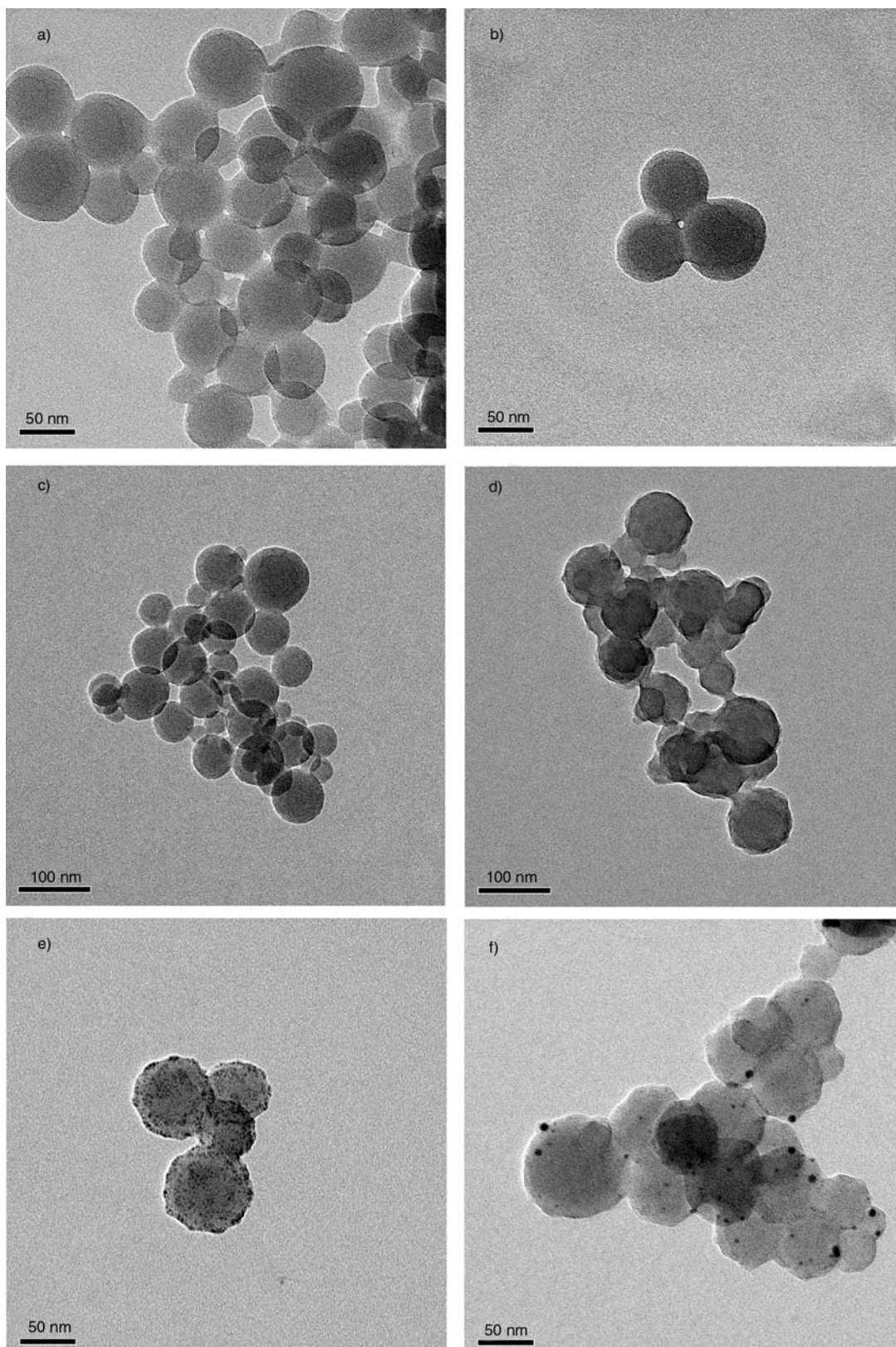
Figure 8. TEM images of a), b) the cross-linked PVBCS nanosphere, c) the PVBCS supporting chain transfer agent: PBCBD nanosphere, d) the PVBCS-*g*-P4VP nanosphere (PVBCS-1 nanosphere) obtained by the surface RAFT polymerization of 4VP for 24 h, e) the Pd/P4VP composite shell nanosphere (PVBCS-2 nanosphere), and f) the Pd/P4VP composite shell nanosphere (PVBCS-2A nanosphere) used in the Heck reaction after four times

leached Pd species can be adsorbed on the polymer support [42], so the catalyst remains good in activity and is stable after being recycled several times.

4. Conclusions

A four-step method for preparing core-crosslinked polymer nanospheres with Pd/P4VP inorganic/ organic hybrid shells via RAFT polymerization was developed. This method allows the control over shell thickness by simply adjusting the RAFT polymerization time, and therefore the content of palladium. The Pd/P4VP shell nanospheres can serve as an efficient and reusable catalyst for the Heck reaction.

Acknowledgements

References

[1] Caruso F.: Nanoengineering of particle surfaces. Advanced Materials, **13**, 11–22 (2001).
DOI: 10.1002/1521-4095(200101)13:1<11::AID-ADMA11>3.0.CO;2-N

[2] Daniel M. C., Astruc. D.: Gold nanoparticles: Assembly, supramolecular chemistry, quantum-size-related properties, and applications toward biology, catalysis, and nanotechnology. Chemical Reviews, **104**, 293–346 (2004).
DOI: 10.1021/cr030698+

[3] Du Y. J., Damron M., Tang G., Zheng H. X., Chu C-J., Osborne J. H.: Inorganic/organic hybrid coatings for aircraft aluminum alloy substrates. Progress in Organic Coatings, **41**, 226–232 (2001).
DOI: 10.1016/S0300-9440(01)00133-3

[4] Lin C. K., Luo Y., You H., Quan Z., Zhang J., Fang J., Lin J.: Sol-gel-derived BPO$_4$/Ba^{2+} as a new efficient and environmentally-friendly bluish-white luminescent material. Chemistry of Materials, **18**, 458–464 (2006).
DOI: 10.1021/cm052109h

[5] Teng X., Shchukin D. G., Möhwald H.: Encapsulation of water-immiscible solvents in polyglutamate/polyelectrolyte nanocontainers. Advanced Functional Materials, **17**, 1273–1278 (2007).
DOI: 10.1002/adfm.200601229

[6] Kim B-S., Taton T. A.: Multicomponent nanoparticles via self-assembly with cross-linked block copolymer surfactants. Langmuir, **23**, 2198–2202 (2007).
DOI: 10.1021/la062692w

[7] Limpanart S., Khunthon S., Taepaiboon P., Supaphol P., Srikhirin T., Udomkichdecha W., Boontongkong Y.: Effect of the surfactant coverage on the preparation of polystyrene-clay nanocomposites prepared by melt intercalation. Materials Letters, **59**, 2292–2295 (2005).
DOI: 10.1016/j.matlet.2005.03.006

[8] Hu Q. Y., Hampsey J. E., Jiang N., Li C. J., Lu Y. F.: Surfactant-templated organic functionalized mesoporous silica with phosphino ligands. Chemistry of Materials, **17**, 1561–1569 (2005).
DOI: 10.1021/cm0491983

[9] Otsu T., Yoshida M.: Role of initiator-transfer agent-terminator (iniferter) in radical polymerizations: Polymer design by organic disulfides as iniferters. Die Makromolekulare Chemie, Rapid Communications, **3**, 127–132 (1982).
DOI: 10.1002/marc.1982.030030208

[10] Wang J. S., Matyjaszewski K.: Controlled/'living' radical polymerization. Atom transfer radical polymerization in the presence of transition-metal complexes. Journal of the American Chemical Society, **117**, 5614–5615 (1995).
DOI: 10.1021/ja00125a035

[11] Chiefari J., Chong Y. K., Ercole F., Krstina J., Jeffery J., Le T. P. T., Mayadunne R. T. A., Meijs G. F., Moad C. L., Moad G., Rizzardo E., Thang S. H.: Living free-radical polymerization by reversible addition-fragmentation chain transfer: The RAFT process. Macromolecules, **31**, 5559–5562 (1998).
DOI: 10.1021/ma9804951

[12] Kasseh A., Ait-Kadi A., Riedl B., Pierson J. F.: Organic/inorganic hybrid composites prepared by polymerization compounding and controlled free radical polymerization. Polymer, **44**, 1367–1375 (2003).
DOI: 10.1016/S0032-3861(02)00905-9

[13] Fulghum T. M., Patton D. L., Advincula R. C.: Fuzzy ternary particle systems by surface-initiated atom transfer radical polymerization from layer-by-layer colloidal core-shell macroinitiator particles. Langmuir, **22**, 8397–8402 (2006).
DOI: 10.1021/la0601509

[14] Lowe A. B., Sumerlin B. S., Donovan M. S., McCormick C. L.: Facile preparation of transition metal nanoparticles stabilized by well-defined (co)polymers synthesized via aqueous reversible addition-fragmentation chain transfer polymerization. Journal of the American Chemical Society, **124**, 11562–11563 (2002).
DOI: 10.1021/ja020556h

[15] Braunecker W. A., Matyjaszewski K.: Controlled/living radical polymerization: Features, developments, and perspectives. Progress in Polymer Science, **32**, 93–146 (2007).
DOI: 10.1016/j.progpolymsci.2006.11.002

[16] Moad G., Rizzardo E., Thang S. H.: Radical addition-fragmentation chemistry in polymer synthesis. Polymer, **49**, 1079–1131 (2008).
DOI: 10.1016/j.polymer.2007.11.020

[17] Lowe A. B., McCormick C. L.: Reversible addition-fragmentation chain transfer (RAFT) radical polymerization and the synthesis of water-soluble (co)polymers under homogeneous conditions in organic and aqueous media. Progress in Polymer Science, **32**, 283–351 (2007).
DOI: 10.1016/j.progpolymsci.2006.11.003

[18] Guo T-Y., Liu P., Zhu J-W., Song M-D., Zhang B-H.: Well-defined lactose-containing polymer grafted onto silica particles. Biomacromolecules, **7**, 1196–1202 (2006).
DOI: 10.1021/bm051011t

[19] Fustin C-A., Colard C., Filali M., Guillet P., Duwez A. S., Meier M. A. R., Schubert U. S., Gohy J-F.: Tuning the hydrophilicity of gold nanoparticles templated in star block copolymers. Langmuir, **22**, 6690–6695 (2006).
DOI: 10.1021/la060758h

[20] Skaff H., Emrick T.: Reversible addition fragmentation chain transfer (RAFT) polymerization from unprotected cadmium selenide nanoparticles. Angewandte Chemie, International Edition, **43**, 5383–5386 (2004).
DOI: 10.1002/anie.200453822

[21] Hong C-Y., You Y-Z., Pan C-Y.: Synthesis of water-soluble multiwalled carbon nanotubes with grafted temperature-responsive shells by surface RAFT polymerization. Chemistry of Materials, **17**, 2247–2254 (2005).
DOI: 10.1021/cm048054l

[22] Perrier S., Takolpuckdee P., Mars C. A.: Reversible addition-fragmentation chain transfer polymerization mediated by a solid supported chain transfer agent. Macromolecules, **38**, 6770–6774 (2005).
DOI: 10.1021/ma0506886

[23] Peng Q., Lai D. M. Y., Kang E. T., Neoh K. G.: Preparation of polymer-silicon(100) hybrids via interface-initiated reversible addition-fragmentation chain-transfer (RAFT) polymerization. Macromolecules, **39**, 5577–5582 (2006).
DOI: 10.1021/ma0607362

[24] Pyun J., Matyjaszewski K.: Synthesis of nanocomposite organic/inorganic hybrid materials using controlled/'living' radical polymerization. Chemistry of Materials, **13**, 3436–3448 (2001).
DOI: 10.1021/cm011065j

[25] Nishi H., Kobatake S.: Photochromism and optical property of gold nanoparticles covered with low-poly-dispersity diarylethene polymers. Macromolecules, **41**, 3995–4002 (2008).
DOI: 10.1021/ma702882t

[26] Hotchkiss J. W., Lowe A. B., Boyes S. G.: Surface modification of gold nanorods with polymers synthesized by reversible addition-fragmentation chain transfer polymerization. Chemistry of Materials, **19**, 6–13 (2007).
DOI: 10.1021/cm0622912

[27] Kim J-H., Lee D-H., Jun B-H., Lee Y-S.: Copper-free Sonogashira cross-coupling reaction catalyzed by polymer-supported *N*-heterocyclic carbene palladium complex. Tetrahedron Letters, **48**, 7079–7084 (2007).
DOI: 10.1016/j.tetlet.2007.08.015

[28] Beletskaya I. P., Khokhlov A. R., Tarasenko E. A., Tyurin V. S.: Palladium supported on poly(*N*-vinylimidazole) or poly(*N*-vinylimidazole-co-*N*-vinylcaprolactam) as a new recyclable catalyst for the Mizoroki-Heck reaction. Journal of Organometallic Chemistry, **692**, 4402–4406 (2007).
DOI: 10.1016/j.jorganchem.2007.06.056

[29] Tzschucke C. C., Andrushko V., Bannwarth W.: Assessment of the reusability of Pd complexes supported on fluorous silica gel as catalysts for Suzuki couplings. European Journal of Organic Chemistry, **24**, 5248–5261 (2005).
DOI: 10.1002/ejoc.200500281

[30] Drelinkiewicz A., Knapik A., Waksmundzka-Góra A., Bukowska A., Bukowski W., Noworól J.: Functional gel-type resin based palladium catalysts: The role of polymer properties in the hydrogenation of the C=C bond of maleic and fumaric acids, the isomers of dicarboxylic acids. Reactive and Functional Polymers, **68**, 1059–1071 (2008).
DOI: 10.1016/j.reactfunctpolym.2008.02.008

[31] Fryling C. F., Harrington E. W.: Emulsion polymerization. Industrial and Engineering Chemistry, **36**, 114–117 (1944).
DOI: 10.1021/ie50410a004

[32] Zhou D., Zhu X. L., Zhu J., Hu L. H., Cheng Z. P.: Influence of the chemical structure of dithiocarbamates with different R groups on the reversible addition-fragmentation chain transfer polymerization. Journal of Applied Polymer Science, **103**, 982–988 (2007).
DOI: 10.1002/app.25280

[33] Barner L., Li C. E., Hao X. J., Stenzel M. H., Barner-Kowollik C., Davis T. P.: Synthesis of core-shell poly(divinylbenzene) microspheres via reversible addition fragmentation chain transfer graft polymerization of styrene. Journal of Polymer Science Part A: Polymer Chemistry, **42**, 5067–5076 (2004).
DOI: 10.1002/pola.20328

[34] Zhao Y., Perrier S.: Synthesis of well-defined homopolymer and diblock copolymer grafted onto silica particles by Z-supported RAFT polymerization. Macromolecules, **39**, 8603–8608 (2006).
DOI: 10.1021/ma061586y

[35] Beamson G., Briggs D.: High-resolution XPS of organic polymers: The scienta ESCA300 Database. Wiley, Chichester (1992).

[36] Moulder J. F., Stickle W. F., Sobol P. E., Bomben K. D.: Handbook of X-ray photoelectron spectroscopy. Perkin-Elmer, Eden Prairie (1992).

[37] Quinn J. F., Chaplin R. P., Davis T. P.: Facile synthesis of comb, star, and graft polymers via reversible addition-fragmentation chain transfer (RAFT) polymerization. Journal of Polymer Science Part A: Polymer Chemistry, **40**, 2956–2966 (2002).
DOI: 10.1002/pola.10369

[38] Wang S. M., Cheng Z. P., Zhu J., Zhang Z. B., Zhu X. L.: Synthesis of amphiphilic and thermosensitive graft copolymers with fluorescence P(St-*co*-(p-CMS))-*g*-PNIPAAM by combination of NMP and RAFT methods. Journal of Polymer Science Part A: Polymer Chemistry, **45**, 5318–5328 (2007).
DOI: 10.1002/pola.22277

[39] Briggs D.: Surface analysis of polymers by XPS and static SIMS. Cambridge University Press, New York (1998).

[40] Cheng Z. P., Zhang L. F., Zhu X. L., Kang E. T., Neoh K. G.: Organic/inorganic hybrid nanospheres coated with palladium/P4VP shells from surface-initiated atom transfer radical polymerization. Journal of Polymer Science Part A: Polymer Chemistry, **46**, 2119–2131 (2008).
DOI: 10.1002/pola.22547

[41] Mathew J. P., Srinivasan M.: Photoelectron spectroscopy (XPS) studies on some palladium catalysts. European Polymer Journal, **31**, 835–839 (1995).
DOI: 10.1016/0014-3057(95)00027-5

[42] Miao S., Zhang C., Liu Z., Han B., Xie Y., Ding S., Yang Z.: Highly efficient nanocatalysts supported on hollow polymer nanospheres: Synthesis, characterization, and applications. The Journal of Physical Chemistry C, **112**, 774–780 (2008).
DOI: 10.1021/jp076596v

[43] Choudary B. M., Madhi S., Chowdari N. S., Kantam M. L., Sreedhar B.: Layered double hydroxide supported nanopalladium catalyst for Heck-, Suzuki-, Sonogashira-, and Stille-type coupling reactions of chloroarenes. Journal of the American Chemical Society, **124**, 14127–14136 (2002).
DOI: 10.1021/ja026975w

Polyimide/silica hybrids via the sol-gel route: High performance materials for the new technological challenges

G. Ragosta*, P. Musto

National Research Council of Italy, Institute of Chemistry and Technology of Polymers (ICTP), Via Campi Flegrei 34, Olivetti Buildings, 80078 Pozzuoli, NA, Italy

Abstract. The present review article describes in detail the state-of-the-art of organic-inorganic hybrid materials based on polyimide/silica components. The article is divided in three parts. In the first the basic processing route for the preparation of these systems is described, i.e. the sol-gel technique, along with the strategies developed to control the final morphology. In the second part the curing characteristics, the dynamic-mechanical and the mechanical and fracture properties of hybrids with different morphologies are reviewed. Finally, the more technologically relevant applications devised for these high performance materials are discussed.

Keywords: nanocomposites, hybrid materials, polyimide, silica, sol-gel

1. Introduction

Polyimides (PI) are a class of high-performance polymers possessing the cyclic imide and aromatic groups in the main chains. The most familiar polyimide is widely known as Kapton, developed by Du Pont in the 1960s. After the marketing of this polyimide, many others were commercially developed with some modified properties. They have gained considerable importance in advanced areas such as microelectronics, aerospace and separation technologies owing to their outstanding properties in terms of thermal stability, mechanical properties, and solvent resistance, coupled with relatively low permittivity and dielectric losses up to very high temperatures [1–3]. In order to facilitate progress of PIs in their application fields, much effort has been spent to further improve their properties. This can been achieved through the formation of *in situ* gen-erated inorganic particles to produce organic-inorganic (O/I) hybrid materials [4–7].

The O/I systems have been recognized as a new class of high performance materials owing to the unique opportunity that these systems provide to combine the excellent properties of inorganic glasses, such as high modulus, thermal stability and low coefficient of thermal expansion, with the ductility and low temperature processing characteristics of organic polymers. When the two phases are interconnected and the domain sizes of these phases approach those of supramolecular entities, these materials are known as nanostructured materials or 'phase-interconnected' nanocomposites [8–11].

Hybrid materials offer a large potential for applications in a variety of advanced technologies, either as structural materials [6], including their use as matrices for high performance composites [12, 13],

---

*Corresponding author, e-mail: rago@ictp.cnr.it

or as functional materials [14] such as catalyst supports [15] and microelectronic devices [16]. The sol-gel route represents the preferred way for the synthesis of polyimide based hybrids. The classical sol-gel process consists in a two step hydrolysis-condensation reaction, starting with a metal alkoxides $M(OR)_4$, typically tetraethoxisilane $Si(OCH_2CH_3)_4$ or titanium isopropoxide $Ti[OCH(CH_3)_2]_4$, to produce hydroxyl groups followed by the polycondensation of the hydroxyl groups and residual alkoxy groups to form a three-dimensional network [5, 17–21].

Polyimides are particularly suited for this type of process because they can be obtained from polyamic acid precursors, which are soluble in hygroscopic solvents and can, therefore, tolerate the addition of water necessary to bring about the hydrolysis of the metal alkoxide. Moreover, the outstanding thermal stability of polyimides allows the hybrids to be post-cured at very high temperatures (300–350°C) making it possible the development of a very dense inorganic network without inducing appreciable degradation of the organic phase.

Polyimide/silica hybrids made by the sol-gel technique are the subject of this review, in which the approaches used for a close control of their final morphology, the effects of the silica phase on the curing process of polyimide precursors, the dynamic-mechanical and the mechanical and fracture properties that these materials can display, and their possible applications will be presented and discussed.

## 2. Processing and morphology

A typical procedure for the preparation of PI/silica hybrids via the sol-gel route, involves the following steps:

i) The polyamic acid (PAA) (PI precursor) is formed by a polyaddition reaction of a dianhydride [e.g., pyromellitic anhydride (PMDA), 3,3′,4,4′-biphenyltetracarboxylic dianhydride (BPDA), or 2,2-bis(3,4-dicarboxy-phenyl)-hexafluoropropane dianhydride (6FDA)] with a diamine [e.g., 4,4′-oxydianiline (ODA), or p-phenylen diamine (PPA)] in a common solvent [e.g., dimethylacetamide (DMAc), or N-methyl pyrolidone (NMP)]. The reaction and chemical structures of monomers are reported in Figure 1.
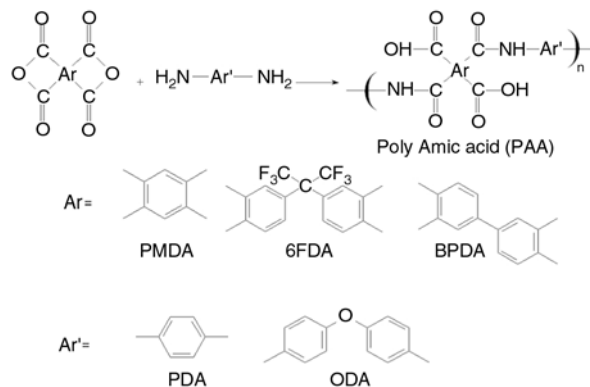
Figure 1. Formation of polyamic acids, the precursor of polyimides

ii) The silica precursor [e.g., tetraethoxysilane (TEOS) or tetramethoxysilane (TMOS) is added to the PAA solution, and the hydrolysis and polycondensation is carried out using an appropriate catalyst.

iii) The PAA/silica solution is film cast by drying the solvent, and then the film is cured by successive heating treatments up to 300°C. The heating induces the imidization reaction to convert PAA to PI and the crosslinking of the
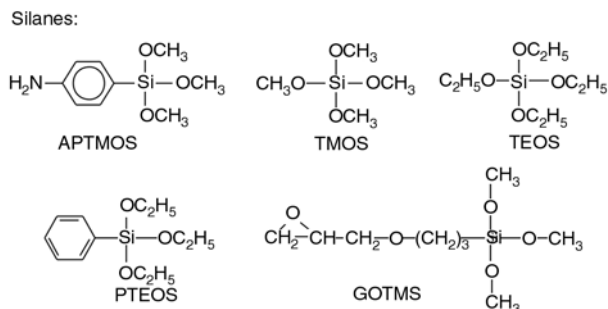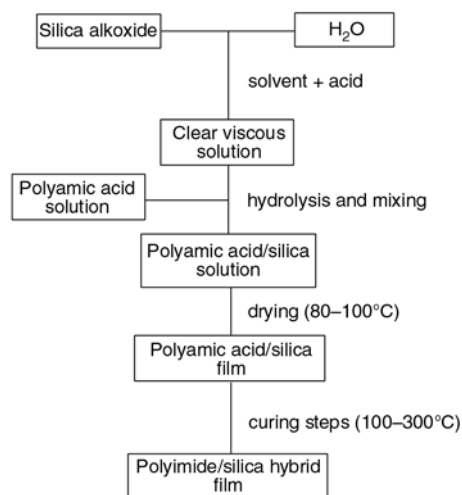
Figure 2. Sol-gel process for the production of a polyimide/silica hybrid and the structures of some alkoxisilanes

siloxane component to form a silica network. This route is outlined in Figure 2 where the structures of some silanes discussed in the present review are also reported.

The types of reactions involved in the preparation of PI/silica hybrids allow to exert a considerable control on the final morphology by preventing premature phase separation. This is achievable by optimizing the processing parameters (temperature, catalyst and nature of the solvent) and by promoting reactions or interactions between the two components, either directly or via a coupling agent. Various methods for effectively introducing a silica phase into PI matrices have been reported by Nandi *et al.* [17, 22], Morikawa *et al.* [7, 11], Wang *et al.* [23], Mascia *et al.* [8, 13], Schmidt and Wolter [24, 25] among other. Given below is an account of some of the approaches used.

In earlier studies, large sized silica domains were generated with inhomogeneous distribution within polyimide matrices. This led to brittle materials with poor mechanical properties. In order to minimize the size of the inorganic particles and to prevent their agglomeration, Nandi and co-workers prepared polyimide-silica hybrids via the *'site isolation method'* [17, 22]. This method consisted of pre-binding an alkoxide precursor to a polyamic acid, forming a carboxylate group, and subsequently curing the system to imidize the polyamic acid and to drive the sol-gel reactions. Homogeneously dispersed silica particles of nanometer dimensions were observed in the polyimide matrix, particularly at low silica content, although micron-sized particles were evident at higher silica concentrations (> 40 wt%). However, this approach had the drawback that the prebinding of the alkoxide precursor prevented a complete imidization of the polyamic acid.

Morikawa *et al.* [7, 26] produced PI/silica hybrids by mixing TEOS solutions and a polyamic acid, obtained from the reaction of PMDA and ODA. Except for systems with low silica content (<10 wt%), the films were opaque and contained coarse silica particles 3–7 µm in diameter. In later studies these authors [11, 27] greatly improved the morphology and properties of these hybrids by introducing different types and concentrations of pendant alkoxysilanes along the polyimide backbone. These pendant groups provided connection points to the silica particles. The SEM results

showed that the silica particle size was 0.5–1.0 µm, i.e. smaller than those in the previous studies, and the particles were homogeneously distributed. These results were attributed to increased compatibility owing to interactions between the organic and inorganic phases.
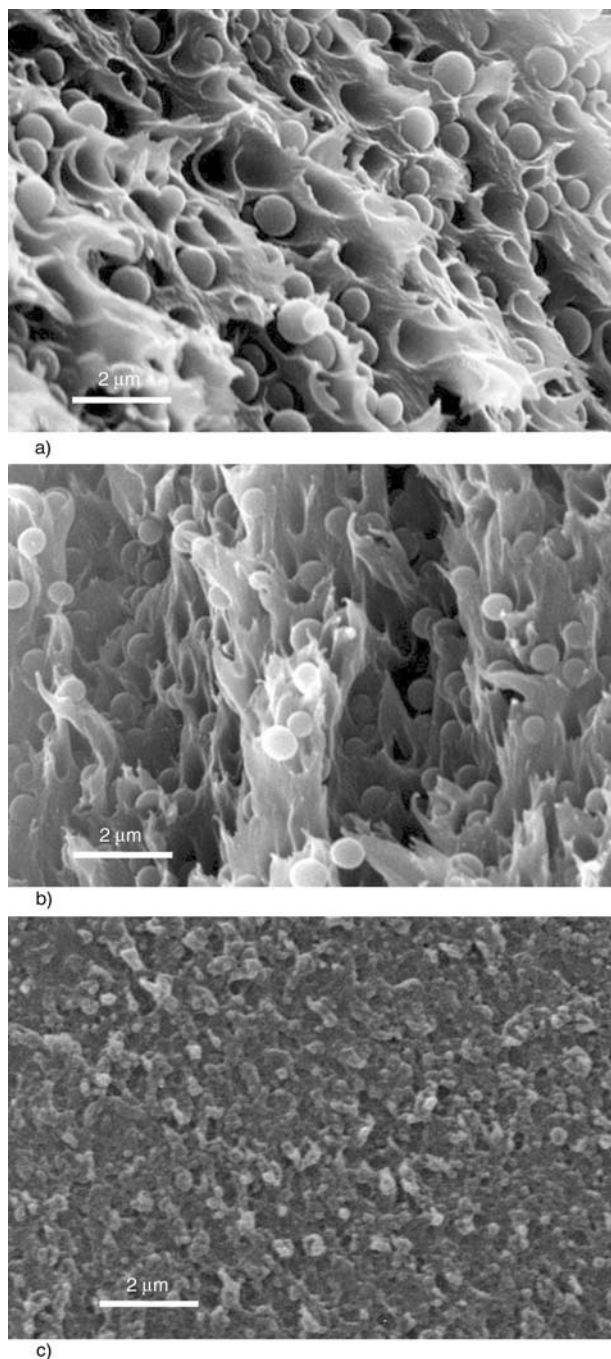
Mascia and Kioul [5, 8, 21] and Mascia and coworkers [28, 29], showed that the compatibility in PI/silica hybrids can be greatly improved by adding to TEOS solutions a functional alkoxysilane coupling agent such as γ-glycidyloxipropyl trimethoxysilane (GOTMS). The SEM micrographs of Figure 3 for PI hybrids with 22.3 wt% of silica illustrate the compatibilization effect of GOTMS, which brings about a morphological transformation from a dispersed particle microstructure (Figure 3a), in absence of GOTMS to a finely interconnected or co-continuous phase morphology (Figure 3b), with the use of GOTMS [28]. For the compatibilized system the size of the interconnected silica domains ranges from 40 to
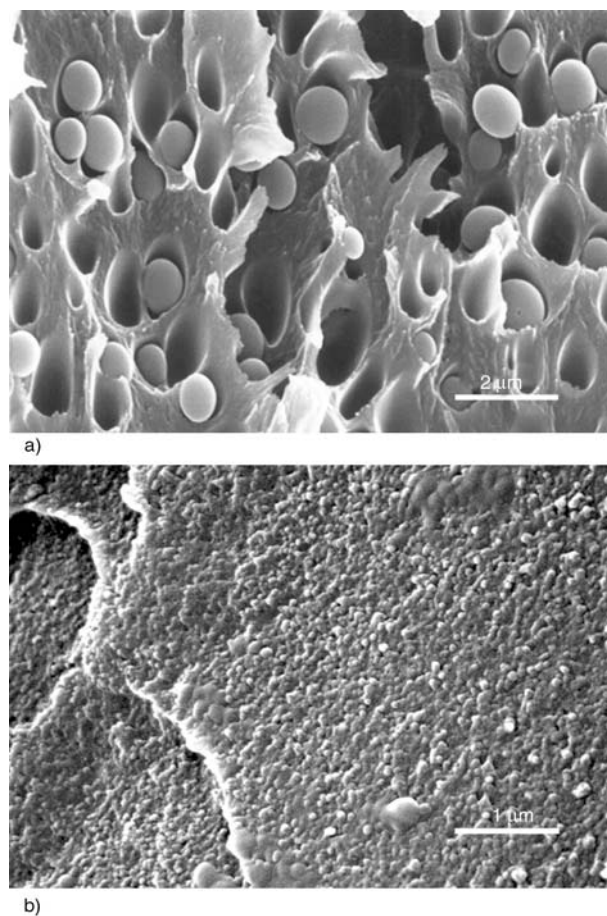
Figure 3. SEM micrographs of PI/silica hybrids with 22.3 wt% of silica: a) hybrid without the coupling agent (GOTMS); b) hybrid with the coupling agent (GOTMS) [28].

100 nm, while for the non-compatibilized system, the average diameter of the silica particles varies from 0.8 to 1.0 µm. These morphologies are the result of a typical phase separation by spinodal decomposition [30, 31] differing from each other in the extent of phase connectivity. The way through which the coupling agent induces and controls the evolution of the morphology in these hybrid sys-

tems was attributed to interactions, possibly by hydrogen bonding, taking place between the epoxy groups of GOTMS and the acid groups of the poly-imide precursor. These interactions delay the onset of phase separation by spinodal decomposition, which results in a higher viscosity of the solution and in a reduction of the rate of particle growth [5, 8, 32]. It was found that a threshold value of the GOTMS/TEOS molar ratio exists for the formation of co-continuous morphologies [8, 32]. This threshold value was found to change with the overall silica content in the hybrid. For a silica concentration of 22.3 wt%, calculated theoretically assuming complete conversion of TEOS and GOTMS to silica [33], the threshold GOTM/TEOS molar ratio is located between 0.06 and 0.08. Figure 4 shows the SEM micrographs of hybrids having 22.3 wt% of silica and GOTMS contents below and above the threshold value [32]. For GOTMS concentrations lower than the limiting value, the hybrids display (Figures 4a and 4b) a particulate morphology like that of Figures 3a, but with smaller particles sizes. The dimensions of these particles decrease from about 0.61 to 0.32 µm with increasing the amount of GOTMS. The micrograph of Figure 4c, on the other hand, illustrates the morphology obtained with a GOTMS content slightly above the threshold value. This morphology is close to that of Figure 3b for which a higher GOTMS concentration was used. TEM examinations for co-continuous structures revealed additional morphological features. In particular, it was found that increasing the amount of GOTMS above the threshold value had the effect of reducing the sizes of the silica domains [33]. Thus the GOTMS/TEOS molar ration represents a parameter which allows us to finely tune the size of the silica particles in the system. This flexibility in the management of the final morphology permits to realize PI/silica hybrids tailored to specific requirements. For instance co-continuous morphologies were found to be much more effective in suppressing molecular relaxation processes, producing higher temperature stability and lower coefficients of thermal expansion. Two-phase micron sized morphologies, on the other hand, gave higher ductility.

Attempts to decrease the extent of phase separation in PI/silica hybrids by enhancing the miscibility of the components were also conduced by Wang and coworkers [23, 34, 35]. They used aminophenyl-

Figure 4. SEM micrographs of PI/silica hybrids with 22.3 wt% of silica and at different GOTMS/TEOS molar ratios: a) GOTMS/TEOS 0.02; b) GOTMS/TEOS 0.03; c) GOTMS/TEOS 0. 1 [32].

trimethoxysilane (APTMOS) as a coupling agent. Whether premixed with the polyamic acid or with the trimethoxysilane (TMOS) solution, this coupling agent was reported to have improved the dispersion of the silica domains in the polyimide matrix. This was attributed to the enhanced interconnectivity of the two phases through chemical interactions with the amine groups of the coupling agent.

Hybrids from TMOS and a pyromellitic polyamic acid, synthesised by replacing the aromatic diamine typically used (ODA) with γ-aminopropyltrimethoxysilane (APTEOS) have been also investigated by Schrotter *et al.* [36]. The resulting microstructure of PMDA/APTEOS-based films showed a better incorporation of the silica than in PMDA/ODA, possibly as a result of the presence of active amino and methoxyl groups in APTEOS [37]. Using a variety of other amine coupling agents, the same authors demonstrated the variability in the siloxane network density, according to the precursor used. Generally, in the absence of alkoxyl functionalities, in favour of methyl groups, linear materials were produced. Conversely, methyl groups imparted hydrophobic character to the final materials.

3. Reactivity and curing behaviour

Several investigations have been reported in which the influence of the inorganic phase on the reactivity of the polyimide precursor has been studied [28, 29, 38]. In all these reports it has been pointed out that the silica phase exerts a considerable influence on the behaviour of the polyamic acid both in terms of its tendency to form molecular interactions with residual solvent, and with respect to the imidization reaction itself. In particular, Musto *et al.* [28] performed a *time-resolved* FTIR analysis on a PI/silica nanocomposite and a pure polyimide (PMDA-ODA) in order to compare the rate and extent of solvent removal from the two systems. It was shown that the presence of the silica precursor within the pre-polymer solution greatly facilitates solvent removal from the film surface. This effect was ascribed to a reduction of the stability of the NMP-PI complexes and, in particular to the destabilization of the most stable complex, i.e. the one with a 1:2 PI repeating units/NMP molar ratio. It was speculated that the comparatively large amount of

OH groups present on the silica phase effectively compete with NMP in forming hydrogen-bonding interactions with the PAA units. The same spectroscopic technique was employed to investigate the kinetics of thermal imidization. In this instance the imidization degree, *i.d.*, was evaluated by monitoring the intensity of the imide band at 1376 cm^{-1} as a function of time. The *i.d.* parameter, relative to three different systems, is reported in Figure 5 as a function of the reaction time. In particular, curve A refers to a nanocomposite with 22.3 wt% of silica, curve B is for the pure polyimide precursor and curve C is relative to a PAA film from which the NMP solvent was completely removed before curing. The kinetic data for the imidization of the polyimide precursor, shown in Figure 5, curve B, are in general agreement with other published results. In particular, two distinct regimes can be distinguished; both being adequately described as first order processes. The initial regime is faster than the second by a factor of about 6.5. It also worth to note that partial imidization (*i.d.* = 0.06) takes place during the heating ramp before reaching the isothermal temperature. For this reason the conversion curve does not start from the origin. The data shown in Figure 5, curve C, relative to a PAA film from which all NMP had been eliminated prior to curing, confirm the fundamental role of residual solvent in the cure kinetics of polyimides. In fact, a drastic reduction of the imidization rate is observed in
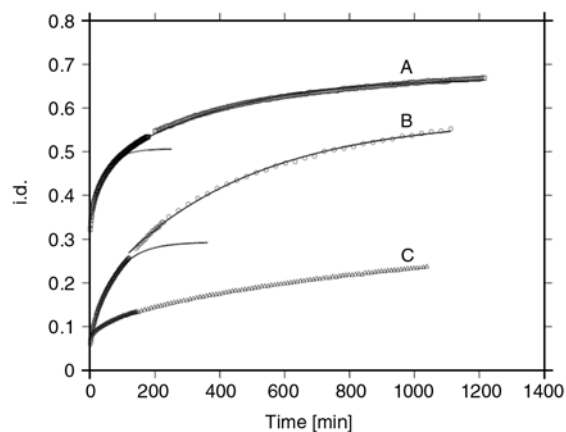

Figure 5. Imidization degree (*i.d.*) as a function of time for the isothermal reaction at 120°C. Curve A: nanocomposite with 23.3 wt% of silica. Curve B: polyimide precursor. Curve C: polyimide precursor from which the solvent had been completely eliminated prior to curing. The symbols indicate the experimental data, while the continuous lines represent the simulation of the first order kinetic model [29].

comparison to the control system (compare curves B and C). The kinetic behaviour of the nanocomposite precursor resembles that of the pure polyamic acid in the presence of solvent, in that it can be adequately described by two first-order regimes. The second regime has a rate constant considerably lower than that of the first regime. However, in the nanocomposite system the first stage is significantly faster than for the pure polyamic acid in solution and the imidization reaches a more advanced stage during the heating ramp from room temperature to 120°C (initial *i.d.* = 0.33). As a consequence of these two effects the final conversion of amic acid is higher in the nanocomposite than in the pure polyimide polyimide (0.67 against 0.58). The second stage of imidization in the two systems, however, is characterized by a comparable rate constant. The kinetic behaviour for the nanocomposite precursor seems to be conflicting with the solvent effect, since the residual amount of solvent is much lower in the nanocomposite formulation than in the in pure polyamic acid solution. Evidently, the inorganic phase exerts a catalytic activity with respect to the imidization of polyamic acid. This effect may arise from the hydroxyl groups present along the outer surface of the silica phase. These may form strong molecular interactions of the hydrogen bonding type with the amic acid moieties of PAA and, in doing so, may force the PAA chains to assume a planar conformation more favourable for cyclization.

4. Dynamic mechanical properties

Dynamic mechanical analysis (DMA) has been extensively used to study the influence of the silica phase on the molecular relaxation processes of the polyimide, which control and determine several material properties including tensile mechanical properties [39–41].

Figures 6 and 7 report the DMA results obtained by Musto *et al.* [42] on two types of PI/silica hybrids having, respectively, a particulate micron sized structure and nano-structured co-continuous morphology. The alkoxysilane solutions used for the production of these hybrids were pure TEOS for the phase separated system and a TEOS/GOTMS mixture for the interconnected hybrid. The PI precursor was a PAA formed by condensation of PMDA and ODA.
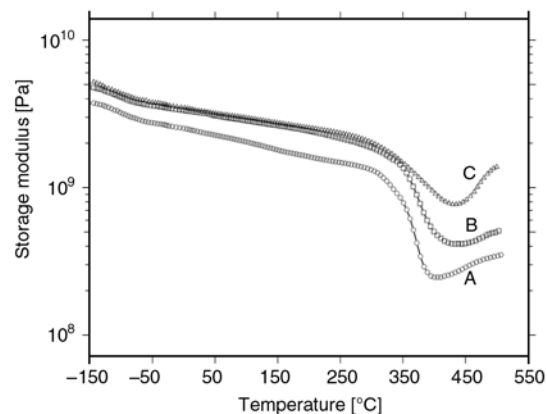
Figure 6. Storage modulus as a function of temperature: A) pure polyimide; B) microcomposite with 22.3 wt% of silica; C) nanocomposite with 22.3 wt% of silica [42].

The presence of silica increases the elastic modulus (Figure 6) both in the glassy region and at temperatures above the glass transition. The upturn in the E' curves above the glass transition was attributed to the occurrence of intermolecular crosslinking reactions.

The tanδ plots (Figure 7) reveal the occurrence of three relaxation processes with increasing tempera-
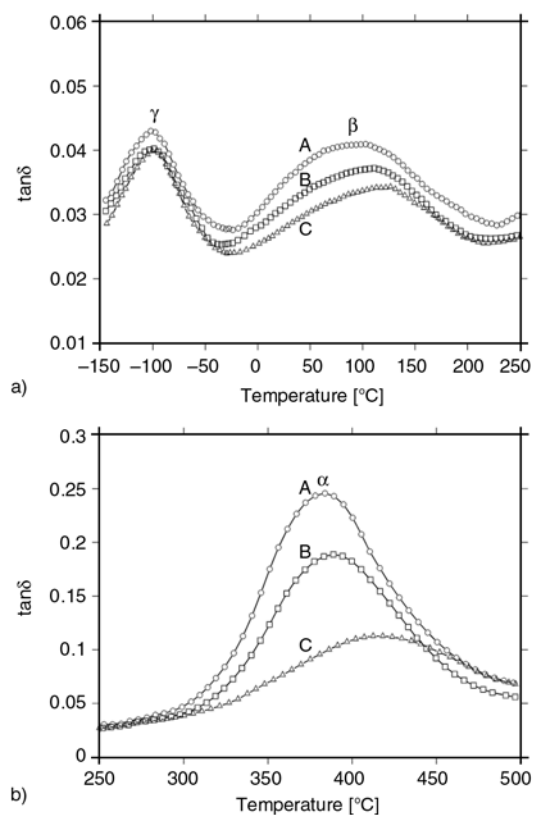
Figure 7. Tanδ spectra as a function of temperature: A) pure polyimide; B) microcomposite with 22.3 wt% of silica; C) nanocomposite with 22.3 wt% of silica [42].

ture. The low and the medium temperature relaxations are defined, respectively, as the γ and β transitions (Figure 7a). The highest temperature transition is an α-relaxation process (Figure 7b) and corresponds to the glass transition temperature (T_g). The β transition is generally associated with local bond rotations along the polyimide backbone, although its exact description is still uncertain [42]. The γ transition is observed only in the presence of absorbed moisture.

The incorporation of the silica phase causes a shift of the γ, β and α peaks toward higher temperatures. The increase in T_β and T_α was about 10°C for the micron sized composite and, respectively, of 24 and 34°C for the nanocomposite. The increase in T_γ was considerably lower. Also the height of these transitions decreases. The effect was larger for the β and α processes and was much more pronounced for the nanocomposite sample. This depression in the relaxation processes was attributed to an increased constrain of the polyimide chain segments due to occurrence of interactions between the silica phase and the polyimide matrix. These interactions are larger for the nanocomposite than for microcomposite and were attributed to the action of the GOTMS coupling agent.

On the same systems Mascia and Kioul [8] found that for phase separated hybrids the depression of the α-relaxations was approximately equal to that predicted by the law of mixtures, showing that all the silica precipitated as spherical particles. For nanocomposites, on the other hand, the reduction in the α-relaxations was considerably lower. This was indicative of the involvement of polyimide chains in the silicate network through the coupling of the two components by the GOTMS.

The effect of the silica precursor on the β and α relaxation processes was also studied by Cornelius and Marand [40]. They produced a series of hybrids by carrying out sol-gel reactions of different alkoxysilanes in the presence of fully imidized polyimides, functionalized with different degrees of triethoxysilane groups. The alkoxysilanes employed included tetramethoxysilane (TMOS), methyltrimethoxysilane (MTMOS), and phenyltrimethoxysilane (PTMOS).

The morphology of these hybrids was found to be largely dependent on the type and content of the alkoxide used. In particular, the higher functionality and reactivity of TMOS gave rise to very fine interconnected homogeneous systems, while the MTMOS and PTMOS based hybrids were phase separated with micron sized silica domains.

The DMA results revealed that the T_g and the T_β of various hybrid materials increased with increasing silica content. However, no clear trends with type or concentration of the alkoxide was observed . On the other hand, the magnitude of tanδ at T_g was found to decrease with increasing the silica content for all the hybrid systems. The larger T_g reduction was displayed for the TMOS based hybrids, followed by MTMOS and PTMOS hybrids. These results confirm that, as found for TEOS/GOTMS based hybrids, highly interconnected morphologies are much more effective in depressing α-relaxations with respect to phase separate systems.

In accordance with the DMA results, larger reductions in the coefficient of thermal expansion were found when the morphology of the dispersed silica phase changed from particulate to co-continuous [8]. This effect became even more pronounced at temperatures above the T_g of the PI.

5. Mechanical and fracture properties

Polyimide/silica hybrids generally exhibit improved mechanical properties when compared to those of pristine polyimides. These enhancements include primarily modulus, strength and toughness and the magnitude of the effect is related to the compatibility of the organic and inorganic components, as well as to the size and dispersion state of the inorganic phase.

In Figures 8 and 9 are shown the results of tensile tests carried out by Musto *et al*. [28] on PI/silica systems obtained using GOTMS as compatibilizing agent. The modulus is found to increase linearly with increasing the concentration of the inorganic phase (Figure 8). In the same figure, the data for the normalized modulus, calculated as the ratio of the modulus of the hybrid to that of the polyimide, reached a value of 2 (i.e. 100% increase) at a silica content of 28.4%. This enhancement was found to be larger than that normally achieved for conventional composites [43, 44]. The tensile strength (Figure 9) showed a gradual increase up to a concentration of silica around 15 wt%, followed by a slight reduction at higher concentrations. The elongation at break, displayed in the same figure, exhibited a monotonic decrease. The increase in the
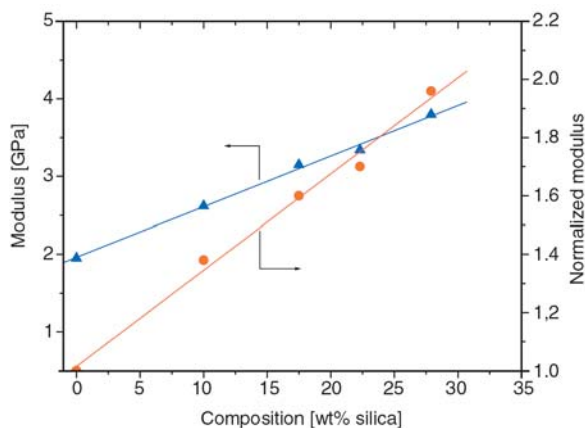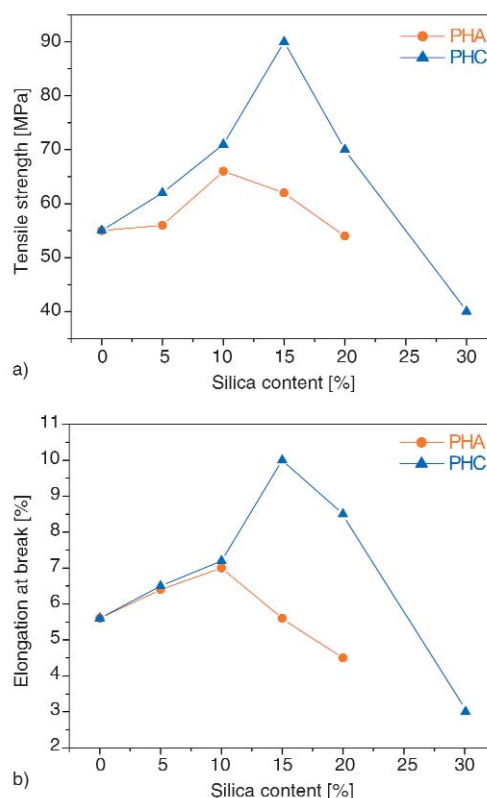
Figure 8. Elastic modulus (▲) and normalized elastic modulus (●) for nanocomposite hybrids as a function of the silica content [28].
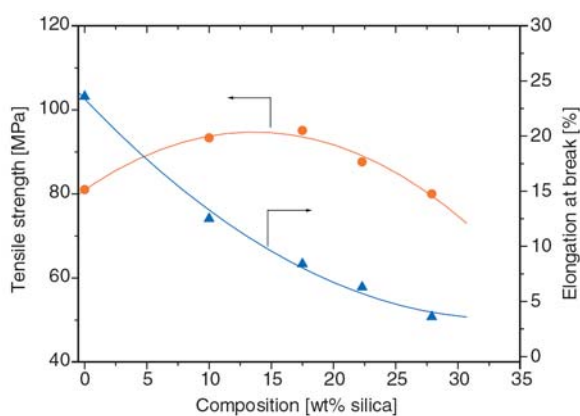
Figure 9. Tensile strength (●) and elongation at break (▲) for nanocomposite hybrids as a function of the silica content [28].


Figure 10. Mechanical properties of PI/silica hybrids with GOTMS (PHC) and without GOTMS (PHA) as a function of silica content: a) Tensile strength; b) Elongation at break. Reproduced from [45] Chen B. C., Chin T. M., Tsay S. Y., by permission of John Wiley & Sons, Ltd.

mechanical strength was attributed to the action of GOTMS, which produced both an improvement in the interfacial adhesion and the formation of finely interconnected morphologies (see Figure 3b), leading to an efficient stress transfer mechanism between the two components. This is consistent with the fact that tensile strengths are known to be reduced if there are no interactions between the organic matrix and the inorganic phase. Chen *et al.* [45] also reported hybrids with a co-continuous phase morphology obtained directly from a soluble PI, functionalized with phenyl hydroxyl groups, and GOTMS as compatibilizer. In Figure 10 are compared the mechanical properties of PI/silica systems obtained with GOTMS (PHC) and without GOTMS (PHA). In both cases the tensile strength (Figure 10a) and the elongation at break (Figure 10b) increase with increasing the silica content up to a concentration of about 15 wt%. After that a fast reduction is observed. Although for both sys-

tems the introduction of hydroxyl groups in the PI increased the miscibility with the silica phase, the superior mechanical properties exhibited by the PHC hybrids were the result of a better compatibility and interfacial strength achieved through the formation of chemical bonds involving the hydroxyl groups of PI and the epoxy groups of the GOTMS.

Changes in the type of coupling agent were found to produce hybrid materials with mechanical properties comparable to those achieved with GOTMS. In this regard several aminoalkoxylanes, including aminopropyltriethoxysilane (APTEOS) and aminophenyltrimethoxysilane (APTMOS) were employed. The presence of both amino and methoxy side groups enabled chemical bonding between the PI and silica, resulting in the formation of homogeneous hybrids with enhanced modulus and ultimate properties. This is shown in Figure 11 where the results of Zhang *et al.* [46] on hybrids containing APTEOS are reported. It can be seen that for silica
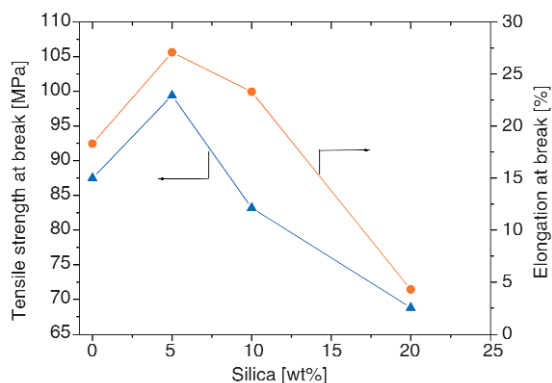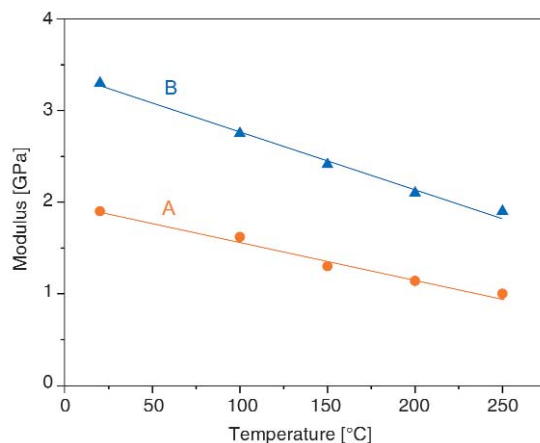
Figure 11. Tensile strength and elongation at break as a function of silica content. Reproduced from [46] Zhang J., Zhu B. K, Chu H. Y., Xu Y. Y, by permission of John Wiley & Sons Ltd.
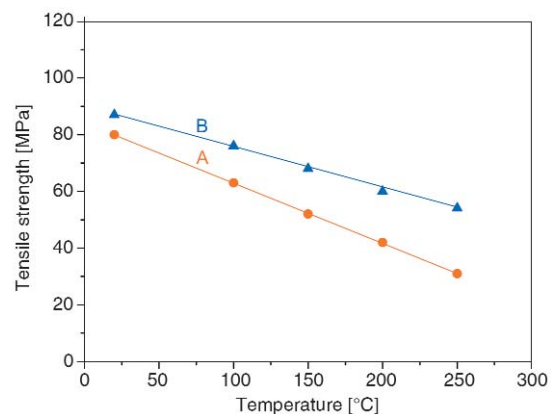

Figure 12. Elastic modulus as a function of temperature for the plain polyimide (Curve A) and for a nanocomposite with 22.3 wt % of silica (Curve B) [28].

Figure 13. Tensile strength as a function of temperature for the plain polyimide (Curve A) and for a nanocomposite with 22.3 wt % of silica (Curve B) [28].

Figure 14. Essential work of fracture, w_e, as a function of temperature: A) polyimide; B) microcomposite with 10 wt% of silica; C) microcomposite with 15 wt% of silica; D) microcomposite with 20 wt% of silica [48].

contents lower than 10 wt% improvements in the ultimate properties are observed, while for silica concentrations exceeding this value both tensile strength and elongation at break sharply decrease. Chen and Iroh [47] also used APTEOS for the production of bonded PI-silica hybrids. These materials exhibited, in comparison with the pure polyimide, higher mechanical strengths and lower elongations at break. Similarly Ahmad *et al.* [23] used APTMOS to bond the PI to the silica phase. This aromatic compound was also chosen for its high thermal stability, which is comparable to that of the pure polyimide. Relatively small amounts of APTMOS were found to improve significantly modulus and mechanical strength.

The effect of temperature on the mechanical properties of PI/silica nanocomposites was also investigated [28]. In Figure 12 the variation of modulus with temperature for a nanocomposite hybrid containing 22.3% of silica is compared with that of the pure PI. The relevant finding is that at 250°C, which is the limiting temperature for the continuous use of polyimides, the value of modulus of the hybrid material is very close to that of the neat polyimide at ambient temperature. An analogous trend was observed for the tensile strength (Figure 13). Thus, properly formulated PI hybrids with silica domains of nanoscale dimensions could make it possible to extend considerably the maximum temperature at which these systems can be reliably employed.
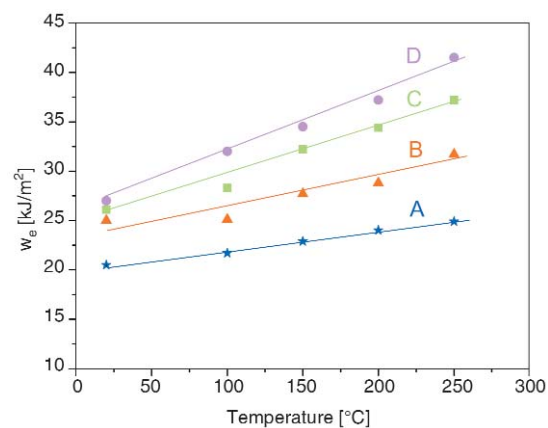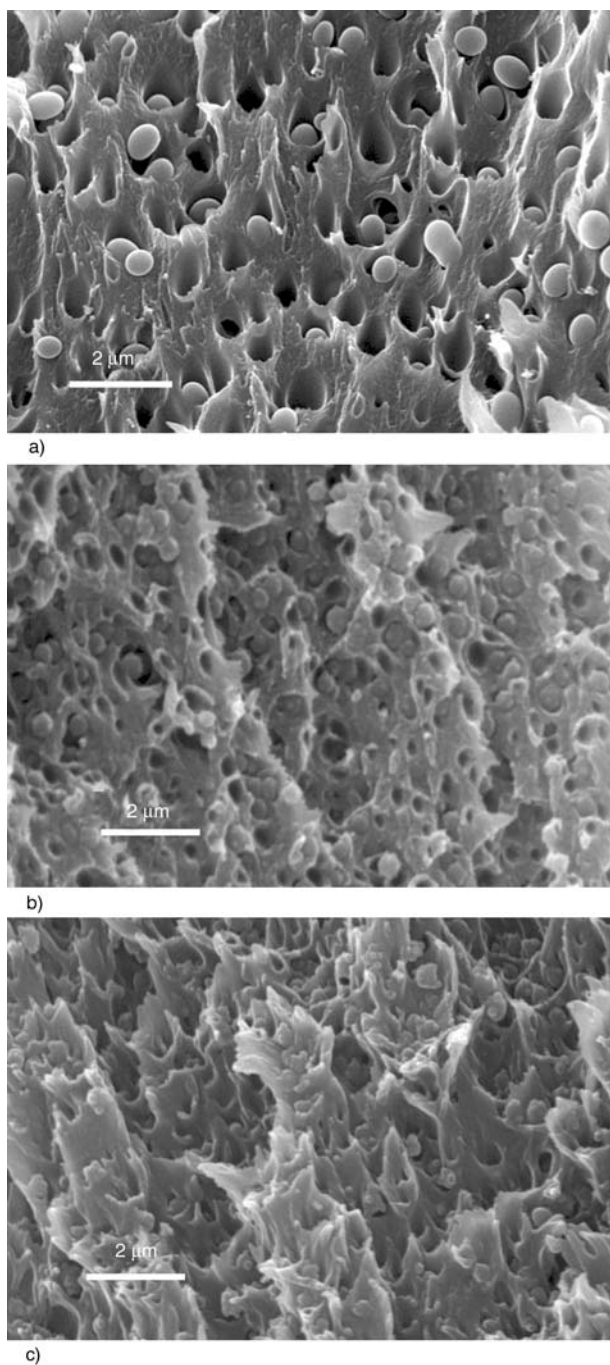
Ragosta and coworkers [32, 48] used the Essential Work of Fracture (EWF) method [49–51] to assess the fracture toughness of phase separated PI/silica hybrids from ambient temperature to 250°C. Fig-

Figure 15. SEM micrographs of the fractured surfaces of particulate composites with 15 wt% of silica, tested at ambient temperature:
a) GOTMS/TEOS 0,0; b) GOTMS/TEOS 0.03; c) GOTMS/TEOS 0.04 [32].

Table 1. The essential work of fracture, w_e, for microcomposites containing 15.0 wt% of silica and different GOTMS/TEOS molar rations

Silica content [wt%]	GOTMS/TEOS [molar ratio]	w_e [kJ/m²]	Temperature [°C]
15.0	0.00	26.5	20
15.0	0.03	28.2	20
15.0	0.04	30.4	20

ure 14 shows the fracture toughness, expressed in term of the essential work of fracture parameter, w_e, versus temperature for a series of particulate PI/silica hybrids and for the pure polyimide. The parameter, w_e, is found to increase linearly with increasing temperature and, at any given temperature, the enhancement of fracture toughness is related to the silica content. It is also found, as shown in Table 1, that for a given silica content the fracture toughness increases further when the GOTMS coupling agent is added to silica precursor.

The fractographic analysis (Figure 15) shows that the fracture process of these hybrids is dominated by interface-initiated cavitations. This mechanism is known to occur in particulate composites with spherical particles when the matrix modulus is lower than that of the particles [52, 53]. In particular, due to the poor adhesion between particles and matrix, a debonding process takes place at both equator and pole regions of the particles. The debonding of the matrix from the particles relaxes the local interfacial stresses promoting shear yielding mechanisms. Thus cavitations and matrix yielding are the deformation mechanisms responsible for the enhancement in the fracture toughness observed for micron sized PI/ silica hybrids.

The addition of GOTMS (compare Figure 15a with Figures 15b and 15c) reduces the particles diameter and improves the interfacial strength, thus favouring the conditions for promoting shear yielding processes in the PI matrix. Accordingly, higher values of w_e are found with respect to those in absence of GOTMS (see Table 1).

5. Applications

The applications areas for PI/silica hybrids have considerably expanded with the current generation of materials in microelectronic, optoelectronic, and advanced membranes [54–57]. Some specific examples will be now briefly described on these particular uses.

Ree *et al.* [58] prepared PI/silica nanocomposite hybrids for the production of microelectronic devices utilizing silica aerogels, which are known to exhibit a low dielectric constant and low thermal expansivity [59]. These hybrids showed improved dielectric and optical properties, whereas the interfacial stress and the thermal expansion coefficient were found considerably reduced owing to the sil-
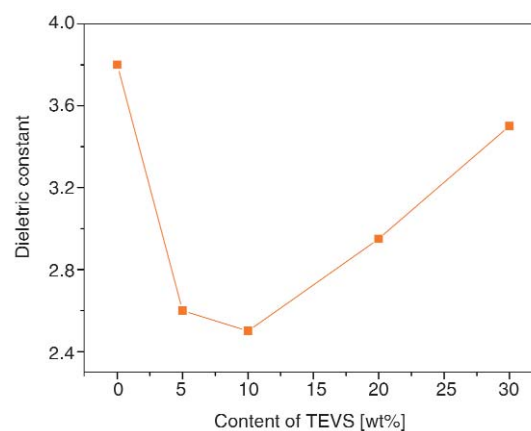
ica aerogels despite their low thermal expansivity. Kim *et al*. [60] studied the effects of TEOS content on the dielectric properties of PI hybrids using two type of soluble precursors chemically convertible to PI [poly(p-phenylene biphenyltetracarboxamic acid) (BPDA-PDA) and BPDA-PDA diethyl ester (BPDA-PDA ES)]. It was found that BPDA-PDA gave homogeneous nanocomposite films, whereas heterogeneous micron sized hybrids were generated with the BPDA-PDA ES precursor. As shown in Figure 16 the dielectric properties increased with TEOS contents, regardless of the polyimide precursor type, due to the inherent higher dielectric constant of silica in comparison to that of the PI. However, the nanocomposites films exhibited higher dielectric constants than those of microcomposites. Accordingly, the decrease in the resistivity observed in these hybrids was found to be less prominent for the nanocomposites than that for the microcomposites. Jiang *et al*. [61] developed a new method for preparing PI/silica films with low dielectric constants. The procedure consisted in two steps. Firstly, PI/silica hybrids were prepared via a sol-gel process. Secondly, the hybrid films were treated with hydrofluoric acid to remove the dispersed silica phase, leaving pores with a size and shape dictated by the initial morphology. It was found that the porous films exhibited lower dielectric constants with respect to the PI/silica hybrids, owing to the presence of air in the pores. Recently, there has been a great deal of interest in using polysilsesquioxane (PSSQ) or poly (vinylsilsesquioxane) (PVSSQ) as novel inorganic components in
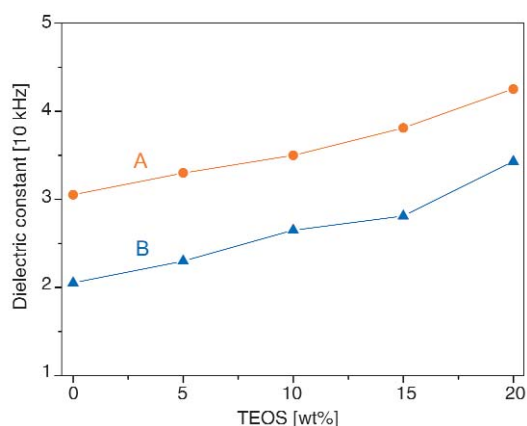
the preparation of PI hybrids for microelectronic devices, owing to their lower dielectric constants and lower moisture absorption compared to the silicon dioxide [62–64]. For instance, Wahab *et al*. [65] produced PI/PVSSQ hybrid films from BPDA-ODA polyamic acid and triethoxyvynilsilane (TEVS). These hybrids exhibited nanocomposite structures for PVSSQ content less than 20 wt%. Figure 17 shows the dielectric constants of the hybrid composites. As small amounts of PVSSQ are added the dielectric constant is remarkably reduced and then it increases with increasing the PVSSQ content. However, even at high PVSSQ contents, the electric constants of the hybrids are still lower than that of the pure polyimide. These hybrids also showed improved mechanical and thermal properties.

PI/silica hybrids were also found to be useful materials for the production of optoelectronic devices (e.g. optical waveguides). For these applications the use of unmodified, conventional photosensitive PIs is strongly limited owing to the large volume shrinkage taking place after curing, which causes a significant distortion on the patterned feature [66]. Therefore, the incorporation of a silica phase within the PI matrix may represent a good solution to overcome this problem. However, only a limited number of PI/silica materials have shown to be photopatternable [67, 68]. For instance, photosensitive PI/silica hybrids were developed by Wang *et al*. [69]. In this study the volume shrinkage of polyimides with pendant photosensitive moieties, such as 2-methylacrylic acid 2-dimethylamino-ethyl ester (MDAE), was largely reduced by pho-

Figure 16. The effect of TEOS on the dielectric constant of silica/polyimide films: A) BPDA-PDA PAA precursor; B) BPDA-PDA ES precursor. Reproduced from [60] Kim Y., Kang E., Kwon Y. S., Cho W. J., Chang M., Ree M., Chang T., Ha C. S., by permission of Elsevier.

Figure 17. Effect of TEVS contents on the dielectric constants of PI/TEVS hybrid films. Reproduced from [65] Wahab M. A., Kim I., Ha C–S., by permission of Elsevier.

tocrosslinking MDAE with a coupling agent and the silica domains. The prepared hybrids exhibited good lithographic resolution, dimensional stability, reduced refractive index and low optical loss in the NIR region. Very recently, Yu *et al.* [70] synthesized fluorinated polyimide/colloidal silica hybrids, using 4.4′-hesafluoroisopropylidenediphthalic anhydride (6FDA), oxydianiline (ODA), aminopropyltriethoxysilane (APTEOS), and colloidal silica, in place of conventional alkoxysilanes. The coupling agent (3-methacryloxypropyl trimethoxysilane, MPTMS) and the silica domains were designed so as to reduce the volume shrinkage and to enhance the thermal properties. The prepared hybrids exhibited lithographical patterns with good resolution, suggesting potential applicability in the field of optoelectronic devices.

Since PI hybrid materials combine the basic properties of organic and inorganic constituents, they can offer specific advantages for the preparation of membranes with enhanced selectivity and permeability, and improved thermal and chemical resistance [71, 72]. In particular, PI/silica membranes have been found to exhibit promising gas permeation qualities and have been tailored to accommodate specific gas separations. Joly *et al.* [73] conduced a study on transport properties of a series of gases (N_2, O_2, H_2, CO_2 and CH_4) in polyimide hybrids charged with silica particles. The composite membranes showed higher permeability coefficients when compared with the pure polyimide. In spite of the permeability enhancement an increase in the selectivity of the H_2 with respect to N_2, O_2 and CO_2 was observed. In a later paper, Joly *et al.* [74] investigated the role of silica in the modification of the membrane microstructure and the resulting effects on gas permeability. Similarly, Hu *et al.* [75] prepared nanocomposite membranes that had higher permeability coefficients and significant improvements in permeselectivity. The diffusivity and selectivity toward gases were also investigated by Cornelius and Marand [76] They prepared, via sol-gel, a series of hybrid composites based on 6FDA-6FpDA and 6FDA-6FDA-DABA polyimides and various organo-silica structures. The gas transport properties of these hybrid membranes were found to be dependent on the type of alkoxide employed and on the final morphology. In particular, systems with low degree of cross-linking between the inorganic and polymer components showed low membrane performances. In contrast, improvements in selectivity and permeability were observed in hybrids with high interactions between the components. This was attributed to the formation of an interphase consisting of constrained polymer segments partially incorporated into the silica structure.

Diffusion studies of ammonia and water vapour in polyimides and polyimide/silica nanocomposite films were conducted by Musto *et al.* [77–80]. They showed that the amount of hydrogen bonded water increased substantially in these hybrids compared to the pure PI as a result of molecular interactions occurring with the inorganic domains. Extensive reactions were found to take place between the ammonia penetrant and the polyimide substrate, which were considerably faster for the hybrids due to the confinement effect imposed by the nanostructured silica domains. This widens the possibility of utilizing PI hybrid systems for catalytic processes involving reactive penetrants.

6. Conclusions

Several examples of polyimide/silica hybrids materials have been presented herein. These showed that the sol-gel process was a versatile tool for the production of such hybrids since it allowed to adapt the structure of the silica phase and the chemical composition of the PI precursor to different applications. The phase separation was found to be the key factor in determining the morphologies that gave the best combination of properties in terms of thermal stability, dynamic and static mechanical properties, and fracture toughness. This can be achieved by promoting interactions between the organic and the inorganic components, either directly by functionalizing the polyimide backbone, or adding coupling agents that interacted with the growing silica network and the PI chains.

References

[1] Ghosh M. K., Mittal K. L.: Polyimides: Fundamental and applications. Marcel Dekker, New York (1996).

[2] Bessonov M. I., Zubkov V. A.: Polyamic acids and polyimides: Synthesis, transformation and structure. CRC Press, Boca Raton (1993).

[3] Thompson L. F., Wilson C. G,. Tagawa S.: Polymers for microelectronics: Resists and dielectrics. ACS Symposium Series, Washington (1994).

[4] Mark J. E., Lee C. Y. C., Bianconi P. A.: Hybrids organic-inorganic composites. ACS Symposium Series, Washington (1995).

[5] Kioul A., Mascia L.: Compatibility of polyimide-silicate ceramers induced by alkoxysilane coupling agents. Journal of Non-Crystalline Solids, **175**, 169–186 (1994).
DOI: 10.1016/0022-3093(94)90009-4

[6] Mascia L.: Developments in organic-inorganic polymeric hybrids: Ceramers. Trends in Polymer Science, **3**, 61–66 (1995).

[7] Morikawa A., Iyoku Y., Kakimoto M., Imal Y.: Preparation of a new class of polyimide-silica hybrid films by sol-gel process. Polymer Journal, **24**, 107–113 (1992).

[8] Mascia L., Kioul A.: Influence of siloxane composition and morphology on properties of polyimide-silica hybrids. Polymer, **36**, 3649–3659 (1995).
DOI: 10.1016/0032-3861(95)93766-F

[9] Didier B., Mercier R., Albrola N. D., Bas C.: Preparation of polyimide/silica hybrid material by sol-gel process under basic catalysis: Comparison with acid conditions. Journal of Polymer Science Part B: Polymer Physics, **46**, 1891–1902 (2008).
DOI: 10.1002/polb.21522

[10] Mark J. E., Sun C-C.: Polymer-modified silica glasses. I. Control of hardness. Polymer Bulletin, **18**, 259–264 (1987).
DOI: 10.1007/BF00255119

[11] Morikawa A., Lyoku Y., Kakimoto M-A., Imai Y.: Preparation of new polyimide-silica hybrid materials via the sol-gel process. Journal of Materials Chemistry, **2**, 679–689 (1992).
DOI: 10.1039/JM9920200679

[12] Mark J. E.: Ceramic-reinforced polymers and polymer-modified ceramics. Polymer Engineering and Science, **36**, 2905–2920 (1996).
DOI: 10.1002/pen.10692

[13] Mascia L., Zhang Z., Shaw S. J.: Carbon fibre composites based on polyimide/silica creamers: Aspects for structure-properties relationship. Composites Part A: Applied Science and Manufacturing, **27**, 1211–1221 (1996).
DOI: 10.1016/1359-835X(96)00082-6

[14] Wei Y., Yeh J-M., Jin D., Jia X., Wang J., Jang G-W., Chen C., Gumbs R. W.: Composites of electronically conductive polyaniline with polyacrylate-silica hybrid sol-gel materials. Chemistry of Materials, **7**, 969–974 (1995).
DOI: 10.1021/cm00053a024

[15] Guizard C. G., Julbe A. C., Ayral A. J.: Design of nanosized structures in sol-gel derived porous solids. Applications in catalyst and inorganic membrane preparation. Journal of Materials Chemistry, **9**, 55–65 (1999).
DOI: 10.1039/a805867i

[16] Wang H., Zhong W., Xu P., Du Q.: Polyimide/silica/titania nanohybrids via a novel non-hydrolytic sol-gel route. Composites Part A: Applied Science and Manufacturing, **36**, 909–914 (2005).
DOI: 10.1016/j.compositesa.2004.12.008

[17] Nandi M., Conklin J. A., Salvati L. Jr., Sen A.: Molecular level ceramic/polymer composite. 2. Synthesis of polymer-trapped silica and titania nanoclusters. Chemistry of Materials, **3**, 201–206 (1991).
DOI: 10.1021/cm00013a040

[18] Huang H-H., Order B., Wilkes G. L.: Ceramers: Hybrid materials incorporating polymeric/oligomeric species with inorganic glasses by a sol-gel process. Polymer Bulletin, **14**, 557–564 (1985).
DOI: 10.1007/BF00271615

[19] Wung C. J., Pang Y., Prasad P. N., Karaz F. E.: Poly(*p*-phenylene vinylene)-silica composite: A novel sol-gel processed non-linear optical material for optical waveguides. Polymer, **32**, 605–608 (1991).
DOI: 10.1016/0032-3861(91)90471-T

[20] Wung C. J., Lee K-S., Prasad P. N., Kim J-C., Jin J-I., Shim H-K.: Study of third-order optical non-linearity and electrical conductivity of sol-gel processed silica: Poly(2-bromo-5-methoxy-*p*-phenylene vinylene) composite. Polymer, **33**, 4145–4151 (1992).
DOI: 10.1016/0032-3861(92)90619-8

[21] Mascia L., Kioul A.: Polyimide-silica hybrid materials by sol-gel processing. Journal of Materials Science Letters, **13**, 641–643 (1994).
DOI: 10.1007/BF00271220

[22] Nandi M., Conklin J. A. Salviati L. Jr., Sen A.: Molecular level ceramic/polymer composites. 1. Synthesis of polymer-trapped oxide nanoclusters of chromium and iron. Chemistry of Materials, **2**, 772–776 (1990).
DOI: 10.1021/cm00012a033

[23] Wang S., Ahmad Z., Mark J. E.: Polyimide-silica hybrid materials modified by incorporation of an organically substituted alkoxysilane. Chemistry of Materials, **6**, 943–946 (1994).
DOI: 10.1021/cm00043a013

[24] Schmidt H.: Inorganic-organic composites by sol-gel techniques. Journal of Sol-Gel Science and Technology, **1**, 217–231 (1994).
DOI: 10.1007/BF00486165

[25] Schmidt H., Wolter H.: Organically modified ceramics and their applications. Journal of Non-Crystalline Solids, **121**, 428–435 (1990).
DOI: 10.1016/0022-3093(90)90171-H

[26] Morikawa A., Jamaguchi H., Kakimoto M., Imai Y.: Formation of interconnected globular structure of silica phase in polyimide-silica hybrid films prepared by the sol-gel process. Chemistry of Materials, **6**, 913–917 (1994).
DOI: 10.1021/cm00043a009

[27] Morikawa A., Yamaguchi H., Kakimoto Y., Imai Y.: Preparation of polyimide-silica hybrid films using sol-gel process. Journal of Photopolymer Science and Technology, **5**, 393–396 (1992).
DOI: 10.2494/photopolymer.5.393

[28] Musto P., Ragosta G., Scarinzi G., Mascia L.: Polyimide-silica nanocomposites: Spectroscopic, morphological and mechanical investigations. Polymer, **45**, 1697–1706 (2004).
DOI: 10.1016/j.polymer.2003.12.044

[29] Abbate M., Musto P., Ragosta G., Scarinzi G., Mascia L.: Polyimide-silica hybrids: Spectroscopy, morphology and mechanical properties. Macromolecular Symposia, **218**, 211–220 (2004).
DOI: 10.1002/masy.200451422

[30] Inoue T.: Reaction-induced phase decomposition in polymer blends. Progress in Polymer Science, **20**, 119–152 (1995).
DOI: 10.1016/0079-6700(94)00032-W

[31] Yamanaka K., Takagi Y., Inoue T.: Reaction-induced phase separation in rubber-modified epoxy resins. Polymer, **30**, 1839–1844 (1989).
DOI: 10.1016/0032-3861(89)90355-8

[32] Ragosta G., Musto P., Abbate M., Russo P., Scarinzi G.: Effect of morphology on the relaxation processes and mechanical properties in polyimide/silica hybrids. Macromolecular Symposia, **247**, 88–98 (2007).
DOI: 10.1002/masy.200750111

[33] Menoyo C. J. D., Mascia L., Shaw S. J.: Compatibilization mechanism of polyimide/silica hybrids with organofuctional trialkoxysilanes. in 'Nanostructured powders and their industrial applications' (eds.: Beaucage G., Mark J. E., Burns G. T., Hua D. W.) Vol 520, 239–267, Materials Research Society, Warrendale (1998).

[34] Wang S., Ahmad Z., Mark J. E.: Polyimide-silica hybrid materials having interfacial bonding through use of a sol-gel technique. Journal of Macromolecular Science, Macromolecular Reports, **31**, 411–419 (1994).

[35] Mark J. E., Wang S., Ahmad Z.: Inorganic-organic composites, including some examples involving polyamides and polyimides. Macromolecular Symposia, **98**, 731–741 (1995).

[36] Schrotter J. C., Smaihi M., Guizard C.: Polyimide-siloxane hybrid materials: Influence of coupling agents addition on microstructure and properties. Journal of Applied Polymer Science, **61**, 2137–2149 (1996).
DOI: 10.1002/(SICI)1097-4628(19960919)61:12 <2137::AID-APP12>3.0.CO;2-4

[37] Goizet S., Schrotter J. C., Smaihi M., Deratani A.: Sol-gel polyimide-silica composite films: Correlation between the microstructure and the synthesis parameters. New Journal of Chemistry, **21**, 461–468 (1997).

[38] Tyan H-L., Liu Y-C., Wei K-H.: Enhancement of imidization of poly(amic acid) through forming poly(amic acid)/organoclay nanocomposites. Polymer, **40**, 4877–4886 (1999).
DOI: 10.1016/S0032-3861(98)00716-2

[39] Wang L., Tian Y., Ding H., Li J.: Microstructure and properties of organosoluble polyimide/silica hybrid films. European Polymer Journal, **42**, 2921–2930 (2006).
DOI: 10.1016/j.eurpolymj.2006.08.004

[40] Cornelius C., Marand J. E.: Hybrid inorganic-organic materials based on a 6FDA-6FpDA-DABA polyimide and silica: Physical characterization studies. Polymer, **43**, 2385–2400 (2002).
DOI: 10.1016/S0032-3861(01)00803-5

[41] Matos M. C., Ilharco L. M., Almeida R. M.: The evolution of TEOS to silica gel and glass by vibrational spectroscopy. Journal of Non-Crystalline Solids, **147–148**, 232–237 (1992).
DOI: 10.1016/S0022-3093(05)80622-2

[42] Musto P., Abbate M., Lavorgna M., Ragosta G., Scarinzi G.: Microstructural features, diffusion and molecular relaxations in polyimide/silica hybrids. Polymer, **47**, 6172–6186 (2006).
DOI: 10.1016/j.polymer.2006.05.074

[43] Iyoku Y., Kakimoto M., Imai Y.: The preparation of poly(methylsilsesquioxane) network-polyimide hybrid materials by the sol-gel process and their properties. High Performance Polymers, **6**, 43–52 (1994).
DOI: 10.1088/0954-0083/6/1/005

[44] Magaraphan R., Lilayuthalert W., Sirivat A., Schwank J. W.: Preparation, structure, properties and thermal behaviour of rigid-rod polyimide/montmorillonite nanocmposites. Composites Science and Technology, **61**, 1253–1264 (2001).
DOI: 10.1016/S0266-3538(01)00026-4

[45] Chen B-K., Chin T-M., Tsay S-Y.: Synthesis and characterization of polyimide/silica hybrid nanocomposites. Journal of Applied Polymer Science, **94**, 382–393 (2004).
DOI: 10.1002/app.20947

[46] Zhang J., Zhu B-K., Chu H-Y., Xu Y-Y.: Silica/polyimide hybrids and their dielectric properties. I. Preparation with an improved sol-gel process with poly(amic acid) as the precursor. Journal of Applied Polymer Science, **97**, 20–24 (2005).
DOI: 10.1002/app.21721

[47] Chen Y., Iroh Y. O.: Synthesis and characterization of polyimide/silica hybrid composites. Chemistry of Materials, **11**, 1218–1222 (1999).
DOI: 10.1021/cm980428l

[48] Musto P., Ragosta G., Scarinzi G., Mascia L.: Toughness enhancement of polyimide by *in situ* generation of silica particles. Polymer, **45**, 4265–4274 (2004).
DOI: 10.1016/j.polymer.2004.03.099

[49] Xenopoulos C., Mascia L., Shaw S. J.: Variables analysis in the gelation of alkoxysilane solutions for the production of polyimide-silica hybrids. Material Science and Engineering: C, **6**, 99–114 (1998).
DOI: 10.1016/S0928-4931(98)00040-X

[50] Ragosta G., Musto P., Abbate M., Russo P., Scarinzi G.: Fracture behaviour and deformation mechanisms of polyimide/silica hybrids. Macromolecular Symposia, **228**, 287–298 (2005).
DOI: 10.1002/masy.200551026

[51] Karger-Kocsis J., Czigany T., Moskala J.: Thickness dependence of work of fracture parameters of amorphous copolyester. Polymer, **38**, 4587–4593 (1997).
DOI: 10.1016/S0032-3861(96)01061-0

[52] Wu S.: A generalized criterion for rubber toughening: The critical matrix ligament thickness. Journal of Applied Polymer Science, **35**, 549–561 (1988).
DOI: 10.1002/app.1988.070350220

[53] Bagheri R., Pearson R. A.: Role of particle cavitation in rubber-toughened epoxies: II. Inter-particle distance. Polymer, **41**, 269–276 (2000).
DOI: 10.1016/S0032-3861(99)00126-3

[54] Premachandra J., Kumudine C., Mark J. E., Dang T. D., Chen J. P., Arnold F. E.: Polymer-silica hybrid materials prepared from some functionalized polybenzoxazoles and polybenzobisthiazoles. Journal of Sol-Gel Science and Technology, **7**, 163–175 (1996).
DOI: 10.1007/BF00401035

[55] Kumudinie C., Premachandra J. K., Mark J. E., Dang T. D., Arnold. F. E.: Preparation and properties of some hybrid aerogels from a sulfopolybenzobis thiazole-silica. Journal of Macromolecular Science Part A: Pure Applied Science, **36**, 73–83 (1999).
DOI: 10.1081/MA-100101517

[56] Suzuki T., Yamada Y.: Physical and gas transport properties of novel hyperbranched polyimide-silica hybrid membranes. Polymer Bulletin, **53**, 139–146 (2005).
DOI: 10.1007/s00289-004-0322-9

[57] Cornelius C., Hibshman C., Marand E.: Hybrid organic-inorganic membranes. Separation and Purification Technology, **25**, 181–193 (2001).
DOI: 10.1016/S1383-5866(01)00102-2

[58] Ree M., Goh W. H., Kim Y.: Thin films of organic polymer composites with inorganic aerogels as dielectric materials: Polymer chain orientation and properties. Polymer Bulletin, **35**, 215–222 (1995).
DOI: 10.1007/BF00312917

[59] Mukherjee S. P., Suryanarayana D., Strope D. H.: Sol-gel processing in electronic packaging materials. Journal of Non-Crystalline Solids, **147–148**, 783–791 (1992).
DOI: 10.1016/S0022-3093(05)80717-3

[60] Kim Y., Kang E., Kwon Y. S., Cho W. J., Cho C., Chang M., Ree M., Chang T., Ha C. S.: Electrical properties of silica-polyimide composite dielectric thin films prepared via sol-gel reaction and thermal imidization. Synthetic Metals, **85**, 1399–1400 (1997).
DOI: 10.1016/S0379-6779(97)80291-3

[61] Jiang L., Liu J., Wu D., Li H., Jin R.: A methodology for the preparation of nanoporous polyimide films with low doelectric constants. Thin Solid Films, **510**, 241–246 (2006).
DOI: 10.1016/j.tsf.2005.12.216

[62] Huang J-C., He C-B., Xiao Y., Mya K. Y., Dai Y., Siow Y. P.: Polyimide/POSS nanocomposites: Interfacial interaction, thermal properties and mechanical properties. Polymer, **44**, 4491–4499 (2003).
DOI: 10.1016/S0032-3861(03)00434-8

[63] Chen Y., Kang E. T.: New approach to nanocomposites of polyimide containing polyhedral oligomerric silsesquioxane for dialectric applications. Materials Letters, **58**, 3716–3719 (2004).
DOI: 10.1016/j.matlet.2004.08.001

[64] Nguyen C. V., Carter K. R., Hawker C. I., Hedrick J. L., Jaffer R. L., Miller R. D., Remunar J. F., Rhee H. W., Rice P. M., Toney M. F., Trollsas M., Yoon D. Y.: Low-dielectric, nanoporous organosilcate film prepared via inorganic/organic polymer hybrid templates. Chemistry of Materials, **11**, 3080–3085 (1999).
DOI: 10.1021/cm990114d

[65] Wahab M. A., Kim I., Ha C-S.: Microstructure and properties of polyimide/poly(vinylsilsesquioxane hybrid composite films. Polymer, **44**, 4705–4713 (2003).
DOI: 10.1016/S0032-3861(03)00429-4

[66] Qiu F., Xu H., Cao Y., Jiang Y., Zhou Y., Liu J., Zhang X.: Nonlinear optical materials: Synthesis, characterization, thermal stability and electro-optical properties. Materials Characterization, **58**, 275–283 (2007).
DOI: 10.1016/j.matchar.2006.05.003

[67] Zhu Z-K. U., Yin J., Cao F., Shang X. Y., Lu Q. H.: Photosensitive polyimide /silica hybrids. Advanced Materials, **12**, 1055–1057 (2000).
DOI: 10.1002/1521-4095(200007)12:14<1055::AID-ADMA1055>3.0.CO;2-#

[68] Liu L., Lu Q., Yin J., Qian X., Wang W., Zhu Z., Zongguang W.: Photosensitive polyimide (PSPI) materials containing inorganic-nano particles (I)PSPI/TiO$_2$ hybrid materials by sol-gel process. Materials Chemistry and Physics, **74**, 210–213 (2002).
DOI: 10.1016/S0254-0584(01)00456-4

[69] Wang W-Y., Yen C-T., Chen W-C.: Photosensitive polyimide/silica hybrid optical materials: Synthesis, properties and patterning. Polymer, **46**, 6959–6967 (2005).
DOI: 10.1016/j.polymer.2005.06.026

[70] Yu Y-Y., Chien W-C., Lai C-L.: Synthesis and optical properties of photosensitive polyimide/silica hybrid thin films. Materials Chemistry and Physics, **113**, 567–573 (2009).
DOI: 10.1016/j.matchemphys.2008.08.012

[71] Zhong S-H., Li C-F., Xiao X-F.: Preparation and characterization of polyimide-silica hybrid membranes on kieselguhr-mullite supports. Journal of Membrane Science, **199**, 53–58 (2002).
DOI: 10.1016/S0376-7388(01)00676-7

[72] Hu Q., Marand E., Dhingra S., Fritsch D., Wen J., Wilkes G.: Poly(amide-imide)/TiO$_2$ nano-composite gas separation membranes: Fabrication and characterization. Journal of Membrane Science, **135**, 65–79 (1997).
DOI: 10.1016/S0376-7388(97)00120-8

[73] Joly C., Goizet S., Schrotter J. C., Sanchez J., Escoubes M.: Sol-gel polyimide-silica composite membrane: Gas transport properties. Journal of Membrane Science, **130**, 63–74 (1997).
DOI: 10.1016/S0376-7388(97)00008-2

[74] Joly C., Smaihi M., Porcar L., Noble R. D.: Polyimide-silica composite materials: How does silica influence their microstructure and gas permeation properties? Chemistry of Materials, **11**, 2331–2338, (1999).
DOI: 10.1021/cm9805018

[75] Hu Q., Marand E., Dhingra S., Fritsch D., Wen D., Wilkes G. L.: Ply(amide-imide)/TiO$_2$ nano-composite gas separation membranes: Fabrication and characterization. Journal of Membrane Science, **135**, 65–79 (1997).
DOI: 10.1016/S0376-7388(97)00120-8

[76] Cornelius C. J., Marand E.: Hybridsilica-polyimide composite membranes: Gas transport properties. Journal of Membrane Science, **202**, 97–118 (2002).
DOI: 10.1016/S0376-7388(01)00734-7

[77] Musto P., Mascia L., Mensitieri G., Ragosta G.: Diffusion of water and ammonia through polyimide-silica bicontinuous nanocomposites: Interactions and reactions. Polymer, **46**, 4492–4503 (2005).
DOI: 10.1016/j.polymer.2005.02.032

[78] Musto P., Ragosta G., Scarinzi G., Mensitieri G.: Spectroscopic studies of the diffusion of water and ammonia in polyimide and polyimide-silica hybrids. in 'New polymeric materials' (eds.: Korugic-Karasz L. S.,. MacKnight W. J., Martuscelli E.) ACS Simposium Series, Washington, Vol 916, 296–308 (2005).

[79] Musto P., Ragosta G., Scarinzi G., Mascia L.: Structure-properties correlation in polyimide/silica hybrids. High Performance Polymers, **18**, 799–816 (2006).
DOI: 10.1177/0954008306068257

[80] Musto P., Ragosta G., Mensitieri G., Lavorgna M.: On the molecular mechanism of H$_2$O diffusion into polyimides: A vibrational spectroscopy investigation. Macromolecules, **40**, 9614–9627 (2007).
DOI: 10.1021/ma071385+

Solvent free microwave assisted preparation of new telechelic polymers based on poly(ethylene glycol)

N. Arsalani[1*]*, P. Zare*[1]*, H. Namazi*[2]

[1]Polymer Research Laboratory, Faculty of Chemistry, University of Tabriz, Tabriz, P.O. Box: 51664, Iran
[2]Laboratory of Dendrimers and Biopolymers, Faculty of Chemistry, University of Tabriz, Tabriz, Iran

Abstract. Poly(ethylene glycol) bis (methylimidazolium chloride) (PEGBMIM) with average molecular weights of 600 and 1000 g/mol and poly(ethylene glycol) bis (2-oxazoline) (PEGBOX) with average molecular weight of 600 g/mol have been prepared using microwave irradiation under solvent-free condition. The method described herein is a very good, safe, clean, economical and environmentally friendly alternative to the classical procedures. The resulted products have been characterized by common spectroscopic methods, such as FT-IR (Fourier transform infrared spectroscopy), ^{1}H NMR (Nuclear magnetic resonance of proton) and elemental analysis. Also, the effects of power levels and irradiation time on the yield of reactions and solubility of products have been studied.

Keywords: polymer synthesis, molecular engineering, green chemistry, microwave, ionic liquid

1. Introduction

Telechelic compounds have found considerable interest as versatile intermediates in many fields. Among these poly(ethylene gycol)-based telechelic compounds due to their salient properties are dominant for many applications in peptide synthesis, modification of enzymes and pharmaceutical industry and so on. Most of these applications require certain end-groups. Therefore, telechelic modification is an important prerequisite for the practical use of such basis telechelics as poly(ethylene glycol) [1–7].

The development of cleaner technologies is a major emphasis in green chemistry. Among the several aspects of green chemistry, using efficient and less hazardous energy sources such as microwave energy is recommended. Polymer synthesis assisted by microwave (MW) has seen spectacular growth over the last few years, specially when this new technique has been coupled with solvent-free procedures, resulting in clean, easy-to-perform, cheap, safe and environmentally friendly conditions which are widely used as synthetic tools under 'Green Chemistry' conditions [8–13]. Therefore, we decided to prepare poly(ethylene glycol) containing imidazolium, which is an ionic liquid, and oxazoline end groups using such a green condition.

Ionic liquids are emerging as a set of new green solvents, mainly as a replacement for conventional volatile organic solvents. Ionic liquids containing 1,3-disubstituted imidazolium cations have shown great promise as an attractive alternative to conventional solvents. The important properties of these ionic liquids are low volatility, negligible vapor pressure, ease of handling, accelerated reaction rates and potential for recycling [13–19]. The preparation of the 1,3-dialkylimidazolium halides via conventional heating method in refluxing the

solvents requires long time to afford reasonable yields and also need to use a large excess of alkyl halides/organic solvents as the reaction medium in contrast with a few minutes of reaction time using microwave [13, 14, 19]. Although for many years oxazoline and its derivatives played an important role in organic chemistry. They were used, for example as chiral catalysts or optically active reagents. Among all of the possible isomers 1,3-oxazoline (2-oxazoline) was the most frequently used [20].

The last few years have brought a growing interest in oxazoline compounds among polymer chemists. Polymer chemistry profits from very high reactivity of oxazoline groups in many ways [21–24]. The examples of using oxazoline functionality for grafting [21], ring opening polymerization [25] or introducing double bonds into polymer [26] are described. Bis-oxazoline compounds were applied as linear chain extenders for polyesters [27, 28] and polyamides [28]. Oxazoline macromonomers [29–31] were used to synthesize hyperbranched polymers of various structures [32]. Oxazoline-grafted polymers were used as a nonionic hydrogel for metal complexation [33].

Polymers with oxazoline ring functionality could be obtained by several methods. Reaction between polymer functional groups (acidic, amine) with oxazoline derivatives or bis-oxazoline compounds [26] is one of those. In the present work we have prepared the functional polymer using poly(ethylene glycol) 600 diacid (PEGDA) and α,α,α-tris(hydroxymethyl)methylamine. The direct condensation of carboxylic acids with β-hydroxylamines requires high temperatures and strongly acidic conditions [34] and therefore is not a synthetically valuable method to access these heterocycles. Here we report the preparation oxazoline ring at the end of a poly(ethylene glycol) under solvent-free condition using microwave irradiation.

Although new hydrophilic ionic liquids, based on poly(ethylene glycol), which are potentially important due to their applications in molecular engineering, secondary batteries, sensors and electrochromic displays have been prepared using the same method.

2. Experimental
2.1. Materials
1-Methylimidazolium, α,α,α-tris(hydroxymethyl) methylamine, thionyl chloride, and poly(ethylene glycol) with average molecular weights of 600 and 1000 (Merck) and poly(ethylene glycol) diacid with average molecular weights of 600 was purchased from Fluka.

2.2. Instruments
The ^{1}H NMR spectra of the products recorded on a FT.NMR-Bruker (400 MHz) spectrometer. The FT-IR spectra obtained on a Bruker FT-IR, Tensor 270 spectrometer. Elemental analysis performed using an Elementar, Vario EL III. Reactions were performed in a domestic microwave oven Butan.

2.3. General Procedure
2.3.1. PEGBMIM (a, b)
Dichloro poly(ethylene glycol) (PEGCl) with different average molecular weights (5 mmol) which were prepared from related poly(ethylene glycol) and thionylchloride [6] and 1-methylimidazole (11 mmol) were placed in a an open glass container. The mixture was irradiated and stirred intermittently in an unmodified household microwave oven under reaction conditions which are outlined in Table 1 (During the reaction the temperature of the mixture reached 115°C). After it was allowed to cool to room temperature, diethylether (5 ml) was added into the mixture to remove excessive starting materials. The residue was washed with diethylether several times and it was vacuum-dried in a desiccator.

Poly(ethylene glycol) bis (methylimidazolium chloride) 1000 g/mol (a)

IR (KBr, cm^{-1}): ν = 3107–3150 (aromatic C–H stretching), 1633 (aromatic C=N stretching), 1469, 1350 (CH$_2$ bending), 1136 (C–O stretching), 625, 655 (aromatic C–H oop). ^{1}H NMR (400 MHz, CDCl$_3$, ppm): δ_H = 3.55 (m, O–CH$_2$–CH$_2$–O), 3.77 (2H, t, O–**CH$_2$**–CH$_2$–N), 3.94 (3H, s, N–CH$_3$), 4.48 (2H, t, N–**CH$_2$**–CH$_2$–O), 7.44, 7.64 (2H, C(4,5)–H), 9.87 (1H, C(2)–H).

Elemental analysis: Calculated for C$_{52}$H$_{100}$Cl$_2$N$_4$O$_{21}$ (1217 g/mol): 51.20 (C%), 8.61 (H%), 4.60 (N%).

Table 1. The yield of the obtained products under different reaction conditions

Product name	Reaction condition: MW/time [W/min]	Yield [%]
a	(300/2)+(300/5)[1]	20
a	(300/2)+(300/5)+(300/5)	36
a	(300/2)+(300/5)+(300/5)+(300/5)	57
a	(300/2)+(300/5)+(300/5)+(300/5)+(300/5)	70
a	**(300/2)+(300/5)+(300/5)+(300/5)+(300/5)+(300/5)**	**83**
b	(300/5)+(300/5)	28
b	(300/5)+(300/5)+(300/5)	34
b	(300/5)+(300/5)+(300/5))+(300/5)	58
b	(300/5)+(300/5)+(300/5)+(300/5)+(300/5)	67
b	**(300/5)+(300/5)+(300/5)+(300/5)+(300/5)+(300/5)**	**76**
c	(600/2)+(600/5)	30
c	(600/2)+(600/5)+(600/5)	45
c	(600/2)+(600/5)+(600/5)+(600/5)	64
c	(600/2)+(600/5)+(600/5)+(600/5)+(600/5)	67
c	**(600/2)+(600/5)+(600/5)+(600/5)+(600/5)+(600/5)**	**79**

[1]Irradiation at 300 W for 2 min, stirring for 1 min out of oven, again irradiation at 300 W for 5 min ...

Found: 52.21 (C%), 8.74 (H%), 4.09 (N%). Conversion: 87.7%.

Poly(ethylene glycol) bis (methylimidazolium chloride) 600 g/mol (b): IR (KBr, cm^{-1}): ν = 3073–3145 (aromatic C–H stretching), 1568 (aromatic C=N stretching), 1456, 1352 (CH$_2$ bending), 1107 (C–O stretching), 627, 655 (aromatic C–H oop). ^{1}H NMR (400 MHz, CDCl$_3$, ppm): δ$_H$ = 3.59 (m, O–CH$_2$–CH$_2$–O), 3.83 (2H, t, O–C**H**$_2$–CH$_2$–N), 4.01 (3H, s, N–CH$_3$), 4.54 (2H, t, N–C**H**$_2$–CH$_2$–O), 7.60, 7.74 (2H, C(4,5)–H), 9.99 (1H, C(2)–H).
Elemental analysis: Calculated for C$_{34}$H$_{64}$Cl$_2$N$_4$O$_{12}$ (791 g/mol): 51.58 (C%), 8.09 (H%), 7.07 (N%). Found: 49.67 (C%), 7.81 (H%), 6.51 (N%). Conversion: 95%.

2.3.2. PEGBOX (c)

Poly(ethylene glycol) 600 diacid (1 mmol) and α,α,α-tris(hydroxymethyl)methylamine (2.2 mmol) were placed in an open glass container in such a way as to occupy only 10% of the overall volume. The mixture was irradiated intermittently in an unmodified domestic (multimode) microwave oven at the power levels indicated in Table 1 (During the reaction the temperature of the mixture reached 138°C).When the irradiation terminated and all of the starting materials disappeared, the mixture was allowed to cool to room temperature. Then, dichloromethane (5 ml) was added at room temperature and the mixture was stirred for some minutes to precipitate unreacted α,α,α-tris(hydroxymethyl) methylamine. The resulted mixture was filtered and the obtained clear solution was added into diethyl ether to precipitate the expected functional polymer.

Poly(ethylene glycol) bis (2-oxazoline) 600 g/mol (c)

IR (KBr, cm^{-1}): ν = 3362 (O–H stretching), 2880 (aliphatic C–H stretching), 1658 (C=N stretching), 1462, 1352 (CH$_2$ bending), 1107 (C–O stretching). ^{1}H NMR (400 MHz, DMSO-d$_6$, ppm): δ$_H$ = 3.62 (m, OCH$_2$O–(CH$_2$CH$_2$O)$_{n-2}$–CH$_2$O), 3.96 (4H, s, C(3)–C**H**$_2$OH), 4.20 (2H, C(4)–H), 4.59 (2H, b, C(3)–CH$_2$O**H**).
Elemental analysis: Calculated for C$_{30}$H$_{56}$N$_2$O$_{16}$ (700 g/mol): 51.40 (C%), 8.00 (H%), 4.00 (N%). Found: 49.25 (C%), 7.88 (H%), 3.80 (N%). Conversion: 99%.

3. Results and discussion

According to Figure 1 derivatives of poly(ethylene glycol) with different average molecular weights have been reacted with 1-methylimidazole and α,α,α-tris(hydroxymethyl)methylamine as reactants, separately. The reactions have been performed using microwave irradiation under solvent-free condition. So poly(ethylene glycol) bis(3-methylimidazolium chloride) and poly(ethylene glycol) containing oxazoline end groups have been prepared. These reactions have been performed in a good yield, quickly and without using chemical solvents.
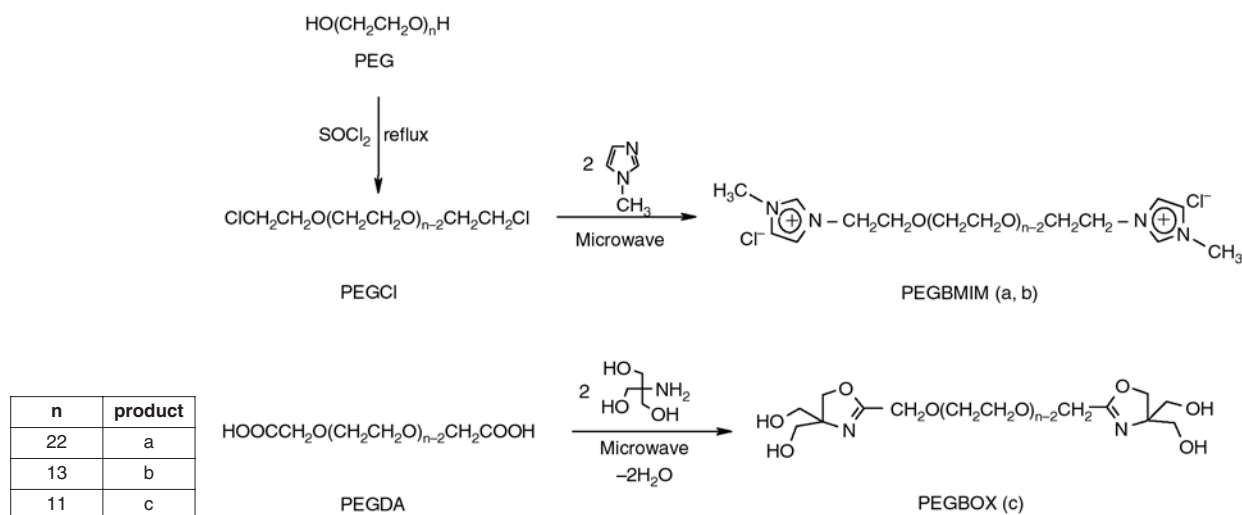
Figure 1. The reaction route for the preparation of PEGBMIM (**a,b**) and PEGBOX (**c**)

The yields of the obtained functional polymers using different reaction conditions are outlined in Table 1. In an unmodified household microwave oven it is not possible to effectively adjust the microwave power. The reduction in power level simply entails that it operates at its full power but for a reduced period of time. Upon microwave irradiation, the product starts forming, which increases the polarity of the reaction medium thereby, increasing the rate of microwave absorption. Perreux and Loupy [35] postulated that a bimolecular reaction between neutral reactants should be assisted by microwave irradiation as the reaction goes through a dipolar transition state. This dipolar transition state is prone to develop more efficient stabilizing electrostatic interactions with the applied electromagnetic field (of a dipole-dipole nature) than the neutral ground state due to dipole formation during the course of the reaction. As a consequence, as the transition state is displaced further along the reaction coordinates (more product-like transition state) the more prone it will be to develop an increased polarity and the more pronounced will be the microwave effect.
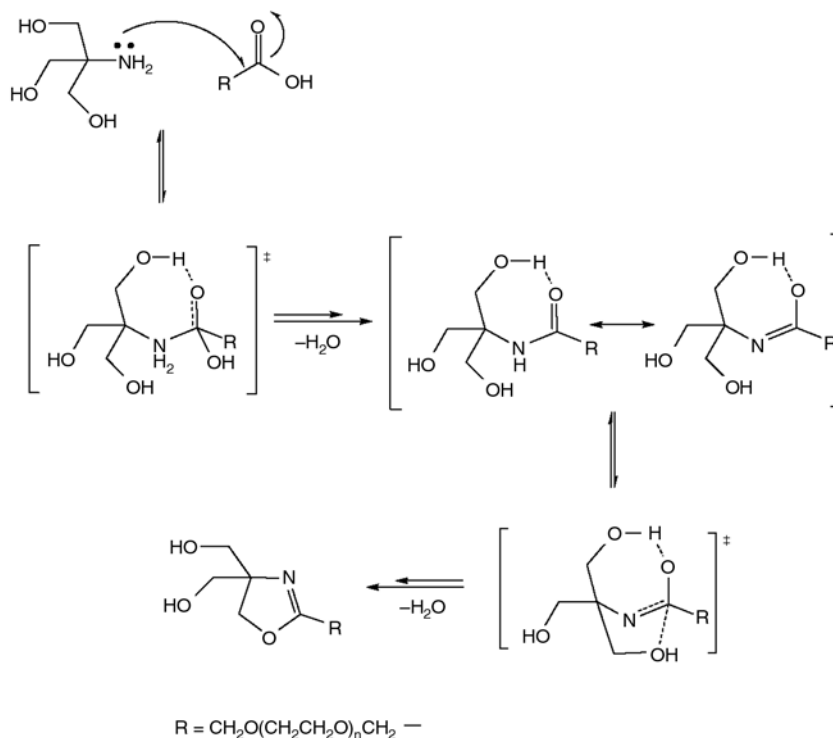
Figure 2. The possible mechanism of the formation of 2-oxazoline from condensation of β-amino alcohol

In the process of preparation of ionic liquids it is observed that at elevated power levels partial decomposition/charring of the ionic liquid occurs possibly owing to the localized overheating of ionic liquid, which eventually results in lower yields. To avoid this problem, the reactions are conducted with intermittent heating and mixing at a moderate power level to obtain better yields and cleaner ionic liquid formation. So, we tried to irradiate samples in various conditions at different power levels for different period of times to obtain an optimized condition.

In the case of condensation of acid with β-amino alcohol, once the amide are formed, subsequent intramolecular condensation between the amide and the free hydroxyl groups present in the molecule can afford 2-oxazoline. The presence of at least two hydroxyl groups in the amino alcohol seems to be crucial to promote the further condensation (Figure 2). In the absence of such a second hydroxyl group, the condensation needs a catalyst to proceed.

Because of the polar nature of the transition states involved in these processes, the microwave irradiation should help to drive the reaction to completion. Furthermore, the final temperature reached ($T \sim 140°C$) implies that the formed water is removed from the reaction medium rendering the global process irreversible, irrespective of the mode of activation (MW irradiation or conventional heating).

It is believed [35] that the key role of the second hydroxyl group is to form an internal H-bond with the carbonyl group of the amide to provide some electrophilic assistance for the next condensation. This mechanism is also highly beneficial for MW specific effects as it involves a dipolar transition state from neutral reactants.

Figure 3 shows the FT-IR spectra of the products in comparison with their primary polymers. According to the spectrum the elimination of C–Cl stretch-
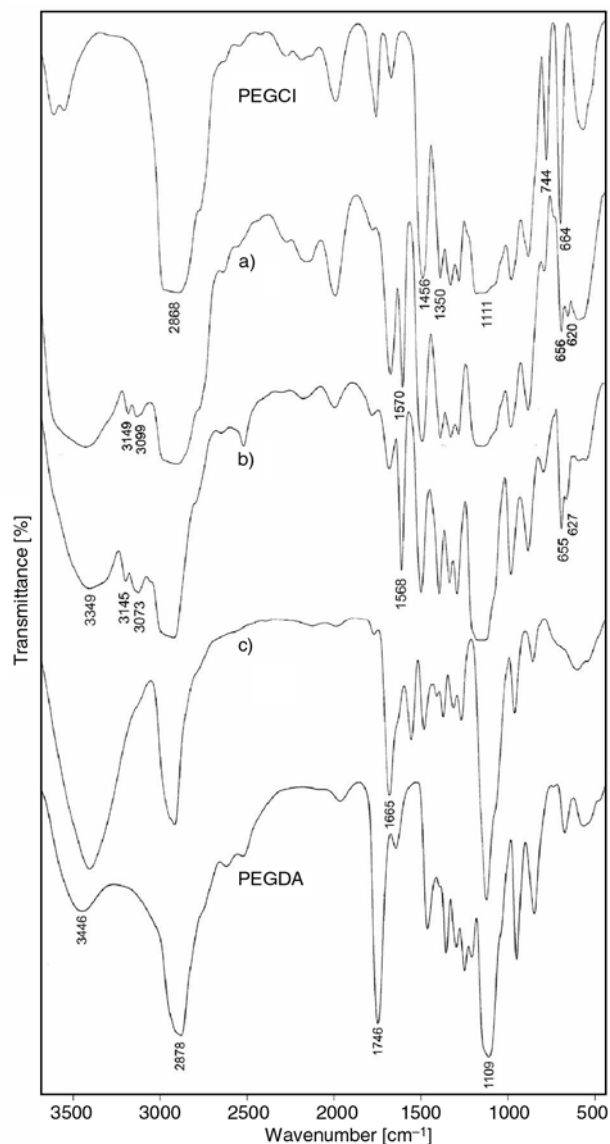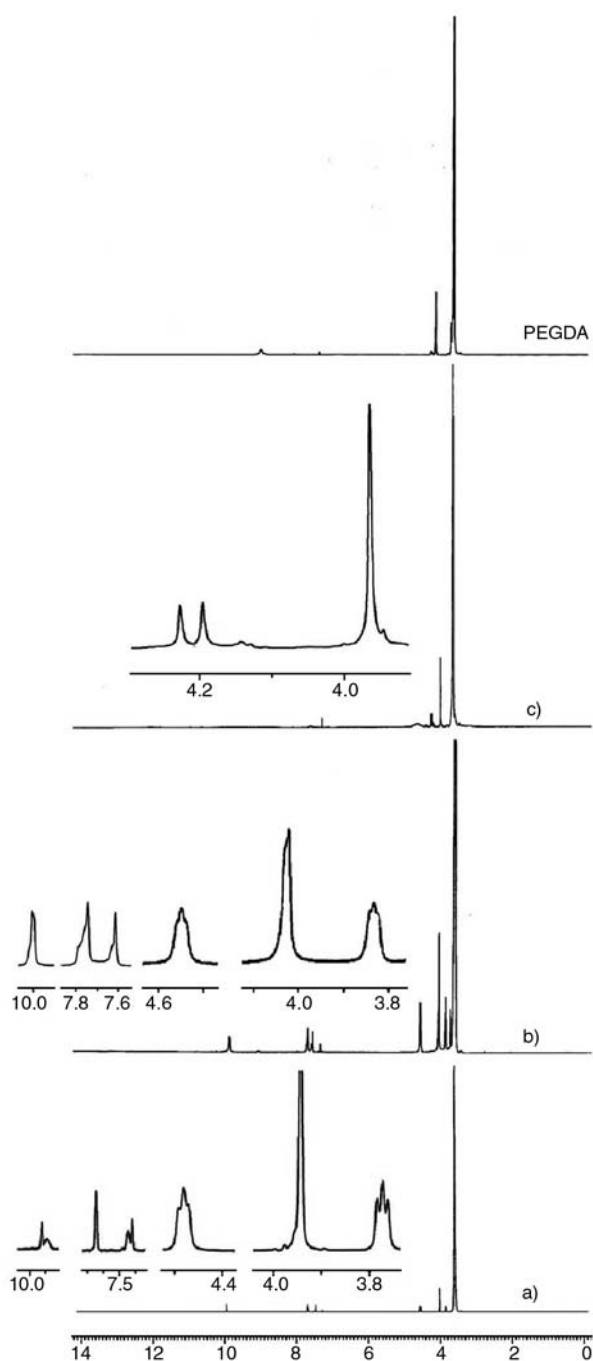

Figure 3. The FT-IR spectra of PEGCl, PEGBMIM (**a,b**), PEGBOX (**c**) and PEGDA

ing bands, and the appearance of aromatic C–H and C=N stretching bands confirm the formation of the expected ionic liquids. Furthermore the elimination of C=O stretching band in 1746 cm^{-1} and the appearance of C=N stretching band in 1658 cm^{-1}, confirm the formation of 2-oxazoline.

Table 2. The elemental analysis results of the products

| | | Content [%] | | | [C]/[N] | Conversion |
		C	H	N	[%]	[%]
PEGMIM(a)	calculated	51.20	8.61	4.60	13.00	
	found	52.21	8.74	4.09	14.89	87.8
PEGMIM(b)	calculated	51.58	8.09	7.07	8.50	
	found	49.67	7.81	6.51	8.90	95.0
PEGOX(c)	calculated	51.40	8.00	4.00	15.00	
	found	49.25	7.88	3.80	15.12	99.0

Figure 4. The ¹H NMR spectra of PEGBMIM (**a**,**b**), PEGBOX (**c**) and PEGDA

Table 3. The solubility behavior of products in comparison with the primary polymers

Solvent	PEGCl	a	b	PEGDA	c
Water	+[1]	+	+	+	+
DMF	+	+	+	+	+
Dichloromethane	+	+	+	+	+
Diethylether	+[2]	–	–	+[3]	–
n-Hexane	–	–	–	–	–
Toluene	+	+	+	±	–

[1]+: soluble, –: insoluble, ±: slightly soluble

[2,3]PEGCl and PEGDA are insoluble in diethylether below 0°C

Figure 4 shows the ¹H NMR spectra of the products. The appearance of the aromatic protons signals in **a** (7.44, 7.64, 9.87 ppm) and **b** (7.60, 7.74, 9.99 ppm), and the elimination of the peak of carboxylic acid groups (8.88 ppm) from PEGDA are evidences of formation of the **a**, **b** and **c** products.

Also the elemental analysis results of the products are shown in Table 2. According to these results, functionalization of the primary polymers has been concluded.

The resulted data showed that, in the case of preparation PEGBMIM (**a**,**b**), the obtained dicationic salts generated from dichloro poly(ethylene glycol) are slightly contaminated with the corresponding monocationic intermediate.

The solubility of the synthesized polymers in water and in common organic solvents were studied and the results are shown in Table 3. The results showed that the solubility of the obtained polymers are similar to their parent polymers, but they became polar than primary polymers.

4. Conclusions

According to the obtained results poly(ethylene glycol) bis methylimidazolium chloride with average molecular weights of 600 and 1000 g/mol and poly(ethylene glycol) bis 2-oxazoline with average molecular weight of 600 g/mol have been prepared as a new telechelic polymers under solvent free condition using an unmodified household microwave oven, a method that precludes the usage of volatile organic solvents and is much faster, efficient, and eco-friendly.

References

[1] Zhang S., Du J., Sun R., Li X., Yang D., Zhang S., Xiong C., Peng Y.: Synthesis of hetrobiofunctional poly(ethylene glycol) with a primary amino group at one end and carboxylate group at the other end. Reactive and Functional Polymers, **56**, 17–25 (2003). DOI: 10.1016/S1381-5148(03)00015-4

[2] Henning T.: Polyethylene glycols (PEGs) and the pharmaceutical industry. PharmaChem, June, 57–59 (2002).

[3] Li J., Kao W. J.: Synthesis of polyethylene glycol (PEG) derivatives and PEGylated-peptide biopolymer conjugates. Biomacromolecules, **4**, 1055–1067 (2003). DOI: 10.1021/bm034069l

[4] Roberts M. J., Bentley M. D., Harris J. M.: Chemistry for peptide and protein PEGylation. Advanced Drug Delivery Reviews, **54**, 459–4796 (2002).
DOI: 10.1016/S0169-409X(02)00022-4

[5] Yao N., Jamiseson A. M.: Synthesis and solution properties of cholesterol end capped poly(ethylene glycol). Polymer, **41**, 2925–2930 (2000).
DOI: 10.1016/S0032-3861(99)00488-7

[6] Bayer E., Zheng H., Geckeler K. E.: Functionalization of soluble polymers. 4. Synthesis of dichloro- and di(4-formylphenyloxyethyl) poly(oxyethelene). Polymer Bulletin, **8**, 585–592 (1982).
DOI: 10.1007/BF00262939

[7] Geckeler K. E., Arsalani N.: Synthesis and properties of hydrophilic polymers. 4. Preparation and characterization of poly(oxyethylene) telechelics with different aromatic termini. Journal of Macromolecular Science: Pure and Applied Chemistry, **33**, 1165–1179 (1996).
DOI: 10.1080/10601329608010912

[8] Tanaka K.: Solvent-free organic synthesis. Wiley-VCH, Weinheim (2003).

[9] Varma R. S.: Solvent-free organic syntheses using supported reagents and microwave irradiation. Green Chemistry, **1**, 43–55 (1999).
DOI: 10.1039/a808223e

[10] Garcia-Tellado F., Loupy A., Petit A., Marrero-Terrero A. L.: Solvent-free microwave-assisted efficient synthesis of 4,4-disubstituted 2-oxazolines. European Journal of Organic Chemistry, **22**, 4387–4391 (2003).
DOI: 10.1002/ejoc.200200469

[11] Wiesbrock F., Hoogenboom R., Schubert U. S.: Microwave-assisted polymer synthesis: State-of-the-art and future perspectives. Macromolecular Rapid Communications, **25**, 1739–1764 (2004).
DOI: 10.1002/marc.200400313

[12] Kappe C. O.: Controlled microwave heating in modern organic synthesis. Angewandte Chemie International Edition, **43**, 6250–6284 (2004).
DOI: 10.1002/anie.200400655

[13] Varma R. S., Namboodiri V.: An expeditious solvent-free route to ionic liquids using microwaves. Chemical Communications, **1**, 643–644 (2001).
DOI: 10.1039/b101375k

[14] Erdmenger T., Vitz J., Wiesbrock F., Schubert U. S.: Influence of different branched alkyl side chains on the properties of imidazolium-based ionic liquids. Journal of Materials Chemistry, **18**, 5267–5273 (2008).
DOI: 10.1039/b807119e

[15] Wasserscheid P., Welton T.: Ionic liquids in synthesis. Wiley-VCH, Weinheim (2003).

[16] Xue H., Varma R., Shreeve J. M.: Review of ionic liquids with flurine-containing anions. Journal of Flurine Chemistry, **127**, 159–176 (2006).
DOI: 10.1016/j.jfluchem.2005.11.007

[17] Welton T.: Room-temperature ionic liquids, solvent for synthesis and catalysis. Chemical Review, **99**, 2071–2083 (1999).
DOI: 10.1021/cr980032t

[18] Bohm V. P. W., Herrmann W. A.: Coordination chemistry and mechanisms of metal-catalyzed C-C coupling reactions, part 12. Nonaqueous ionic liquids: Superior reaction media for the catalytic heck-vinylation of chloroarenes. Chemistry A, European Journal, **6**, 1017–1025 (2000).
DOI: 10.1002/(SICI)1521-3765(20000317)6:6<1017:: AID-CHEM1017>3.0.CO;2-8

[19] Lewandowski A., Swiderska A.: New composite solid electrolytes based on a polymer and ionic liquids. Solid State Ionics, **169**, 21–24 (2004).
DOI: 10.1016/j.ssi.2003.02.004

[20] Kronek J., Luston J., Bohme F.: Reactions of 2-oxazolines and their utilization (in Czech). Chemicke' Listy, **92**, 475–485 (1998).

[21] John J., Tang J., Bhattacharya M.: Grafting of oxazoline functional group to polycaprolactone. Journal of Applied Polymer Science, **67**, 1947–1955 (1998).
DOI: 10.1002/(SICI)1097-4628(19980314)67:11<1947:: AID-APP14>3.0.CO;2-R

[22] Vocke C., Anttila U., Heino M., Hietaoja P., Seppälä J.: Use of oxazoline functionalized polyolefins and elastomers as compatibilizers for thermoplastic blends. Journal of Applied Polymer Science, **70**, 1923–1930 (1998).
DOI: 10.1002/(SICI)1097-4628(19981205)70:10 <1923:: AID-APP6>3.0.CO;2-4

[23] Hu G-H., Scaffaro R., La Mantia F.: Chemical modification of nitrile to oxazoline functionality on a styrene-acrylonitrile copolymer in the melt. Journal of Macromolecular Science Part A: Pure and Applied Chemistry, **35**, 457–474 (1998).
DOI: 10.1080/10601329808001989

[24] Wörner Ch., Müller Ph., Mülhaupt R.: 1,3-oxazoline intermediates in reactive processing applications. Polymer, **39**, 611–620 (1998).
DOI: 10.1002/macp.1995.021960612

[25] Wiesbrock F., Hoogenboom R., Leenen M. A. M., Meier M. A. R., Schubert U. S.: investigation of the living cationic ring-opening polymerization of 2-methyl-, 2-ethyl-, 2-nonyl-, and 2-phenyl-2-oxazoline in a single-mode microwave reactor. Macromolecules, **38**, 5025–5034 (2005).
DOI: 10.1021/ma0474170

[26] Luston J., Böhme F., Komber H., Pompe G.: Unsaturated 2-oxazoline modification of polyethylene containing carboxylic groups. Journal of Macromolecular Science: Pure and Applied Chemistry, **35**, 1045–1054 (1998).
DOI: 10.1080/10601329808002099

[27] Inata H., Matsumura S.: Chain extenders for polyesters. IV. Properties of the polyesters chain-extended by 2,2′-bis(2-oxazoline). Journal of Applied Polymer Science, **33**, 3069–3079 (1987).
DOI: 10.1002/app.1987.070330838

[28] Chalamet Y., Taha M.: Carboxyl terminated polyamide 12 chain extension using a dioxazoline coupling agent. Journal of Polymer Science Part A: Polymer Chemistry, **35**, 3697–3705 (1997).
DOI: 10.1002/(SICI)1099-0518(199712)35:17<3697:: AID-POLA9>3.0.CO;2-P

[29] Christova D., Velichkova R., Goethals E.: Bis-macro-monomers of 2-alkyl-2-oxazolines-synthesis and polymerization. Macromolecular Rapid Communications, **18**, 1067–1073 (1997).
DOI: 10.1002/marc.1997.030181210

[30] Weber C., Becer R., Baumgaertel A., Hoogenboom R., Schubert U. S.: Preparation of methacrylate end-functionalized poly(2-ethyl-2-oxazoline) macro-monomers. Designed Monomers and Polymers, **12**, 149–165 (2009).
DOI: 10.1163/156855509X412090

[31] Ito K.: Polymeric design by macromonomer technique. Progress in Polymer Science, **23**, 581–620 (1998).
DOI: 10.1016/S0079-6700(97)00049-X

[32] Lach C., Hanselmann R., Frey H., Mülhaupt R.: Hyperbranched carbosilane oxazoline-macromono-mers: Polymerization and coupling to a trimesic acid core. Macromolecular Rapid Communications, **19**, 461–465 (1998).
DOI: 10.1002/(SICI)1521-3927(19980901)19:9<461:: AID-MARC461>3.0.CO;2-8

[33] Pantchev I., Velichkova R., Lakov L., Peshev O., Goethals E.: Amphiphilic polyelectrolyte networks derived from 2-oxazolines. Polymer, **39**, 7089–7097 (1998).
DOI: 10.1016/S0032-3861(98)00083-4

[34] Vorbrüggen H., Krolikiewicz K.: A simple synthesis of Δ^2-oxazines, Δ^2-oxazines, Δ^2-thiazolines and 2-sub-stituted benzoxazoles. Tetrahedron, **49**, 9353–9372 (1993).
DOI: 10.1016/0040-4020(93)80021-K

[35] Perreux L., Loupy A.: A tentative rationalization of microwave effects in organic synthesis according to the reaction medium, and mechanistic considerations. Tetrahedron, **57**, 9199–9223 (2001).
DOI: 10.1016/S0040-4020(01)00905-X

Electrospinning of polyacrylonitrile (PAN) solution: Effect of conductive additive and filler on the process

P. Heikkilä[1]*, A. Harlin[2]

[1]Department of Materials Science, Tampere University of Technology, P.O. Box 589, FI-33101 Tampere, Finland
[2]VTT Technical Research Centre of Finland, P.O. Box 1000, FI-02044 VTT, Finland

Abstract. Electrospinning utilizes electric forces and hence the electrical properties of the solution have an effect the process. The study examined the effect of conductive additive and filler on the electrospinning process with polyacrylonitrile (PAN). Electrospinning trials were performed using a pure PAN solution, a salt-containing solution, and a solution containing carbon nanotubes (CNTs). Different nozzle sizes were used, and the spinning voltage and distance were also varied. The composition of the solution had a greater effect on fibre diameter than varying the process parameters. Conductivity of the solution increased the probability of process problems such as the formation of three-dimensional (3D) structures and the occurrence of larger, micro-sized fibres. When the viscosity of the solution was increased, as was the case with the PAN/CNT solution, the severity of the problems became less acute than with the PAN/Salt solution.

Keywords: nanocomposites, electrospinning, polyacrylonitrile, nanofibres, conductive additives

1. Introduction

Sub-micron and nanofibres can be prepared from a polymer solution utilizing electrospinning [1–5]. In electrospinning, the electrostatic field stretches the polymer solution into fibres as the solvent is evaporating. During the process the polymer jet undergoes instabilities, which together with the solution properties, determines the morphology of the forming nano-sized structures obtained onto the collector [6–8]. The instabilities are caused by two opposing forces that affect the jet as follows: 1) the surface tension, which stabilizes the jet and tends to minimize its surface; and 2) the charge repulsion, which destabilizes the jet and increases its surface [9]. Three distinguishable competing instability modes can occur: 1) a classical (axisymmetric) Rayleigh break-up instability mode, 2) an axisymmetric conducting instability mode; and 3) a whipping conducting instability mode [10, 11], also

known as bending instability [12, 13]. Numerous solution and process variables affect these instabilities. Conducting modes, especially whipping, are enhanced with increased voltage and electric field strength, while Rayleigh instability is suppressed by them [6, 10].

Electrospun fibres can be functionalized by the use of additives, and fillers of many kinds can be used to form composite fibres [14, 15]. The properties of electrospun fibres can be modified using nano-sized fillers. Carbon nanotubes (CNTs) are widely used as filler in electrospun fibres [16–29]. Typically, their function is to serve as a reinforcement component [16–19] in electrospun polymeric fibres, but they are also used to modify the electrical properties of fibres [20–23].

The use of filler in the solution may affect the different properties of the solution. The filler particles may, for example, act as charge carriers which

cause the conductivity of the solution to increase the charge density of the jet and, thereby, enhance instabilities. Charge carriers such as salts or conductive filler particles have an influence on the conductivity of the solution and they may promote two phenomena having opposite effects on fibre formation and diameter [8]. Firstly, they may increase flow rate, which can lead to larger fibres [30]. Secondly, they may increase net charge density, which suppresses the Rayleigh instability and enhances the whipping instability, leading to the formation of bead-free fibres and smaller fibre diameter [31]. In addition, additives may affect the interactions in the solution and thus also have an effect on fibre diameter and morphology [8].

Salts and other conductive additives have been found to reduce [32, 33] and also increase fibre diameter [30, 34]. Ju *et al*. [24] and Ra *et al*. [23] obtained finer fibres with CNT-containing solution compared to a CNT-free one. It was also observed that beads formed especially when CNT concentration was high or the dispersion of the CNTs in solution was poor [23]. Mathew *et al*. [35], on the other hand, found that CNTs led to broader fibre diameter distribution and especially the occurrence of fibres having larger diameters. According to the authors this can be explained by the increase in solution viscosity or by the creation of new interfaces between polymer and CNTs [35]. The effect of fillers and additives on fibre diameter varies from system to system depending on the polymer, solvent as well as the additive [8, 36].

Fillers and additives may also interact with solvent, with polymer or with both. The electrospinnability of the solution may also change as a result of these interactions, but it may also remain unchanged, regardless of the additive. [8] It has, for example, been shown [36] that conductive solutions can form different kinds of three-dimensional (3D) loose structures on the substrate, instead of a thin coating layer attached to the substrate surface. The form of these structures can vary from fibrils perpendicular to the substrate surface to a fluffy layer of cotton-like structure. Fibrils can even extend to cover the entire electrospinning zone. If this kind of conductive fibrous structure connects nozzle and plate, the electric field discharges and the process stops [36, 37]. The optimization of process parameters for ternary systems can be even more challenging than for binary systems composed only of polymer and solvent [8].

This study examined the phenomena caused by conductivity. Polyacrylonitrile (PAN), whose behaviour in electrospinning is well known [30, 38–41], was used in the experiments. Electrospun PAN fibres have many possible applications, one of which is the production of carbon nanofibres (CNF) by carbonization of electrospun precursor fibres [17, 21, 25, 26, 29, 40–45]. CNTs can be used in precursor fibres since CNT filler may effectively resist heat shrinkage in composite fibres during the carbonization process [29]. CNTs may have a positive effect on crystallinity and the order of polymer [25] and the presence of CNTs may also promote the growth of carbon crystals during PAN carbonization [26]. Since the addition of CNT has an effect on the viscosity of the solution, the conductivity of polymer solution was also modified with salt, for comparison. Process parameters such as voltage, distance, and nozzle size were varied in order to determine the optimum process for each solution. The study observed and evaluated the functioning of the electrospinning process as well as the quality of electrospun web.

2. Experimental

2.1. Materials

Spinning solutions of pure PAN and salt-containing PAN were prepared by dissolving polymer (13 wt%) in heated DMF. The solution was heated and stirred until the polymer dissolved, after which $ZnCl_2$ salt (0.25 wt%) was dissolved into salt-containing polymer solution. Dispersing of CNTs evenly into pure DMF or into viscous polymer solution is a difficult process, and so the composite solution was prepared in three steps. First, a small amount of PAN was dissolved in DMF because this acts as a dispersing agent. Then CNTs (0.25 wt%, MWCNT NC7000 from Nanocyl S.A., average diameter 9.5 nm, average length 1.5 μm) were added and dispersed in dilute polymer solution by ultrasonic homogenizing. Finally, the rest of the polymer was added to achieve the desired polymer concentration (13 wt%). Dispersion of CNTs in solution prepared this way has been found to be relatively good, even though some agglomerates might still be present [46].

2.2. Electrospinning experiments

Electrospinning was performed using continuous process equipment in which a horizontal electric field was generated between a nozzle system and a collector plate (Figure 1a). A web having a width of 300 mm was conveyed past the front side of the collector. The nozzle system used in the trials was composed of one tube having places for ten nozzles. A metal rod within the tube was connected to the voltage source (Simco Chargemaster BP 50) from one end of the tube. The solution was fed from the opposite end of the tube, and nitrogen gas with controlled pressure was attached to the feeding system of the tubes. The collector plate was connected to ground. The fibres were collected on paper and metal grid substrates, which were attached onto nonwoven web.
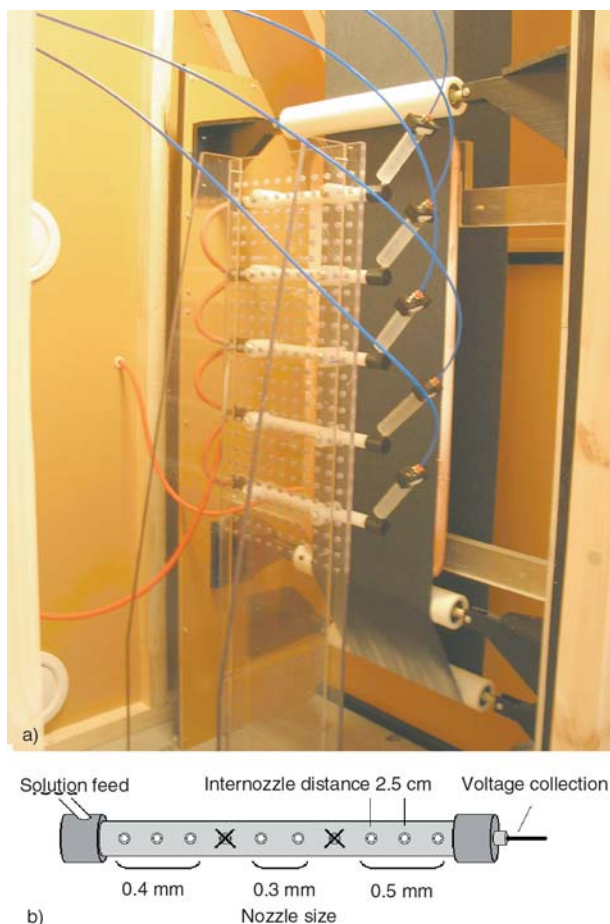
Figure 1. a) Electrospinning equipment equipped with five tubes: a horizontal electric field is generated between the nozzle system and the collector plate and a web is conveyed past the collector. b) Nozzle arrangement on one tube used in this study. Nozzle diameter on the left was 0.4 mm, in the middle 0.3 mm and on the right 0.5 mm – two nozzle places were blocked.

Samples were prepared by conveying substrates at a fixed line speed through the electrospinning zone. Three nozzle sizes were used. Each of three right side nozzles was 0.5 mm in internal diameter and each of the two middle and three left side nozzles was 0.3 and 0.4 mm respectively, two nozzle places were blocked (Figure 1b). Each nozzle formed a stripe of fibre on the substrate (stripes on the substrate are in reverse order to the nozzles on the tube). Two distances, 100 mm (*S*) and 150 mm (*L*), were used in electrospinning trials. The voltage was varied (10–40 kV) so that electric field strengths in the trials measured 67, 133, 200 and 267 kV/m.

2.3. Characterization

Conductivity of the solution was measured with Schott Instruments, Handylab LF11. Viscosity was measured with Brookfield DV-II + viscometer. The production rate and the quality of the fibrous coating were evaluated from photographed samples. SEM imaging was used to observe fibre quality and Philips XL30 and Zeiss Ultra Plus SEM equipment was used to determine the fibre diameter of selected samples. Image Tool 3.0 software was used for diameter measurements from SEM images. Over 100 measurements were made at each trial, and mean diameter [nm] and its standard deviation [nm] were also calculated.

3. Results and discussion

3.1. Formation of electrospun web

Conductivity of PAN solution was 115 µS/cm while the conductivity of the PAN/Salt and PAN/CNT solutions were higher: 196 and 158 µS/cm, respectively. The viscosity of both the PAN and PAN/Salt solutions was around 1150 mPa·s, while the viscosity of the PAN/CNT solution was around 4650 mPa·s. Due to this difference in viscosity optimum nozzle size varied. Solutions having lower viscosity dripped from the largest nozzle, while those with higher viscosity could barely flow through the smallest nozzles. Dripping of solution was more pronounced at low electric field strengths. Short distance seems to increase the dripping tendency even with constant electric field strength, though this may be partially attributable to the horizontal arrangement of the field. The amount of droplets may remain unchanged, but a longer dis-
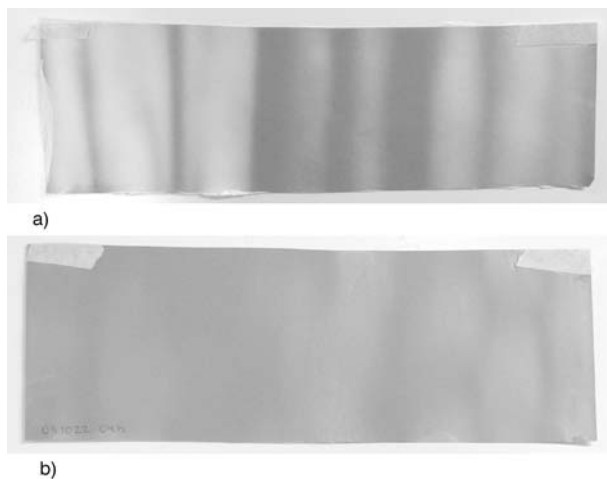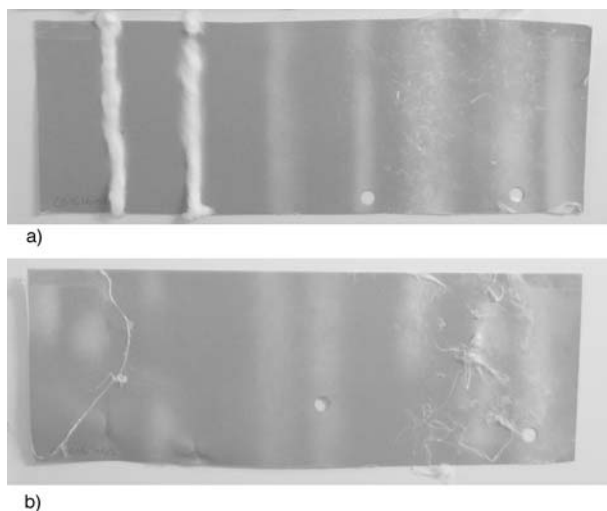
Figure 2. Appearance of white PAN nanofibre stripes on dark paper: a) 40 kV/150 mm, b) 10 kV/150 mm. Nozzle size on the left was 0.5 mm, in the middle 0.3 mm and on the right 0.4 mm. Higher voltage and larger nozzle size increased the amount of fibres on substrate.

tance may increase the likelihood that the droplet trajectory does not reach the substrate. Overall the 0.4 nozzles were best for PAN and PAN/Salt solutions and the 0.5 nozzles for the PAN/CNT solution since they enable sufficient solution flow and thus, relatively high productivity. Besides nozzle size, electric field strength had a significant effect on productivity. The effect of nozzle size and voltage on the amount of fibres can be seen in Figure 2.

The electrospinning process usually produces a smooth fibre layer fixed on the surface of the sub-


Figure 3. Appearance of white PAN/Salt nanofibre stripes on dark paper: a) 40 kV/150 mm, b) 20 kV/100 mm. Nozzle size: left 0.5 mm, middle 0.3 mm and right 0.4 mm. Inclusion of salt increased the occurrence of 3D fibre structures and visible fibre bundles.

strate, but the fibres made of conducting PAN/Salt solution often produced fluffy cotton-like 3D structures or otherwise loose fibre structures on top of the substrate (Figure 3). These structures can be considered as defects from a production point of view. Another slightly less disruptive defect, which occurred in association with 3D, was the formation of larger fibres or fibre bundles visible to the naked eye. Pure PAN solution and PAN/CNT composite solutions produced 3D structures and visible fibre bundles on paper only at the highest voltages and shortest distances. The formation of 3D structures with PAN/Salt fibres was also more pronounced at higher voltages.

Occurrence with high conductivity and high voltage indicated that 3D structures would be induced by high electrical forces. This is supported by our finding that use of a conductive metallic grid as a substrate increases the probability of 3D structures, especially with PAN/Salt and PAN/CNT solutions. PAN/Salt and PAN/CNT solutions differed in 3D tendency even though they contained conductive component. This can, however, be explained by the fact that PAN/CNT solution had high viscosity, which tends to stabilize the process and also reduce the flow of the solution. Short distance seemed to increase 3D tendency even at constant electric field strength, but this might be attributed to reduced stretching and the larger diameter of the jet, and thus a larger charge density on the surface of the jet and larger electric forces affecting it. Electrical forces are not, however, the only factors affecting the occurrence of this tendency, since large nozzle size also increased 3D structures. High electrical forces and large nozzle size both have an increased effect on solution flow rate, which in addition to electrical forces, seem to contribute to the occurrence of 3D structures.

3.2. Electrospun fibres

The composition of the solution affected the diameters and appearance of the fibres. The appearance of PAN, PAN/Salt and PAN/CNT fibres electrospun under the same conditions (voltage 20 kV, distance 150 mm, nozzle 0.4 mm) are exemplified in Figures 4a–4c. In PAN/CNT composite fibres, filler showed more pronounced surface roughness and markedly larger fibre diameters than the PAN and PAN/Salt fibres. Surface roughness is a typi-
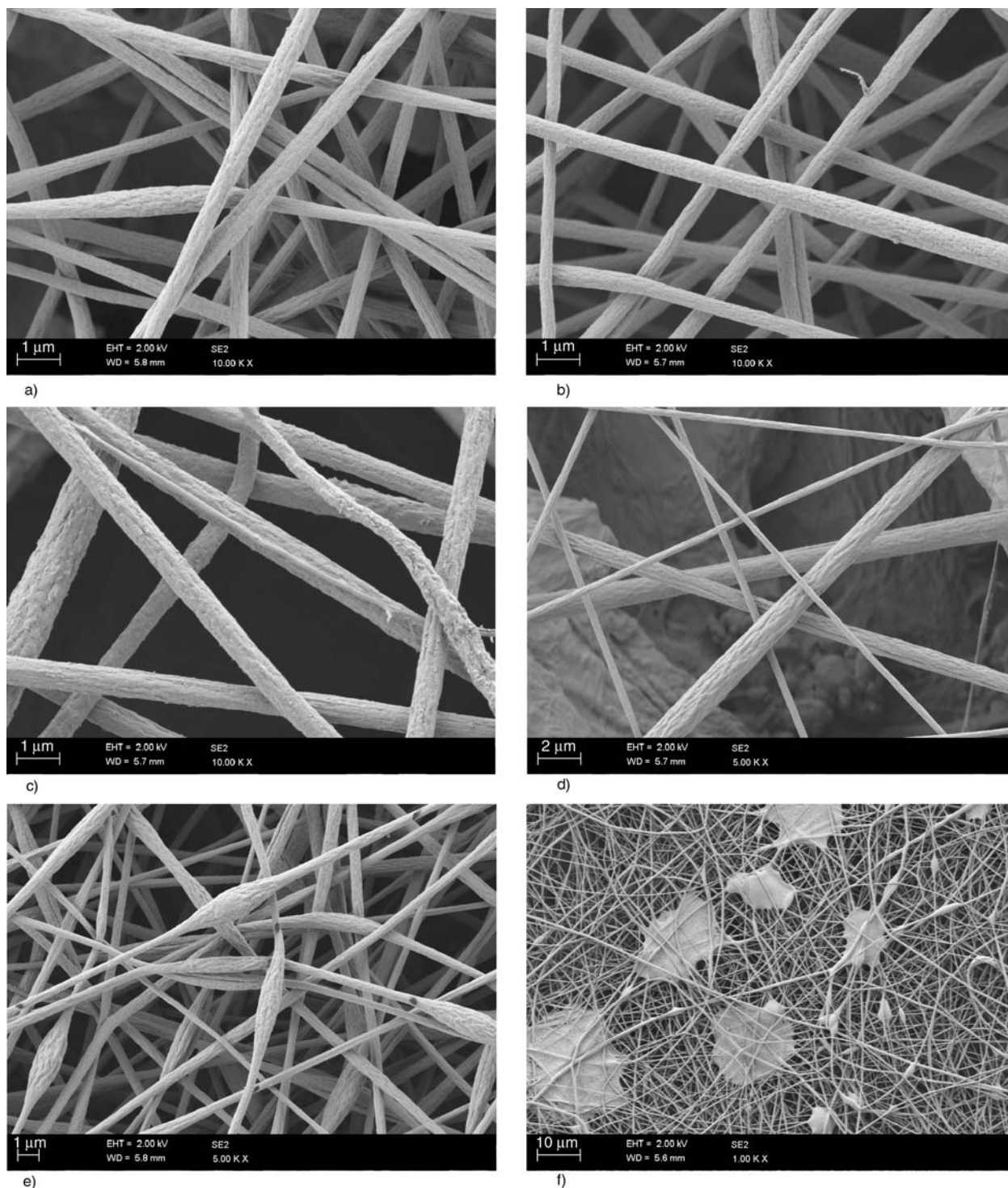
Figure 4. Appearance of a) PAN, b) PAN/Salt and c) PAN/CNT fibres electrospun (voltage 20 kV, distance 150 mm, nozzle 0.4 mm) (magnification in SEM imaging 10000×), d) bimodal fibre distribution composed of two distinctive fibre diameter ranges (SEM 5000×), e) beaded fibres (SEM 5000×), and f) larger fibres and micro sized solution splatters (SEM 1000×).

cally observed characteristic of CNT composite fibres [23, 24], and increased fibre diameter can be explained by increased viscosity [35]. The difference in viscosity is the reason for the difference in the fibre diameter of PAN/CNT and PAN/Salt solutions even though the conductivities of the solutions were nearly at the same level.

In addition to 3D structures, certain other imperfections were observed. In some trials with small nozzles and low field strength we also observed that

the PAN and PAN/Salt solutions produced a clear bimodal fibre diameter distribution (Figure 4d). Spindle-shaped beads (Figure 4e) occurred occasionally with PAN and PAN/Salt solution in trials conducted using shorter distance (100 mm). Other defects observed in the electrospun webs were enlarged fibres and micro-sized solution splatters (Figure 4f). While larger fibres were regularly observed with the PAN/Salt solution, their occurrence with PAN and PAN/CNT solutions was mainly limited to cases where the distance was short or the electric field strength was high.

The dependence of fibre diameter on solution composition is illustrated in Figure 5. PAN/Salt fibres had a slightly larger diameter than PAN fibres, in contrast to the conventional view that a more conductive solution causes a reduction in diameter [32]. In this case higher conductivity seems to have led to increased mass flow and thus larger fibre diameters. Our findings are consistent with those of Qin *et al*. [30]. In their studies on the effect of different salts on the electrospinning of PAN, they observed that salt, which has the greatest effect on conductivity, also produced fibres with the largest diameters. Slightly varying diameters in fibres typically occurs with the use of fillers [8]. However, this variation in individual fibre diameter had no effect on the standard deviation of fibre diameter.

In general, solution composition had greater influence on fibre diameter than either spinning distance or strength of the electric field. Gu *et al*. [41] have also reported that voltage is not a significant factor in determining the diameter of PAN fibres. The differences in the diameters of fibres prepared using a single solution in different spinning distances and
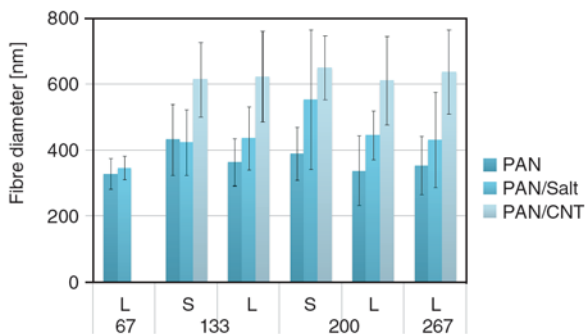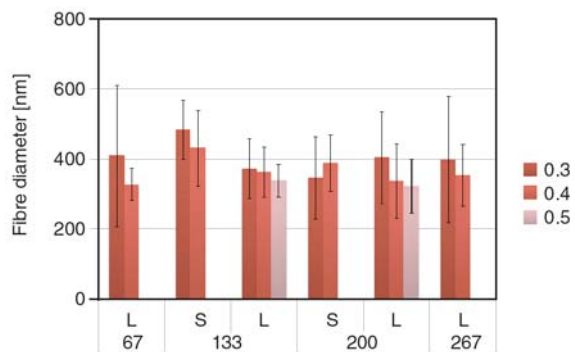
Figure 6. Fibre diameters of PAN solution electrospun using different nozzle sizes (0.3 mm, 0.4 mm and 0.5 mm). Spinning distances ($S = 100$ mm and $L = 150$ mm) and electric field strengths [kV/m] are presented in *x*-axis.

electric field strengths were not significant, though a slight trend could be detected (Figure 5). If electric field strength remained constant, and the distance was increased, fibre diameters were slightly decreased. Longer distance enables greater stretching of the solution jet. Although fibre diameters can be expected to decrease in the presence of a stronger electric field due to increased stretching, our studies showed no evidence for such a trend. An increase in electrical force can produce contradictory effects since it can increase both whipping instability and mass flow [36].

The effect of nozzle diameter with PAN solution is illustrated in Figure 6. Somewhat surprisingly, the fibre diameters produced from larger nozzles were often smaller than those from smaller nozzles, even though such differences were statistically insignificant. We suggest that this tendency is because the more stable spinning process obtained with larger nozzles might promote an adequate and continuous solution flow. This view is also supported by the finding that there was less variation in fibre diameter when larger nozzles were used.

4. Conclusions

This study demonstrated the electrospinning of PAN solutions with salt as the conductive additive, and CNTs as conductive filler. Parameters such as voltage, distance, and nozzle size, were varied. The quality of the electrospun web and the fibres was studied, as well as the functioning of the process.

The PAN and PAN/Salt solutions had similar viscosity but the PAN/Salt solution produced slightly larger fibres because increased conductivity

Figure 5. Fibre diameters of PAN, PNA/Salt and PAN/CNT solutions electrospun using 0.4 mm nozzles. Spinning distances ($S = 100$ mm and $L = 150$ mm) and electric field strengths [kV/m] are presented in *x*-axis.

enhanced the mass flow. The higher conductivity of the PAN/Salt solution increased the instabilities in the electrospinning process. This was also the most probable cause of the increased process problems, such as the formation of 3D structures and defects in fibrous web such as larger fibres. These phenomena were less common with PAN/CNT solution, which also contains a conductive component. The conductivity of the PAN/Salt solution was higher than that of the PAN/CNT solution. The addition of CNTs in the solution also had a significant impact on the viscosity of the solution, which tends to stabilize the process. As expected, increased viscosity gave rise to larger fibre diameters compared to PAN and PAN/Salt solutions.

Even though the composition of the solution was the major factor influencing fibre diameter, varying the parameters also had an effect on the process and fibre diameters. Increase in distance typically reduced fibre diameter when electric field strength remained constant. A longer distance is preferable since shorter distance also increased the likelihood of solution dripping onto the substrate and the occurrence of beaded fibres. At the lower end of the electric field strength range used in our study, we observed dripping and also a low production rate. At the higher end of the range, we observed 3D structures and the occurrence of larger fibres and micro range droplets on the web. Hence intermediate field strength seems optimal.

Acknowledgements

References

[1] Reneker D. H., Chun I.: Nanometre diameter fibres of polymer, produced by electrospinning. Nanotechnology, **7**, 216–223 (1996).
DOI: 10.1088/0957-4484/7/3/009

[2] Li D., Xia Y.: Electrospinning of nanofibers: Reinventing the wheel? Advanced Materials, **16**, 1151–1170 (2004).
DOI: 10.1002/adma.200400719

[3] Reneker D. H., Fong H.: Polymeric nanofibers. ACS Symposium Series, Washington (2006).

[4] Ramakrishna S., Fujihara K., Teo W-E., Yong T., Ma Z., Ramaseshan R.: Electrospun nanofibers: Solving global issues. Materials Today, **9**, 40–50 (2006).
DOI: 10.1016/S1369-7021(06)71389-X

[5] Greiner A., Wendorff J. H.: Electrospinning: A fascinating method for the preparation of ultrathin fibers. Angewandte Chemie International Edition, **46**, 5670–5703 (2007).
DOI: 10.1002/anie.200604646

[6] Zuo W., Zhu M., Yang W., Yu H., Chen Y., Zhang Y.: Experimental study on relationship between jet instability and formation of beaded fibers during electrospinning. Polymer Engineering and Science, **45**, 704–709 (2005).
DOI: 10.1002/pen.20304

[7] Deitzel J. M., Kleinmeyer J., Harris D., Beck Tan N. C.: The effect of processing variables on the morphology of electrospun nanofibers and textiles. Polymer, **42**, 261–272 (2001).
DOI: 10.1016/S0032-3861(00)00250-0

[8] Heikkilä P.: Nanostructured fibre composites and materials for air filtration. PhD thesis, Tampere University of Technology (2008).

[9] Lin T., Wang H., Wang H., Wang X., Brenner M. P.: The charge effect of cationic surfactants on the elimination of fibre beads in the electrospinning of polystyrene. Nanotechnology, **15**, 1375–1381 (2004).
DOI: 10.1088/0957-4484/15/9/044

[10] Hohman M. M., Shin M., Rutledge G., Brenner M. P.: Electrospinning and electrically forced jets. I. Stability theory. Physics of Fluids, **13**, 2201–2220 (2001).
DOI: 10.1063/1.1383791

[11] Hohman M. M., Shin M., Rutledge G.: Electrospinning and electrically forced jets. II. Applications. Physics of Fluids, **13**, 2221–2236 (2001).
DOI: 10.1063/1.1384013

[12] Reneker D. H., Yarin A. L., Fong H., Koombhongse S.: Bending instability of electrically charged liquid jets of polymer solutions in electrospinning. Journal of Applied Physics, **87**, 4531–4547 (2000).
DOI: 10.1063/1.373532

[13] Yarin A. L., Koombhongse S., Reneker D. H.: Bending instability in electrospinning of nanofibers. Journal of Applied Physics, **89**, 3018–3026 (2001).
DOI: 10.1063/1.1333035

[14] Kim G. M., Lach R., Michler G. H., Poetschke P., Albrecht K.: Relationships between phase morphology and deformation mechanisms in polymer nanocomposite nanofibres prepared by an electrospinning process. Nanotechnology, **17**, 963–972 (2006).
DOI: 10.1088/0957-4484/17/4/021

[15] Dersch R., Steinhart M., Boudriot U., Greiner A., Wendorff J. H.: Nanoprocessing of polymers: Applications in medicine, sensors, catalysis, photonics. Polymers for Advanced Technologies, **16**, 276–282 (2005).
DOI: 10.1002/pat.568

[16] Ye H., Lam H., Titchenal N., Gogotsi Y., Ko F.: Reinforcement and rupture behavior of carbon nanotubes-polymer nanofibers. Applied Physics Letters, **85**, 1775–1777 (2004).
DOI: 10.1063/1.1787892

[17] Wan Y-Q., He J-H., Yu J-Y.: Carbon nanotube-reinforced polyacrylonitrile nanofibers by vibration-electrospinning. Polymer International, **56**, 1367–1370 (2007).
DOI: 10.1002/pi.2358

[18] Pan C., Ge L-Q., Gu Z-Z.: Fabrication of multi-walled carbon nanotube reinforced polyelectrolyte hollow nanofibers by electrospinning. Composites Science and Technology, **67**, 3271–3277 (2007).
DOI: 10.1016/j.compscitech.2007.03.036

[19] Lam H., Titchenal N., Naguib N., Ye H., Gogotski Y., Ko F.: Electrospinning of carbon nanotubes reinforced nanocomposite fibrils and yarns. Materials Research Society Symposium Proceeding, **791**, 353–358 (2004).

[20] Seoul C., Kim Y-T., Baek C-K.: Electrospinning of poly(vinylidene fluoride)/ dimethylformamide solutions with carbon nanotubes. Journal of Polymer Science Part B: Polymer Physics, **41**, 1572–1577 (2003).
DOI: 10.1002/polb.10511

[21] Park S. H., Jo S. M., Kim D. Y., Lee W. S., Kim B. C.: Effects of iron catalyst on the formation of crystalline domain during carbonization of electrospun acrylic nanofiber. Synthetic Metals, **150**, 265–270 (2005).
DOI: 10.1016/j.synthmet.2005.02.010

[22] Jeong J. S., Jeon S. Y., Lee T. Y., Park J. H., Shin J. H., Alegaonkar P. S., Berdinsky A. S., Yoo J. B.: Fabrication of MWNTs/nylon conductive composite nanofibers by electrospinning. Diamond and Related Materials, **15**, 1839–1843 (2006).
DOI: 10.1016/j.diamond.2006.08.026

[23] Ra E. J., An K. H., Kim K. K., Jeong S. Y., Lee Y. H.: Anisotropic electrical conductivity of MWCNT/PAN nanofiber paper. Chemical Physics Letters, **413**, 188–193 (2005).
DOI: 10.1016/j.cplett.2005.07.061

[24] Ju Y-W., Choi G-R., Jung H-R., Lee W-J.: Electrochemical properties of electrospun PAN/MWCNT carbon nanofibers electrodes coated with polypyrrole. Electrochimica Acta, **53**, 5796–5803 (2008).
DOI: 10.1016/j.electacta.2008.03.028

[25] Vaisman L., Wachtel E., Wagner H. D., Marom G.: Polymer-nanoinclusion interactions in carbon nanotube based polyacrylonitrile extruded and electrospun fibers. Polymer, **48**, 6843–6854 (2007).
DOI: 10.1016/j.polymer.2007.09.032

[26] Prilutsky S., Zussman E., Cohen Y.: The effect of embedded carbon nanotubes on the morphological evolution during the carbonization of poly(acrylonitrile) nanofibers. Nanotechnology, **19**, 165603/1–165603/9 (2008).
DOI: 10.1088/0957-4484/19/16/165603

[27] Dror Y., Salalha W., Khalfin R. L., Cohen Y., Yarin A. L., Zussman E.: Carbon nanotubes embedded in oriented polymer nanofibers by electrospinning. Langmuir, **19**, 7012–7020 (2003).
DOI: 10.1021/la034234i

[28] Yeo L. Y., Friend J. R.: Electrospinning carbon nanotube polymer composite nanofibers. Journal of Experimental Nanoscience, **1**, 177–209 (2006).
DOI: 10.1080/17458080600670015

[29] Hou H., Ge J. J., Zeng J., Li Q., Reneker D. H., Greiner A., Cheng S. Z. D.: Electrospun polyacrylonitrile nanofibers containing a high concentration of well-aligned multiwall carbon nanotubes. Chemistry of Materials, **17**, 967–973 (2005).
DOI: 10.1021/cm0484955

[30] Qin X-H., Yang E-L., Li N., Wang S-Y.: Effect of different salts on electrospinning of polyacrylonitrile (PAN) polymer solution. Journal of Applied Polymer Science, **103**, 3865–3870 (2007).
DOI: 10.1002/app.25498

[31] Lin T., Wang H., Wang H., Wang X.: The effect of surfactants on the formation of fibre beads during the electrospinning of polystyrene nanofibres. in 'Polymer Fibres 2004, Meetings management' Manchester, UK, p4 (2004).

[32] Haghi A. K., Akbari M.: Trends in electrospinning of natural nanofibers. Physica Status Solidi A: Applications and Materials Science, **204**, 1830–1834 (2007).
DOI: 10.1002/pssa.200675301

[33] Seo J. M., Arumugam G. K., Khan S., Heiden P. A.: Comparison of the effects of an ionic liquid and triethylbenzylammonium chloride on the properties of electrospun fibers, 1-Poly(lactic acid). Macromolecular Materials and Engineering, **294**, 35–44 (2009).
DOI: 10.1002/mame.200800198

[34] Arumugam G. K., Khan S., Heiden P. A.: Comparison of the effects of an ionic liquid and other salts on the properties of electrospun fibers, 2-Poly(vinyl alcohol). Macromolecular Materials and Engineering, **294**, 45–53 (2009).
DOI: 10.1002/mame.200800199

[35] Mathew G., Hong J. P., Rhee J. M., Lee H. S., Nah C.: Preparation and characterization of properties of electrospun poly(butylene terephthalate) nanofibers filled with carbon nanotubes. Polymer Testing, **24**, 712–717 (2005).
DOI: 10.1016/j.polymertesting.2005.05.002

[36] Heikkilä P., Harlin A.: Parameter study of electrospinning of polyamide-6. European Polymer Journal, **44**, 3067–3079 (2008).
DOI: 10.1016/j.eurpolymj.2008.06.032

[37] Morton W. J.: Method of dispensing fluids. US Patent 705691, USA (1902).

[38] Baumgarten P. K.: Electrostatic spinning of acrylic microfibers. Journal of Colloid and Interface Science, **36**, 71–79 (1971).

[39] He J-H., Wan Y-Q., Yu J-Y.: Effect of concentration on electrospun polyacrylonitrile (PAN) nanofibers. Fibers and Polymers, **9**, 140–142 (2008).
DOI: 10.1007/s12221-008-0023-3

[40] Gu S. Y., Ren J., Wu Q. L.: Preparation and structures of electrospun PAN nanofibers as a precursor of carbon nanofibers. Synthetic Metals, **155**, 157–161 (2005).
DOI: 10.1016/j.synthmet.2005.07.340

[41] Gu S. Y., Ren J., Vancso G. J.: Process optimization and empirical modeling for electrospun polyacrylonitrile (PAN) nanofiber precursor of carbon nanofibers. European Polymer Journal, **41**, 2559–2568 (2005).
DOI: 10.1016/j.eurpolymj.2005.05.008

[42] Zussman E., Chen X., Ding W., Calabri L., Dikin D. A., Quintana J. P., Ruoff R. S.: Mechanical and structural characterization of electrospun PAN-derived carbon nanofibers. Carbon, **43**, 2175–2185 (2005).
DOI: 10.1016/j.carbon.2005.03.031

[43] Sutasinpromprae J., Jitjaicham S., Nithitanakul M., Meechaisue C., Supaphol P.: Preparation and characterization of ultrafine electrospun polyacrylonitrile fibers and their subsequent pyrolysis to carbon fibers. Polymer International, **55**, 825–833 (2006).
DOI: 10.1002/pi.2040

[44] Agend F., Naderi N., Fareghi-Alamdari R.: Fabrication and electrical characterization of electrospun polyacrylonitrile-derived carbon nanofibers. Journal of Applied Polymer Science, **106**, 255–259 (2007).
DOI: 10.1002/app.26476

[45] Saiyasombat C., Maensiri S.: Fabrication, morphology, and structure of electrospun PAN-based carbon nanofibers. Journal of Polymer Engineering, **28**, 5–18 (2008).

[46] Heikkilä P., Harlin A.: Electrospun nanofibres containing carbon nanotubes. in 'Autex 2008, 8th Annual World Textile Conference'Biella, Italy, p6 (2008).

Novel oligocarbosilazanes bearing promesogenic end groups

D. Grande[1], T. Ganicz[2], W. A. Stańczyk[2], N. Lacoudre[1], S. Boileau[1]*

[1]Equipe «Systèmes Polymères Complexes», Institut de Chimie et des Matériaux Paris-Est, CNRS-Université Paris XII, 2, rue Henri Dunant, 94320 Thiais, France
[2]Centre of Molecular and Macromolecular Studies, Polish Academy of Sciences, Sienkiewicza 112, 90-363 Lódź, Poland

Abstract. A series of novel oligomers with promesogenic groups on both termini were prepared by a hydrosilylation reaction between well-defined telechelic oligocarbosilazanes end-fitted with vinylsilane (SiVi) groups and promesogenic compounds containing one reactive hydrosilane (SiH) group. We investigated the correlations between the structure of the resulting mesogen end-capped oligomers and their phase behavior as examined by differential scanning calorimetry (DSC) and polarizing optical microscopy (POM).

Keywords: polymer synthesis, molecular engineering, telechelic oligomers, carbosilazane units, phase behavior

1. Introduction

The studies on oligomers with mesogenic chain-end groups are generally undertaken for two main reasons:

– to investigate the structure-property relationships, especially the dependence of liquid crystalline (LC) properties on the length of oligomeric linkages, and

– to obtain materials with relatively low molar mass which have reduced melt viscosity in a mesophase in comparison with traditional LC side-chain polymers, which is an important feature for many optoelectronic applications.

Current research in this area proved that many structures of intermediate molar mass (especially cyclic siloxanes) exhibit the fast electro-optical response characteristic for molar mass liquid crystals, and therefore they can find miscellaneous applications [1]. For many applications, such as LC displays, optical data storage materials, switches and shutters, linear, high molar mass materials exhibit too long response time, when supramolecular orientation is driven by changes in external electric or magnetic fields [2].

LC dimeric compounds with various organosilicon linkages are already well known [3]. Nevertheless, very few papers are concerned with intermediate molar mass systems based on mesogen end-capped oligomers, especially with organosilicon linkages. According to Allen *et al.* [4], the LC materials derived from mesogen-terminated oligodimethyl-siloxanes exhibit many interesting properties, among which the ability to generate biphasic materials with regularly distributed LC domains in a continuous amorphous phase.

The aim of this work was to prepare and characterize a series of telechelic organosilicon oligomers bearing the promesogenic groups on both chain-ends, and containing different linkages constituted of regularly distributed carbosil(ox)azane units.

*Corresponding author, e-mail: tg@bilbo.cbmm.lodz.pl

2. Experimental section

2.1. Materials

All syntheses were carried out under argon with exclusion of moisture. Solvents were distilled by standard methods and stored over a sodium mirror or molecular sieves. All substrates were used as received from suppliers.

The syntheses of SiH-containing mesogens were performed as reported elsewhere [5].

2.2. Synthesis of telechelic vinyl end-capped oligomers

The telechelic copolymers were synthesized by polyaddition *via* hydrosilylation using an excess of the divinyl-functionalized organosilicon monomers, according to a general procedure described previously [6]. Typically, an oligomer with an initial ratio $[SiH]_0/[SiVi]_0$ equal to 0.5 (oligomer 5, Table 1) was prepared as follows. In a flame-dried flask, 6.3 ml (25.30 mmol) of 1,4-divinyl-1,1,4,4-tetramethyldisilethylene, 2.2 ml (12.65 mmol) of 1,1,3,3-disilazane, and 8.5 ml of n-hexane were introduced *via* oven-dried syringes under argon. 27.5 µl ($3.16 \cdot 10^{-6}$ mol) of Karstedt's catalyst (PCO72 from ABCR, $1.15 \cdot 10^{-7}$ mol·µl^{-1}) were then added under stirring and argon at room temperature. The reaction medium was heated at 60°C for 24 h. The oligomer was recovered by several precipitations in methanol, and finally dried under vacuum to yield a colorless viscous oil-type material. Yield: 60%.

2.3. Synthesis of mesogen end-capped oligomers

The hydrosilylation reactions leading to the formation of oligocarbosilazanes bearing promesogenic end groups were performed following a procedure described previously with some minor changes [7]. In a typical experiment, 1 g (1.84 mmol) of mesogen B (see Figure 3), 1,1,3,3-tetramethyl-1-[5-(4′-undecyloxy-biphenyl-4-yloxy)-pentyl]-disiloxane) was dissolved in toluene (10 ml) in a flame-dried Schlenk tube equipped with an argon inlet. The telechelic oligomer 5 (see Table 1) (1 g, 1.66 mmol of Si-Vi end groups) and Karstedt's catalyst (PCO72 from ABCR, 10 µl of 3.5% solution in xylenes) were then added under argon, and the

reaction mixture was stirred at 60°C. The reaction was stopped after 24 h, and the solvent was removed under vacuum, yielding a yellowish solid. The oligomeric product was purified by multiple precipitations from dichloromethane/methanol, and finally dried under vacuum (75°C, 1 mmHg). Yield: 78%.

2.4. Physico-chemical techniques

^{1}H and ^{29}Si NMR spectra were recorded on a Bruker DRX spectrometer at resonance frequencies of 200 and 500 MHz respectively. FTIR spectra were obtained with a Perkin-Elmer 1760 spectrometer from 4000 to 450 cm^{-1}.

Differential scanning calorimetry (DSC) analyses were realized using a Perkin-Elmer DSC 4 calorimeter between –100 and 110°C, at heating and cooling rates of 10°C·min^{-1}. Phase transitions were examined by polarizing optical microscopy (POM). POM studies were performed on thin (50 µm) specimens sandwiched between two glass slides. The samples were preconditioned and heated with a Linkam THMS hot stage (Linkam Scientific Instruments Ltd., Epsom, UK) at a rate of 5°·min^{-1}. Relative intensity of light and digital images were recorded with a microscope (Polish Optical Works, Warsaw) and a CCD-4012A TV camera (Videotronic, Neumunster, Germany) using a PC computer for data acquisition and analysis.

3. Results and discussion

3.1. Preparation of starting oligomers with vinyl groups on both termini

Well-defined telechelic oligocarbosilazanes end-fitted with vinylsilane (SiVi) groups were first prepared by polyaddition *via* hydrosilylation using non-stoichiometric initial molar ratios of two reactive difunctional monomers, namely one deficient monomer with two hydrosilane (SiH) end groups and another one, used in excess, containing two Si-Vi terminal moieties (Figure 1).

By changing the nature of difunctional precursors (dicarbosilanes, disilazanes or disiloxanes), it was possible to obtain telechelic oligomers with different chemical structures in their main chains. This polymerization process provided a unique opportunity to generate alternating copolymers with car-
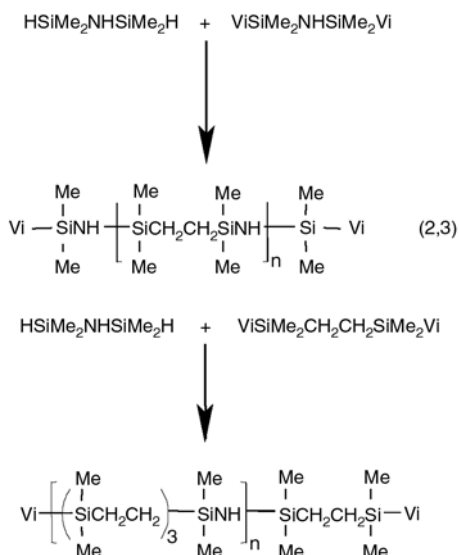
Figure 1. Synthesis of telechelic vinyl end-capped oligomers
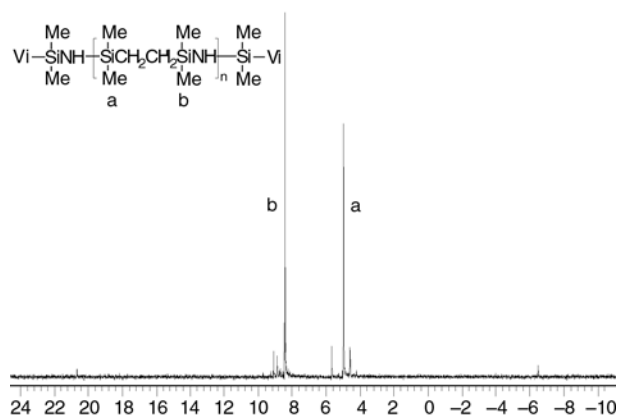
Figure. 2. ^{29}Si NMR (CDCl$_3$) spectrum of telechelic vinyl end-capped oligomer 3 (see Table 1)

bosilane, silazane, and/or siloxane units arranged in a very regular way. The regularity of the copolymer structure was proved by ^{29}Si NMR (Figure 2 as an example).

Additionally, the variation of the initial molar ratio of precursors allowed for the synthesis of oligomers with varying molar masses [6]. The nature and proportions of difunctional monomers, as well as the molar masses of the resulting divinyl-functionalized oligomers are given in Table 1.

3.2. Synthesis of mesogen end-capped oligomers

Two promesogenic compounds (A, B, Figure 3) containing one reactive SiH group were obtained by hydrosilylation of the corresponding alkene-terminated analogues with a large excess of commercially available tetramethyldisiloxane (HSiMe$_2$OSiMe$_2$H), as described previously [5]. The oligomers end-fitted with promesogenic groups were derived from the hydrosilylation reaction of divinyl-functionalized oligomers with SiH-containing mesogens. The reaction was monitored by FTIR, through the disappearance of the Si–H stretching band at 2130 cm^{-1}. The reaction conditions were typical for this type of process [7]. All the syntheses were carried out at 60°C in toluene under an inert atmosphere (Figure 3).
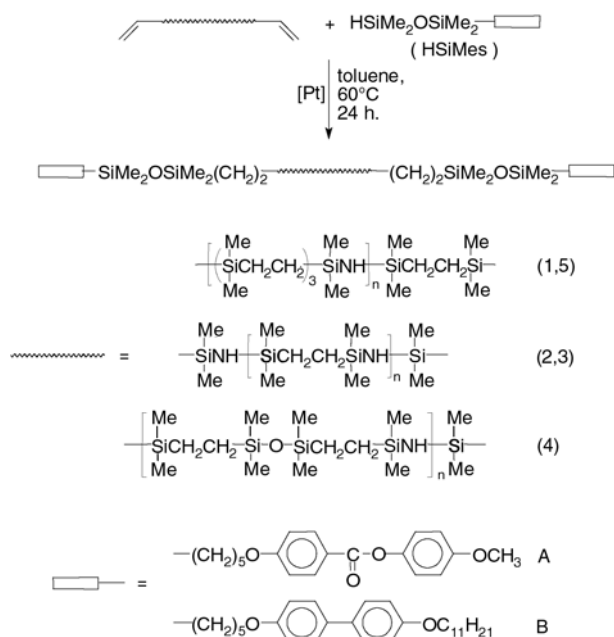
Figure 3. Synthesis of mesogen end-capped oligomers

Table 1. Structure and initial molar ratio (*r*) of precursor monomers and molar masses of divinyl-functionalized oligomers[a]

No.	SiH-ended monomer	SiVi-ended monomer	r = [SiH]$_0$/[SiVi]$_0$	M$_n^b$ (^{1}H NMR)
1	HSi(Me)$_2$NHSi(Me)$_2$H	Vi(Me)$_2$SiCH$_2$CH$_2$Si(Me)$_2$Vi	0.75	2200
2	HSi(Me)$_2$NHSi(Me)$_2$H	Vi(Me)$_2$SiNHSi(Me)$_2$Vi	0.75	2200
3	HSi(Me)$_2$NHSi(Me)$_2$H	Vi(Me)$_2$SiNHSi(Me)$_2$Vi	0.80	1500
4	HSi(Me)$_2$OSi(Me)$_2$H	Vi(Me)$_2$SiNHSi(Me)$_2$Vi	0.85	1900
5	HSi(Me)$_2$NHSi(Me)$_2$H	Vi(Me)$_2$SiCH$_2$CH$_2$Si(Me)$_2$Vi	0.50	1200

[a]Experimental conditions: solvent: n-hexane, *T* = 60°C, Karstedt's catalyst: PCO72, [Pt]$_0$/[SiH]$_0$ =2.5·10^{-4}

[b]Molar mass as determined by ^{1}H NMR using the ratio of intensities associated with resonance signals due to vinylic protons (5.6–6.4 ppm) from SiVi end groups and methylene protons (0.4 ppm) from carbosilane units of organosilicon skeleton
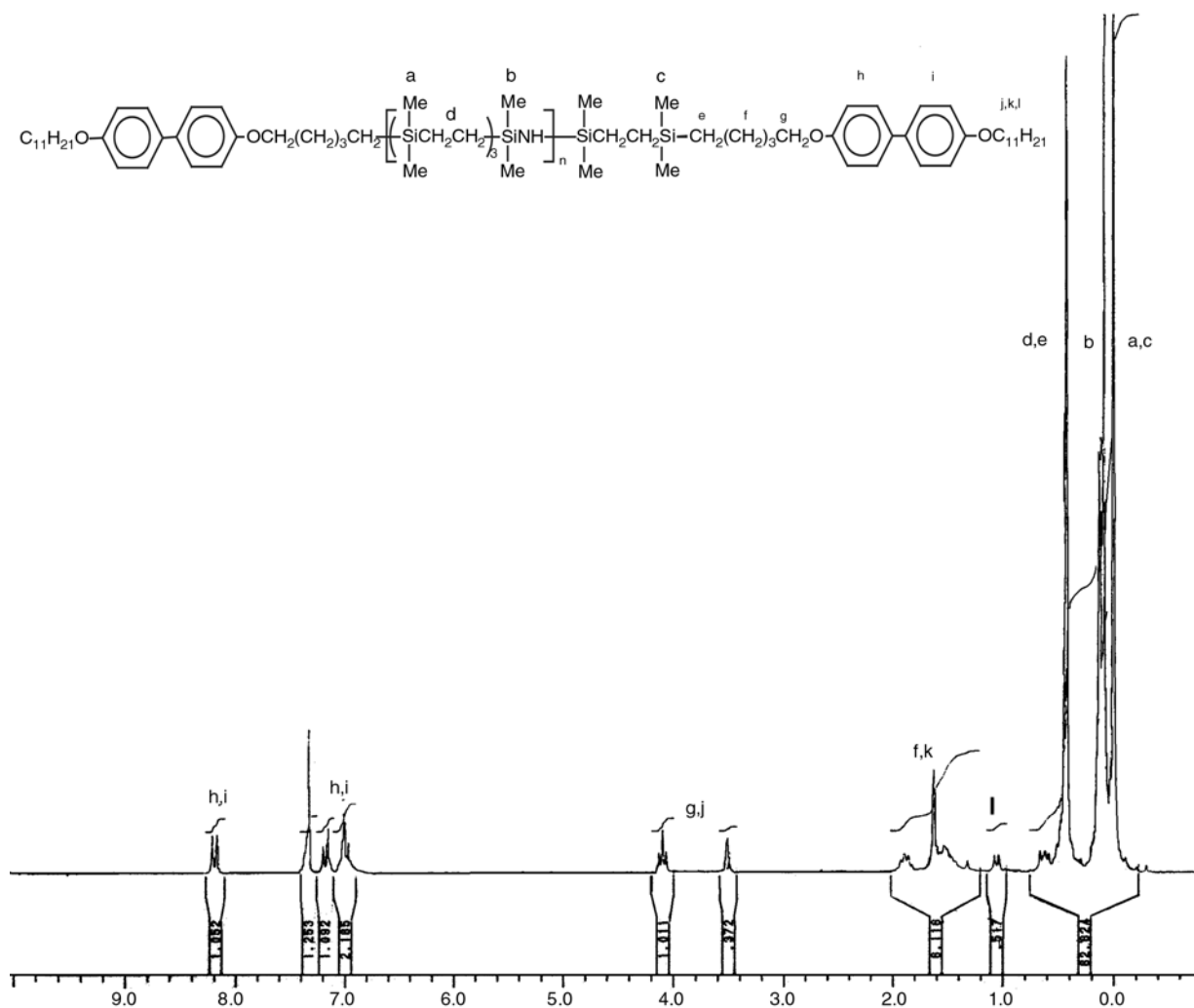
Figure 4. ¹H NMR (CDCl₃) spectrum of telechelic mesogen end-capped oligomer B5 (see Table 2)

In all instances, the reactions were completed within 24 h, and led to the formation of the desired products. The structures of the resulting mesogen-terminated oligomers were confirmed by ¹H (Figure 4 as an example) and ²⁹Si NMR.

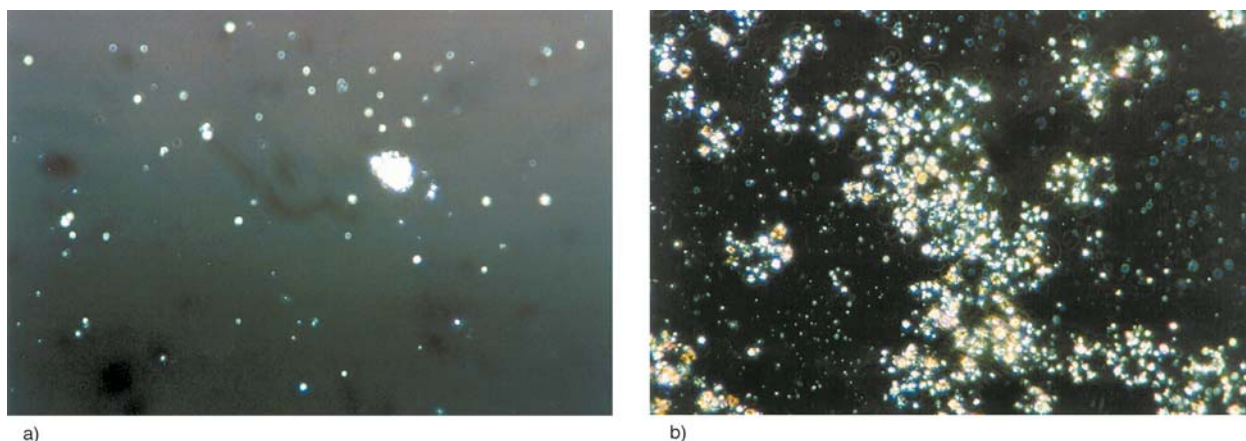## 3.3. Properties of mesogen end-capped oligomers

The mesomorphic properties of the telechelic oligocarbosil(ox)azanes end-capped by a promesogenic group were evaluated through DSC and POM analyses. The results of the studies are summarized in Table 2.

Table 2. Properties of telechelic oligomers end-capped by promesogenic groups

Starting oligomers			MesSiH	Resulting oligomers			
No.	M_n [g/mol]	T_g [°C]	No.[a]	No.	T_g [°C]	other phase transitions [°C]	microscopic observations
1	2200	–69	A	A1	–61	none	isotropic liquid
			B	B1	–58	none	birefringent droplets disappearing at 77°C
2	2200	–82	A	A2	–65	none	isotropic liquid
			B	B2	–63	none	birefringent droplets disappearing at 72°C
3	1500	–77	A	A3	nd	none	isotropic liquid
4	1900	–89	B	B4	–83	K –37 M(?) 84 I (heating) none (cooling)	birefringent droplets disappearing at 85°C
5	1200	–81	B	B5	–63	K –40 M(1) 35 M(2) 57 I (heating) I 57 M(2) 45 M(1) (cooling)	various LC-like textures seen in the whole volume of the sample

nd: not detected, K: crystal, M(?), M(1), M(2): possible mesophases of unknown nature, I: isotropic
[a]Temperature transitions of starting vinyl-terminated mesogens (in °C): A: K 56 N 74 I [8], B: K 89 SmA 141 I (according to POM and DSC analyses)

Figure 5. POM micrographs of mesogen end-capped oligomers: (a) B1 at 23°C; (b) B2 at 23°C
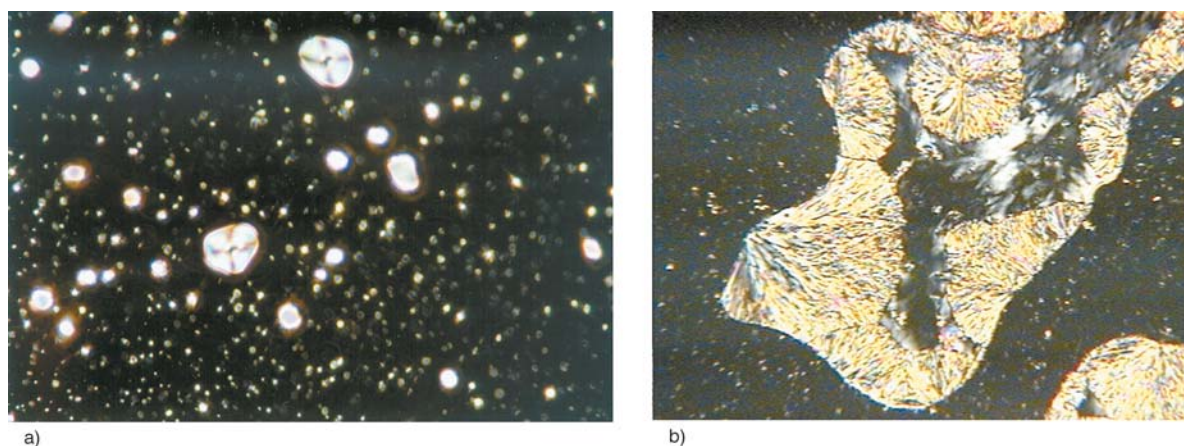
Figure 6. POM micrographs of mesogen end-capped oligomers: (a) B4 at 63°C; (b) B5 at 37°C

Birefringent droplets of LC-like textures were observed only for the products based on mesogen B. In contrast, judging from DSC and microscopic studies, oligomers containing mesogen A (compounds A1, A2 and A3, Table 2) did not exhibit any mesomorphic properties. Although both starting mesogens exhibit LC properties in a free form [8, 9], it was previously found that mesogen A, when attached as a side chain to polymers with relatively low molar ratio of functional units, produced materials with poor or even no LC properties [5, 7, 8]. Therefore, during the course of our research, we directed our attention to mesogen B which was reported to be more effective in systems with a low degree of functionalization [7, 9].

In the case of samples B1 and B2, small birefringent droplets 'dissolved' in an amorphous phase were observed by POM (Figure 5).

The birefringent droplets underwent isotropization at 72–77°C, which was well-visible in microscopic images. However, there were no signals corresponding to these typical phase transitions in the DSC traces.

The oligomers B4 and B5 were characterized by shorter carbosil(ox)azane linkages than those of B1 and B2, and therefore possessed higher contents of promesogenic groups within their structure. Thus, they displayed much higher 'density' of the birefringent droplets, and exhibited weak transition peaks on DSC thermograms, corresponding to phase transitions observed by microscopy (Figure 6). In the case of sample B5, the droplets were of such a large size that the internal change of their textures at 37°C could be observed by POM, which was in accordance with the DSC analysis (Figure 7).

4. Conclusions

The phase behavior of telechelic oligocarbosil(ox)azanes end-capped by a promesogenic group seems to depend on two main parameters, namely the
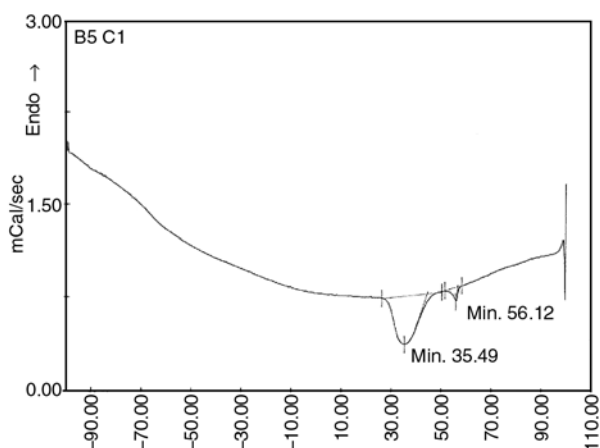
Figure 7. DSC thermogram (on cooling) of mesogen end-capped oligomer B5

structure of the promesogenic precursor and the molar mass of the starting oligomer.

It turns out that the most relevant parameter is the structure of promesogenic entities, although the molar mass of oligomeric linkages is also an important factor, strongly influencing the phase behavior of mesogen-terminated oligomers.

None of the materials containing mesogen A exhibited birefringence, regardless of the structure and length of the oligomeric linkages used. However, the oligomers based on mesogen B displayed birefringent droplets, whose size increased with decreasing the length of the carbosilazane linkages. These novel mesogen end-capped oligocarbosil(ox) azanes should be more thoroughly investigated by complementary techniques, such as X-ray diffraction, in order to characterize precisely their mesophases and to get a better insight into their potential liquid crystalline properties.

Acknowledgements

References

[1] Robinson W. K., Carboni C., Kloess P., Perkins S. P., Coles H.: Ferroelectric and antiferroelectric low molar mass organosiloxane liquid crystals. Liquid Crystals, **25**, 301–307 (1998).
DOI: 10.1080/026782998206092

[2] Ponomarenko S. A., Agina E. V., Boiko N. I., Rebrov E. A., Muzafarov A. M., Richardson R. M., Shibaev V. P.: Liquid crystalline carbosilane dendrimers with terminal phenyl benzoate mesogenic groups: Influence of generation number on phase behaviour. Molecular Crystals and Liquid Crystals, **364**, 93–100 (2001).
DOI: 10.1080/10587250108024979

[3] Ganicz T., Stańczyk W. A., Bialecka-Florjańczyk E., Śledzińska I.: Liquid crystal dimers with organosilicon spacers as models for side chain LC polymers. Polymer, **40**, 4733–4739 (1999).
DOI: 10.1016/S0032-3861(98)00673-9

[4] Allen R. C., Wilkes G. L., Yilgor I., Wu D., McGrath J. E.: Synthesis and characterization of poly(dimethylsiloxane) based liquid crystals. Die Makromolekulare Chemie, **187**, 2909–2931 (1986).
DOI: 10.1002/macp.1986.021871217

[5] Ganicz T., Stańczyk W. A.: Synthesis of novel tripodal mesogenic alkenes and side-chain polysiloxanes. Journal of Organometallic Chemistry, **689**, 2606–2613 (2004).
DOI: 10.1016/j.jorganchem.2004.05.019

[6] Jallouli A., Lestel L., Tronc F., Boileau S.: Polycarbosilanes containing siloxy and/or silanamine units by polycondensation using hydrosilylation. Macromolecular Symposia, **122**, 223–228 (1997).

[7] Ganicz T., Pakula T., Fortuniak W., Bialecka-Florjańczyk E.: Linear and hyperbranched liquid crystalline polysiloxanes. Polymer, **46**, 11380–11388 (2005).
DOI: 10.1016/j.polymer.2005.10.052

[8] Mauzac M., Hardouin F., Richard H., Archard M. F., Sigaud G., Gasparoux H.: Effect of the chemical constitution of the side-chain on the formation and the structure of mesophases in some polysiloxanes. European Polymer Journal, **22**, 137–144 (1986).
DOI: 10.1016/0014-3057(86)90108-4

[9] Itoh M., Lenz R. W.: Side-chain liquid crystalline polymers with silphenylene-siloxane main chains. II. Preparation and characterization of polymers containing biphenyl mesogens. Journal of Polymer Science Part A: Polymer Chemistry, **29**, 1407–1419 (1991).
DOI: 10.1002/pola.1991.080291005

eXPRESS
Polymer Letters

Amorphous and crystalline phase interaction during the Brill transition in nylon 66

Y. Wolanov, A. Y. Feldman, H. Harel, G. Marom*

Casali Institute of Applied Chemistry, The Institute of Chemistry, The Hebrew University of Jerusalem, 91904 Jerusalem, Israel

Abstract. A prominent α' process in specifically treated nylon 66 and microcomposite samples is identified by dynamic mechanical analysis and proposed to be an amorphous phase counterpart of the Brill transition identified by synchrotron wide-angle X-ray diffraction (WAXD). It is suggested that this α' process, which marks a critical free volume change and an onset of segmental chain movement in the amorphous phase, precedes and prompts the Brill transition in the crystalline phase.

Keywords: *thermal properties, Brill transition, α' relaxation*

1. Introduction

The existence of certain associations between second and first order transitions in polymers is by now a proven fact. Many examples exist in the literature, of which the most prominent is the fact that a constant ratio exists between the glass transition temperature in the amorphous phase and the melting point. By and large, for polymers that are free from side groups (so called symmetrical) this ratio (T_g/T_m) is ~0.5, whereas for most of the common vinyl, vinylidene and condensation polymers the ratio is ~0.66 [1]. Another example comes from the solid state crystallization process where the crystallization temperature T_c is directly related to T_g. In this particular example, the relation between the second to the first order transition is causative, wherein the occurrence of the latter is consequent to the first, resulting from the necessity of sufficient free volume, attained at T_g, to allow chain segmental movement and crystallization. Two examples of our own studies are shown here. The first, describes

an investigation of the effect of the cooling rate of a quenching process on the structure of glycolic acid (GA) and lactic acid (LA) [2]. The second, investigated the effect of quenching on the degree of crystallininity in carbon fibre-reinforced poly(ether ether ketone) (PEEK) composites. [3].

The bilateral phase interaction can also work in the opposite direction so that structural changes in the crystalline phase influence the morphology of the amorphous one. An appropriate example from our own research is of high density polyethylene (HDPE), which in its pristine form exhibits a single second order transition, namely, T_g. However, after undergoing a certain solid state crystallization stage, which results in crystalline restructuring, the same HDPE exhibits an untypically immense β transition in the amorphous phase [4, 5].

In the present study we deal with yet another first order transition, namely the Brill transition in polyamides (e.g., nylon 66), for which a counterpart transition in the amorphous phase is explored.

The Brill transition, discovered in 1942 [6], is a sharp reversible polymorphic phase transition, from the triclinic to the pseudo-hexagonal structure at 162°C. It is preceded by gradual crystallographic changes, occurring over a relatively wide temperature range and entailing dimensional changes of the triclinic crystallographic unit cell, wherein the room temperature spacings of 0.44 nm (d_{100}) and 0.37 nm ($d_{010/110}$) are shifted to lower and higher values, respectively. At the transition point the two diffraction maxima are replaced by one with a spacing of 0.42 nm [6–8]. Over the years since its discovery, the Brill transition has been studied for various types of even-even and odd-even polyamides [9–13] and for different crystallization conditions [10].

In a recent study on the Brill transition in transcrystalline nylon 66 we pointed out that the explanation for the effect of the crystalline structure on this first order transition must be based on the existence of reciprocal interactions between the crystalline and amorphous phases [14], which corresponded to the finding that structural changes within the crystalline domains in the lamellae (as in the Brill transition) are accompanied by changes in the packing of the amorphous chain segments outside the lamellae [15]. According to the scientific literature, nylon 66 exhibits three loss peaks, labeled α, β and γ (see e.g., [16–18]), representing different processes in the amorphous phase. Perhaps the only reference to an additional peak (shoulder) was made by Takayanagi in his study of nylon 6 [19]. Because this shoulder was most prominent for specimens with maximum crystallinity it was ascribed to a relaxation process involving the *crystalline* regions and was attributed to a crystal structure change from monoclinic to hexagonal [20]. This is taken by us as strong evidence for the assumption that the Brill transition in the crystalline phase is preceded or even triggered by a second order process in the amorphous phase. Accordingly, the present study has been undertaken in order to identify such a process that can be correlated with the Brill transition.

2. Experimental

2.1. Materials

Nylon 66 pellets were obtained from Nilit, Israel (M_w = 325 000 and M_n = 16 800).

Aramid fibers, Kevlar 49 (Du-Pont 1420 denier yarn) were used as reinforcement.

2.2. Sample preparation

Films of approximately 100 μm thickness were prepared by pressing the pellets at 290°C under minimal pressure for 20 min in a hydraulic press (Carver 2518), followed by isothermal treatment at 250°C for 3–8 h in the press followed by slow cooling.

Unidirectional microcomposites of nylon 66 reinforced by aramid fibers and displaying a transcrystalline layer (tcl) were prepared according to the procedure published in [21]. The condition ranges were similar to those used for the films. A fully developed tcl was observed with 3 h isothermal treatment at 250°C followed by ice-water quenching.

2.3. In situ WAXD

Synchrotron microbeam wide-angle X-ray diffraction (WAXD) measurements were performed at the European Synchrotron Radiation Facility (ESRF) on the Materials Science Beamline (ID-11). The X-ray microbeam was monochromated at a wavelength of λ = 0.4876 Å and collimated to dimension 2 μm (vertical) by 4 μm (horizontal). The exposure time for each sample varied from 20 to 30 s. Samples were inserted into 1 mm diameter Li-glass capillaries and mounted inside a hot stage (Linkam Scientific Instruments, THMS600, Waterfield, UK). The distance between the sample and the detector was set at approximately 143 mm. Each sample was scanned during heating at different heating rates, from 25 to 400°C. Data were taken at 5 or 10°C intervals. The one-dimensional diffraction profiles were calculated from the two-dimensional X-ray diffraction patterns using the image analysis programs Fit2D (ESRF, Dr. Hammersley).

2.4. Dynamic mechanical analysis (DMA)

Thermomechanical properties were investigated by dynamic mechanical analysis. A TA Instruments (New Castle, DE) DMA, model 983 was used to measure the transition temperatures. All samples (of the dimensions 10×6×0.1 mm³) were tested at fixed frequency mode under shear stress. The tem-

perature was scanned from 25–220°C at a heating rate of 5°C/min, recording simultaneously the real and the imaginary components of the shear modulus and tanδ. The microcomposite specimens were loaded along the fiber axis.

3. Results and discussion

The essential changes that occur at the Brill transition are expressed clearly by 2D WAXD images below and above the transition temperature T_B, an example of which is presented in Figure 1 (scanned at a heating rate of 15°C/min). The typical features in the diffraction patterns are the clear 100 and 010/110 diffraction rings of the triclinic phase below T_B and the 'shifted 100' diffraction ring of the pseudo-hexagonal phase above it. For the detection of the Brill transition, a series of such 2D diffraction patterns obtained during synchrotron WAXD in situ measurements can then be processed to produce 3D representations of the diffraction profiles as a function of temperature. The results for the nylon 66 films isothermally treated at 250°C are presented in Figure 2 for heating in the temperature range from 25 to 220°C. For this particular material the Brill transition temperature is determined to be T_B = 175°C.

The values of T_B can be determined by measuring the *d* spacings for the 100 and 010/110 diffraction maxima, shown in Figure 2, and plotting them as a

function of temperature as presented in Figure 3; T_B is the intercept of the two curves. It is noted that the point at 175°C (in Figure 3) represents the merging
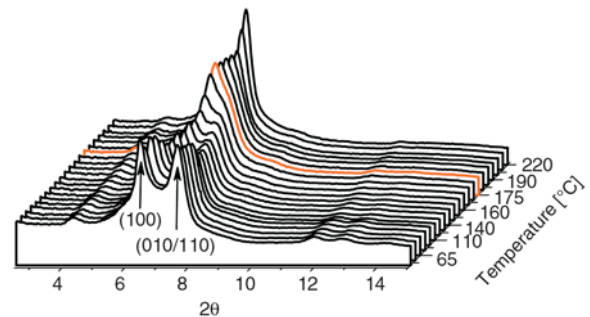
Figure 2. Three-dimensional representation of X-ray diffraction profiles of a nylon 66 film during heating at a rate of 15°C/min from 25 to 220°C
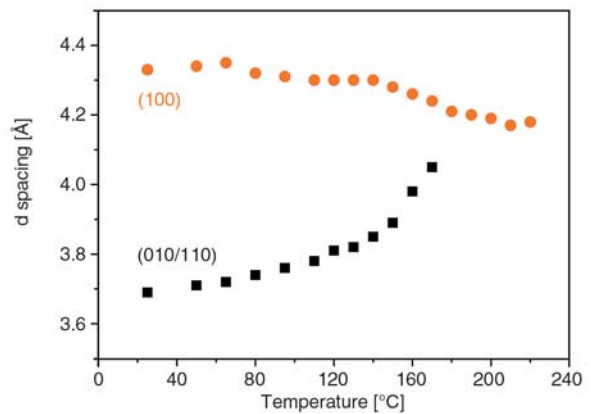
Figure 3. Temperature dependence of the *d* spacings of the 100 and 010/110 diffraction maxima of a nylon 66 film
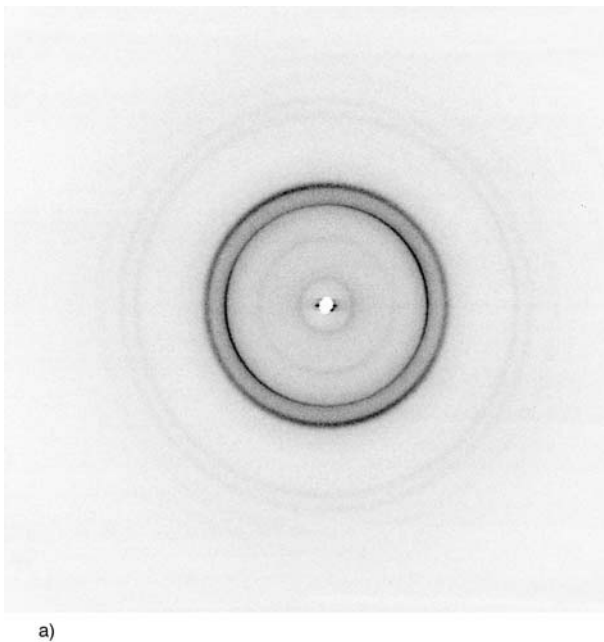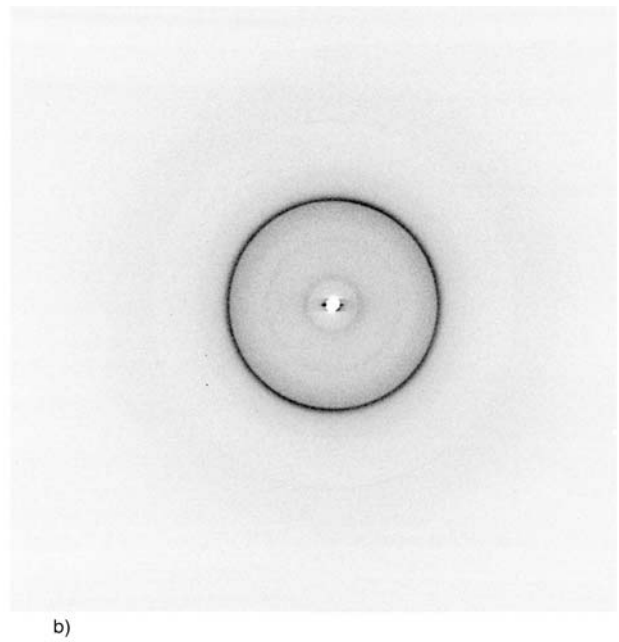
Figure 1. 2D WAXD images of a nylon 66 film, at (a) 65 and (b) 210°C, below and above the Brill temperature

of the 010/110 and 100 *d* spacings. Alternatively, T_B can be determined by plotting the arithmetic difference between these two *d* spacings of the triclinic cell (designated the index of chain packing, ICP) against temperature and extrapolating the linear region to ICP equals zero (not shown here) [14]. Looking at Figure 3 again, it is apparent that whereas the change in the *d* spacings with temperature of the 100 diffraction is relatively gradual and small (with a few minor fluctuations), that of the 010/110 diffraction is characterized by a two step behavior. Over the first step, at the lower temperature range, the spacing change with temperature is minimal. Then at around 130°C a marked change is observed, followed by a steeper increase from approximately 3.8 to 4.2 Å at T_B.

Assuming that this sharp change marks a critical free volume change and an onset of segmental chain movement in the amorphous phase, it was reasonable to assume that if a second order counterpart transition of the Brill transition existed it should be found at around this temperature. Accordingly, a range of nylon 66 samples and microcomposites [22] was prepared under different crystallization conditions and then subjected to DMA measurements. The DMA traces by and large revealed the typical three transitions α, β and γ, however, in a small number of specific cases, limited only to samples with a history of a long crystallization treatment, a clear α′ peak was observed. Particularly, a prominent α′ peak was observed for the microcomposites. It is well known that aramid fiber reinforced nylon 66 composites transcrystallize in such a way that a transcrystalline layer invades the whole space between the fibers and replaces most of the bulk crystallinity [23]. The amplification of the α′ peak can then be associated with the transcrystalline structure, similar to the β peak in HDPE [5].

Two examples of samples that exhibit an apparent α′ peak are shown in Figure 4. It is noted that the microcomposite in Figure 4b exhibits a clear split α process, wherein the glass transition is followed by a separate smaller process. The α′ process reaches its maximum at 110°C for the pure nylon 66 and at 125°C for the microcomposite, which correspond to the sharp tilt at around 130°C observed in the *d* spacings for the 010/110 diffraxtion maxima of the triclinic crystalline phase in Figure 3. This is considered as strong evidence that the α′ process in
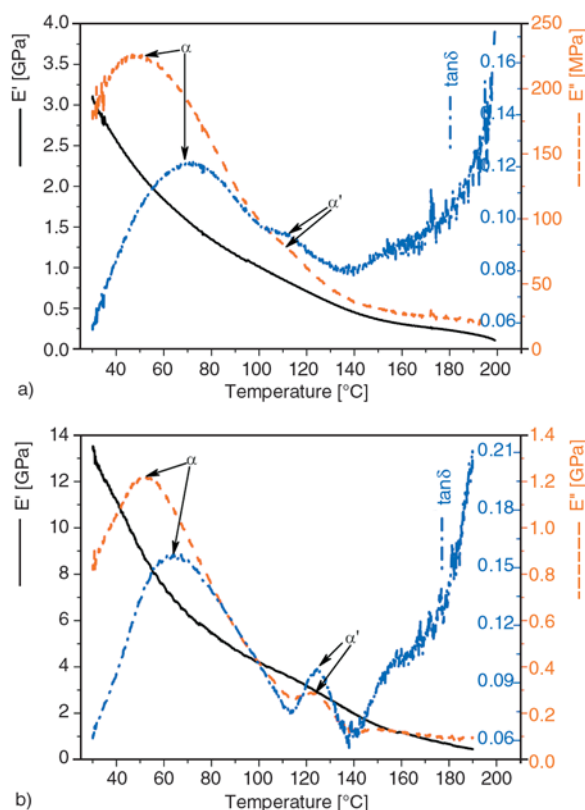
Figure 4. DMA traces of: (a) nylon 66 (250°C/5 h, slow cooling) and (b) microcomposite transcrystalline nylon 66 (250°C/3 h, quenching) films

the amorphous phase with its associated chain mobility permits the onset of movement of the 010/110 triclinic crystalline planes until the pseudo-hexagonal structure is attained at T_B. This conclusion is supported by an overview of transition phenomenon in nylon 6 [24], stating that the Brill transition is observed between 80–170°C and claiming that this transition cannot be detected usually by DMA, for an especially long annealing period at a high temperature (220°C/60 h) where an α′ relaxation at 170°C is observed. It is interesting to note that that study [24] claimed that the 'α′ relaxation was associated with the mobility of interfacial amorphous phase which requires crystal mobility as a precursor', which is the reverse order of the causative relation suggested in our study. We maintain, however, that the causative relation aught not to be determined on the basis of a temperature comparison of the α′ relaxation and T_B. Rather, it is determined by the relation between the α′ relaxation and the temperature of the sharp tilt in the *d* spacings of the 010/110 diffraction which precedes T_B.

4. Conclusions

The change in the *d* spacings with temperature of the 010/110 diffraction, which precedes the Brill transition, is characterized by a two step behavior. The step change is characterized by a sharp tilt followed by a steep increase of the *d* spacing all the way to the Brill transition temperature. It is claimed that this step change reflects a critical free volume change and an onset of segmental chain movement in the amorphous phase. Dynamic mechanical analysis identified in specifically treated nylon 66 and microcomposite samples a prominent α′ process, which corresponds to this step change. Hence, the observed α′ relaxation and the Brill transition are taken as counterparts, wherein the occurrence of the first triggers that of the latter.

Acknowledgements

References

[1] Sperling L. H.: Introduction to physical polymer science. John Wiley and Sons, Hoboken (2006).

[2] Cohn D., Younes H., Marom G.: Amorphous and crystalline morphologies in glycolic acid and lactic acid polymers. Polymer, **28**, 2018–2022 (1987).
DOI: 10.1016/0032-3861(87)90035-8

[3] Tregub A., Harel H., Marom G., Migliaresi C.: The influence of thermal history on the mechanical properties of poly(ether ether ketone) matrix composite materials. Composites Science and Technology, **48**, 185–190 (1993).
DOI: 10.1016/0266-3538(93)90135-4

[4] Pegoretti A., Ashkar M., Migliaresi C., Marom G.: Relaxation processes in polyethylene fibre-reinforced polyethylene. Composites Science and Technology, **60**, 1181–1189 (2000).
DOI: 10.1016/S0266-3538(00)00024-5

[5] Alon Y., Marom G.: On the ß transition in high density polyethylene: The effect of transcrystallinity. Macromolecular Rapid Communication, **25**, 1387–1391 (2004).
DOI: 10.1002/marc.200400185

[6] Brill R.: Behavior of polyamides on heating (in German). Journal für Praktische Chemie, **161**, 49–64 (1942).
DOI: 10.1002/prac.19421610104

[7] Brill R.: Relations between the structures of polyamides and silk fibers (in German). Zeitschrift für Physikalische Chemie, B **53**, 61–74 (1943).

[8] Sandeman I., Keller A.: Crystallinity studies of polyamides by infrared, specific volume and X-ray methods. Journal of Polymer Science, **19**, 401–435 (1956).
DOI: 10.1002/pol.1956.120199303

[9] Jones N. A., Atkins E. D. T., Hill M. J., Cooper S. J., Franco L.: Chain-folded lamellar crystals of aliphatic polyamides. Comparisons between nylons 4 4, 6 4, 8 4, 10 4, and 12 4. Macromolecules, **29**, 6011–6018 (1996).
DOI: 10.1021/ma9603490

[10] Jones N. A., Atkins E. D. T., Hill M. J., Cooper S. J., Franco L.: Chain-folded lamellar crystals of aliphatic polyamides. Investigation of nylons 4 8, 4 10, 4 12, 6 10, 6 12, 6 18 and 8 12. Polymer, **38**, 2689–2699 (1997).
DOI: 10.1016/S0032-3861(97)85603-0

[11] Jones N. A., Atkins E. D. T., Hill M. J.: Comparison of structures and behavior on heating of solution-grown, chain-folded lamellar crystals of 31 even-even nylons. Macromolecules, **33**, 2642–2650 (2000).
DOI: 10.1021/ma9919559

[12] Li W., Huang Y., Zhang G., Yan D.: Investigation on Brill transition of nylons 6/16, 4/16 and 2/16 by variable-temperature WAXD and FTIR. Polymer International, **53**, 1905–1908 (2003).
DOI: 10.1002/pi.1267

[13] Cui X., Yan D.: Preparation, characterization and crystalline transitions of odd-even polyamides 11, 12 and 11,10. European Polymer Journal, **41**, 863–870 (2005).
DOI: 10.1016/j.eurpolymj.2004.10.045

[14] Feldman A. Y., Wachtel E., Vaughan G. B. M., Weinberg A., Marom G.: The Brill transition in transcrystalline nylon-66. Macromolecules, **39**, 4455–4459 (2006).
DOI: 10.1021/ma060487h

[15] Murthy N. S., Wang Z-G., Hsiao B. S.: Interactions between crystalline and amorphous domains in semi-crystalline polymers: Small-angle X-ray scattering studies of the Brill transition in nylon 6,6. Macromolecules, **32**, 5594–5599 (1999).
DOI: 10.1021/ma990475e

[16] Klein N., Marom G., Pegoretti A., Migliaresi C.: Determining the role of interfacial transcrystallinity in composite materials by dynamic mechanical thermal analysis. Composites, **26**, 707–712 (1995).
DOI: 10.1016/0010-4361(95)91137-T

[17] Nuriel H., Kozlovich N., Feldman Y., Marom G.: The dielectric properties of nylon 66/aramid fibre microcomposites in the presence of transcrystallinity. Composites Part A: Applied Science and Manufacturing, **31**, 69–78 (2000).
DOI: 10.1016/S1359-835X(99)00050-0

[18] Nuriel H., Klein N., Marom G.: The effect of the transcrystalline layer on the mechanical properties in the fibre direction of composite materials. Composites Science and Technology, **59**, 1685–1690 (1999).
DOI: 10.1016/S0266-3538(99)00026-3

[19] Takayanagi M., Harima H., Iwata Y.: Viscoelastic behavior of polymer blends and its comparison with model experiments. Reports on Progress in Polymer Physics (in Japanese), **6**, 121–125 (1963).

[20] McCrum N. G., Read B. E., Williams G.: Anelastic and dielectric effects in polymeric solids. John Wiley and Sons, London, 478–500 (1967).

[21] Feldman A., Gonzalez M. F., Wachtel E., Moret M. P., Marom G.: Transcrystallinity in aramid and carbon fiber reinforced nylon 66: Determining the crystallographic structure by synchrotron X-ray micro diffraction. Polymer, **45**, 7239–7245 (2004).
DOI: 10.1016/j.polymer.2004.08.027

[22] Wagner H. D., Rubins M., Marom G.: The significance of microcomposites as experimental models. Polymer Composites, **12**, 233–236 (1991).
DOI: 10.1002/pc.750120404

[23] Klein N., Wachtel E., Marom G.: The microstructure of nylon 66 transcrystalline layers in carbon and aramid fibre reinforced composites. Polymer, **37**, 5493–5498 (1996).
DOI: 10.1016/S0032-3861(96)00361-8

[24] Khanna Y. P.: Overview of transition phenomenon in nylon 6. Macromolecules, **25**, 3298–3300 (1992).
DOI: 10.1021/ma00038a043

Effects of synthesis conditions on chemical structures and physical properties of copolyesters from lactic acid, ethylene glycol and dimethyl terephthalate

M. Opaprakasit[1], A. Petchsuk[2], P. Opaprakasit[3], S. Chongprakobkit[4]*

[1]Department of Materials Science, Faculty of Science, Chulalongkorn University, Bangkok, 10330 Thailand
[2]National Metal and Materials Technology Center, Thailand Science Park, Pathumthani 12120 Thailand
[3]Department of Common and Graduate Studies, Sirindhorn International Institute of Technology (SIIT), Thammasat University, Pathumthani 12121 Thailand
[4]Nanoscience and Technology Program, Chulalongkorn University, Bangkok, 10330 Thailand

Abstract. Lactic acid/ethylene terephthalate copolyesters were synthesized by the standard melt polycondensation of lactic acid (L), ethylene glycol (EG) and dimethyl-terephthalate (DMT). Effects of reaction temperatures and types of catalysts on the structures and properties of the copolymers were examined. In addition, feasibility of promoting the copolymerization process by a novel synthesis step of using thermo-stabilizers was investigated. The results show that a reaction temperature of higher than 180°C is necessary to produce copolymers with appreciable molecular weight. However, degradation was observed when the reaction temperature is higher than 220°C. Triphenyl phosphate (TPP) shows promising results as a potential thermo-stabilizer to minimize this problem. It was found that Sb_2O_3 and Tin(II) octoate are most effective among 4 types of catalysts employed in this study. ^{1}H-NMR results indicate that copolymers have a random microstructure composed mainly of single L units alternately linked with ET blocks at various sequential lengths. The longer ET sequence in the chain structure leads to the increase in melting temperature of the copolymer. TGA results show that the resulting copolymers possessed greater thermal stability than commercially-available aliphatic PLA, as a result of the inclusion of T (terephthalate) units in the chain structure.

Keywords: biodegradable polymers, poly(lactic acid), poly(ethylene terephthalate), aliphatic aromatic copolyester, polymer synthesis

1. Introduction

Global warming is regarded as the most important and serious environmental issue. The major cause of this problematic phenomenon is the rapid increase in the release of greenhouse gases to the atmosphere as a result of high petroleum consumption. From the polymer science point of view, this issue is related to the rapid increase in consumption of petroleum-based commodity plastics, which are mostly non-degradable. In the past, the typical

method for disposing of these plastic wastes was landfills. However, reduction in the number of landfill sites presently causes an accumulation of tremendous amounts of plastic waste. Alternatively, polymer recycling, i.e., mechanical recycling and energy recycling have been employed. This method, in turn, causes deterioration in physical properties of the recycled products, and emits some toxic products and greenhouse gases from incineration. Therefore, (bio)degradable plastics

have been taken into consideration to reduce the impact of plastic waste on the environment. Moreover, polymers synthesized from renewable resources have been considered more sustainable than the conventional ones to overcome a shortage and the high cost of petroleum sources.

During the past two decades, more than 16 million kilograms of (bio)degradable polymers have been commercialized per year, of which 80% were used in loose-fill packaging applications. Other applications included compost bags, agricultural mulch films, paper coating, medical applications, and hygienic products [1]. Commercially available (bio)degradable polymers are classified into three groups: polyolefin/additives, starch blends, and polyesters [2]. Among these, aliphatic polyesters have received the most attention due to their (bio)degradability and versatile physical, mechanical, and biological properties. Susceptibility of carboxyl groups in the main chain of aliphatic polyesters to hydrolysis is well known. The common example of these materials is poly(lactic acid) or polylactide (PLA).

PLA is the most popular material among aliphatic polyesters due to its environmentally friendly properties. Its monomer, lactic acid, is derived from fermentation of agricultural products such as starch or sugar. In addition, high molecular weight PLA is proven as a biocompatible material with mechanical properties comparable to other commodity plastics, e.g., PE, PS and PP. In contrast, aromatic polyesters such as poly(ethylene terephthalate) (PET) have been reported as non-degradable materials [3]. Their physical properties, however, are much better than those of their aliphatic counterparts. This fact has initiated an idea of combining the degradability of aliphatic polyesters and the superior mechanical properties of aromatic polyesters to achieve novel copolyesters. This concept has been employed in improving degradability of PET [4–10], poly(propylene terephthalate) (PPT) [10–12], Poly(butylene terephthalate) (PBT) [10, 13–14], and poly(1,2-propanediyl phthalate) (PPP) [15] by incorporating diols and/or diacids into their main chains. The results revealed that the degradation rate of the resulting copolymers was influenced by the content of aromatic constituents [10, 13], chemical structures, i.e., random, block or alternating structure, solid state structure (semi-

crystalline or amorphous), and chain mobility [14]. For example, copolyester derived from butanediol, adipic acid, and terephthalic acid under a trade name Ecoflex® is claimed to have good mechanical properties and a fully biodegradable property with minimum toxicological effect on the environment [16].

Many reports in the literature have focused on aliphatic-aromatic copolyesters derived from petroleum-based monomers. Only a small number of studies on copolyesters based on renewable lactic acid have been reported [17–20]. Olewnik and co-workers reported that a degradable poly(lactic acid-co-ethylene terephthalate) can be synthesized from lactic acid and PET-glycolized products [19–20]. However, to our knowledge, limited information on the effect of reaction conditions on the properties and microstructures of the synthesized copolymers is available in the literature.

In this communication, we report results on the synthesis and characterization of poly(lactic acid-co-ethylene terephthalate) from lactic acid and dimethyl terephthalate monomers, and ethylene glycol. Although the standard method of polycondensation is employed in the synthesis, this work attempts to enhance the synthesis reaction by focusing on effects of reaction conditions on the chemical structure and properties of the copolyesters; especially reaction temperature and time, type of catalysts, and the stoichiometry of the comonomer feed. Additionally, a novel synthesis step of employing thermo-stabilizers in the reaction to enhance the extent of reaction at high temperature will be discussed.

2. Experimental

2.1. Materials

Lactic acid (88% wt aqueous solution) and ethylene glycol were purchased from Carlo Erba. Dimethyl terephthalate was supplied by Acros. p-Toluene sulfonic acid (PTSA), Titanium(IV) tetra(n-butoxide) Ti(OBu)$_4$, Antimony trioxide (Sb$_2$O$_3$) and Triphenyl phosphate (TPP) were obtained from Sigma-Aldrich. Tin(II) octoate and tin chloride were provided by Wako Chemicals and Fluka, respectively. Irganox-1076 and Zn-stearate were supplied by Ciba Specialty Chemicals. All chemicals were used without purification.

2.2. Synthesis of lactic acid/ethylene terephthlate copolymers

Copolymers were synthesized via polycondensation reaction by using lactic acid (LA) and monomers of PET, i.e., dimethyl terephthlate (DMT) and ethylene glycol (EG). Effects of reaction temperature and time were first investigated. Essentially, DMT, LA and 0.5% wt of Tin(II) octoate catalyst were added into a round bottom flask equipped with condenser, nitrogen gas inlet, thermometer and vacuum line. The mixture was kept isothermally at 160°C for a certain time after DMT was completely melted. EG was then added and the temperature was raised stepwise and kept isothermally between 180 and 220°C. Isothermal time at each temperature increment was varied in reaction batches no.1–4, as indicated in Table 1. A 1:1:1 molar ratio of LA, DMT, and EG was used unless other composition is indicated.

Effects of different types of thermo-stabilizers (i.e., Irganox-1076, Zn-stearate, and TPP), and catalysts (i.e., Tin chloride with PTSA, Ti(OBu)₄, and Sb₂O₃) on the extent of polymerization reaction were also investigated by keeping a constant content of thermo-stabilizers and catalysts at 0.1% and 0.5% by weight of comonomers, respectively. The optimum reaction temperature and time obtained from batch no.4 was employed in these successive reactions (batches no.5–11).

2.3. Characterizations of lactic acid/ethylene terephthlate copolymers

2.3.1. Gel Permeation Chromatography (GPC)

Molecular weight of the as-synthesized copolyesters was examined by a Waters 150CV, using THF as a solvent with a flow rate of 1 ml/min. Mono-dispersed polystyrenes were used as standard materials for constructing a calibration curve.

2.3.2. ^{1}H-NMR spectroscopy

Chemical and sequential structures of copolyesters were determined by 300 MHz ^{1}H-NMR analysis on a Bruker DPX300 spectrometer using chloroform-d as a solvent and TMS reference, with a repetition delay of 2 seconds. For copolyesters insoluble in chloroform, chloroform-d/trifluoroacetic acid mixed solvent was employed.

Assuming the exclusion of side reactions, the possible sequential structures of copolyesters obtained in this work are illustrated in Figure 1. The chemical shift and assignments of proton signals observed in NMR spectra are shown in Figure 2. The average length of ET and L sequences, $X_{(ET)}$ and $Y_{(L)}$, in the copolymers can be calculated according to Grzebieniak *et. al.* [17, 18] from the integrals of the signals LT (~5.33 ppm), LL (~5.16 ppm), TET (~4.66 ppm), and TEL (~4.52 ppm) (Equations (1) and (2)):

$$Y_{(L)} = (LL/LT) + 1 \tag{1}$$

$$X_{(ET)} = (TET/TEL) + 1 \tag{2}$$

Table 1. Effects of reaction temperature and time on reaction yield [%], molecular weight, chemical structure, and transition temperatures of the as-synthesized copolyesters

| Batch No.	Yield [%]	Reaction time [hr] at			Molecular weight[a] (10⁻³)		Sequential length[b]		Number-average sequential length[b]		T/L ratio[b]	B[b]	Transition temperatures [°C]	
		180°C	200°C	220°C	M_n	M_w	$Y_{(L)}$	$X_{(ET)}$	$L_{n,L}$	$L_{n,ET}$			T_g	T_m (ΔH_m [J/g])
1	75	1	–	–	0.3	0.6	N/A	N/A	N/A	N/A	N/A	N/A	N/A	N/A
		5	–	–	0.7	0.9	N/A	N/A	N/A	N/A	N/A	N/A	N/A	N/A
		7	–	–	0.8	1.1	1.7	1.9	1.4	4.1	1.5	0.96	–	119,134
2	66	1	4	–	1.6	2.1	1.3	2.4	1.4	4.4	1.6	0.95	9.6	149.4 (5)
3	N/A	1	2	2	1.7	2.3	N/A	N/A	N/A	N/A	N/A	N/A	N/A	N/A
	70	1	2	4	3.3	5.4	1.2	2.9	1.9	5.1	1.3	0.71	52.2	173.2 (10)
4[c]	58	1	2	4	6.7	12.4	1.2	2.9	1.3	5.2	1.9	0.94	48.1	176.6 (2)

[a]Results from GPC experiments

[b]Calculated from ^{1}H-NMR spectra

[c]After holding the temperature at 220°C for 1 hour, an equivalent molar of EG to DMT was added to ensure an adequate amount of EG remained in polymerization reaction
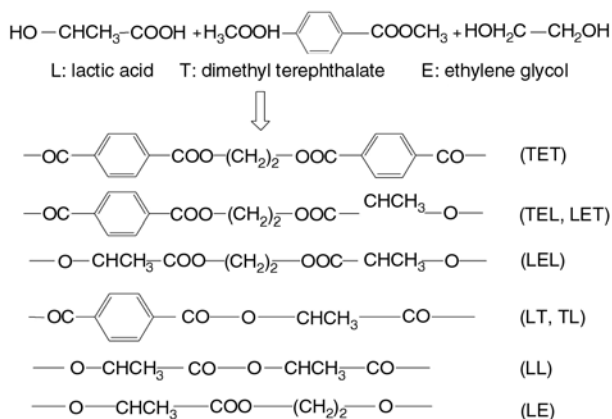
Figure 1. Possible E-centered triads and diads of the resulting copolyesters
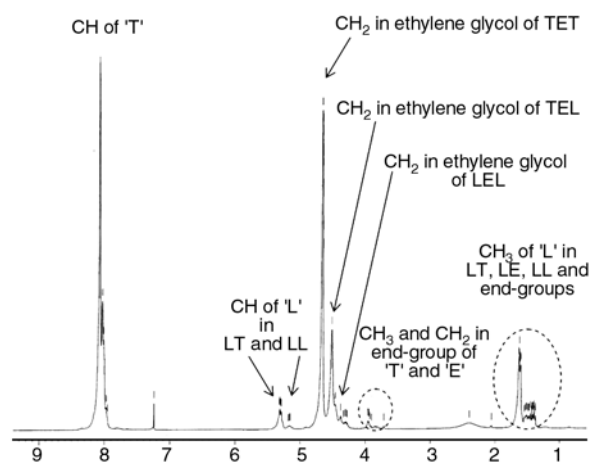
Figure 2. ^{1}H-NMR spectrum of as-received copolyester obtained from batch no.4 and its signal assignments

In Olewnik *et al.* [19], results on chemical and sequential structure of copolyesters synthesized from lactic acid and bis(2-hydroxyethyl terephthalate) (BHET) by employing NMR spectra were reported. The authors extensively discussed proton assignments of the resulting poly(lactic acid-co-terephthalate). Furthermore, number-average molar mass (M_n), degree of randomness (B), T/L ratio, and number-average number of ET and L units in the copolyester chains ($L_{n,ET}$ and $L_{n,L}$) were also calculated [19, 21]. Although, copolyesters synthesized in our work are derived from different monomers used in Olewnik *et al.* [19], the NMR spectra of our copolymers show signals associated with all possible E-centered triads and diads in 3.5–5.5 ppm region. This indicates that the copolymers are consisting of all similar possible connections to those synthesized from lactic acid and

BHET [19]. Therefore, the calculation method was adopted in this work. However, the relative integration of these signals varies with the synthesis conditions in our work. This reflects that the microstructure of the copolyesters can be controlled by using lactic acid, ethylene glycol and DMT as monomers, and varying synthesis conditions.

2.3.3. Differential Scanning Calorimetry (DSC)

DSC thermograms were recorded by employing a Mettler Toledo DSC822^e. First and second heating thermograms were collected from samples of 10–15 mg. The sample was heated from –20 to 200°C at a rate of 10°C/min. After the 1st heating scan, the sample was cooled to –10°C at a rate of 10°C/min. Glass transition temperature (T_g), melting temperature (T_m), and heat of melting (ΔH_m) were derived from the 2nd heating thermograms.

2.3.4. Thermogravimetric Analysis (TGA)

Thermo-stability of the copolyesters was characterized by a Mettler Toledo TGA/SDTA 851 under oxygen atmosphere. Samples of 10–15 mg were heated from 50 to 1000°C at a rate of 20°C/min.

2.3.5. Reduced viscosity

Reduced viscosity of the copolyesters was determined at 25°C using a 0.2g/dl solution in a 7% trichloroacetic acid/chloroform mixed solvent. The solutions were freshly prepared and measured to prevent the possibility of copolymer degradation.

2.3.6. Solubility test

Solubility of copolymers was determined by dissolving 0.5 g of samples in 10 ml of chloroform or a trichloroacetic/chloroform mixed solvent at room temperature. The solubility is indicated by number of '+'. Essentially, the samples were first dissolved in chloroform. If a complete dissolution is achieved within 10 minutes at ambient temperature, solubility is rated as '+++'. For samples taken longer time to completely dissolve in chloroform, the solubility was measured in a trichloroacetic acid/chloroform mixed solvent. The rating of '++' and '+' indicates

that the samples are fully dissolved in 2% (w/w) and 5% of trichloroacetic acid/chloroform mixed solvent within 10 minutes, respectively.

3. Results and discussion
3.1. Effects of reaction temperature and time

Effects of reaction temperature and time on the extent of polymerization, chemical structure, and transition temperatures of the copolyesters, using a typical Tin(II) octoate catalyst, were conducted in batches no.1–4. The results are shown in Table 1, where average molecular weights derived from GPC experiments and chemical structure parameters; including T/L ratio, degree of randomness (B) and sequential length of ET and L examined from ^{1}H-NMR using the methods of Grzebieniak *et al.* [17, 18], Olewnik *et al.* [19], and Tessier and Fradet [21] are compared. The results clearly indicate that number and weight average molecular weights of the copolyesters are strongly dependent on reaction temperature. Results from batches no.1–3 show that higher molecular weight copolymers were obtained at higher polymerization temperatures, when similar reaction time was employed. The drastic increase in molecular weight of copolyesters observed in batches no.2–4 compared to that of batch no.1 indicates that a reaction temperature higher than 180°C is required in order to successfully synthesize high molecular weight material at a practical reaction time.

An attempt to use a reaction temperature higher than 220°C was conducted, but a serious degradation of the copolyesters was observed, where darker color product was produced. Therefore, the reaction condition used in batch no.3, i.e., reaction temperature of 180 to 200 and 220°C with total reaction time of 7 hours, was employed as optimum conditions for successive batches. Copolymer with M_w of 5.4·10[3] g/mole and reduced viscosity of 0.12 dl/g was obtained in this batch. It was speculated that some EG might be removed along with the removal of condensed water and methanol molecules during the reaction when the reaction temperature higher than 200°C was employed. This leads to a lowering of EG content in the mixture and, hence, inhibits the polymerization in reaching a higher extent. To prove this hypothesis, the reaction in batch no.4 was carried out by employing a similar reaction temperature and time to that of

batch no.3, but an additional amount of EG (1 equivalent molar to DMT) was introduced into the reaction flask after a certain time at 220°C. This results in an increase in M_w (approximately twofold compared to that of batch no.3). Since the copolymers from these two batches were synthesized using similar reaction conditions, this clearly provides good evidence that a non-stoichiometric effect is the origin of the lower molecular weight materials obtained in batch no.3. Furthermore, the addition of the excess EG employed in batch no.4 also affects the T/L ratio of the resulting copolyesters, where a much higher ratio was obtained. The reason for this is probably because EG acts as diol that is required for incorporating diacids (DMT) into the copolymer chain. Therefore, the T content of the chain is promoted when EG composition in the reaction is maintained.

NMR spectra of copolyesters obtained from batches no.1–4 are shown in Figures 3a–d, respectively. The presence of proton signals of LT (~5.33 ppm) and TEL (~4.52 ppm) sequences provides a good evidence for linkages of lactic acid and ethylene terephthalate groups, indicating a successful production of lactic acid-co-ethylene terephthalate structure. Additionally, the spectra show significant difference in intensities of signals
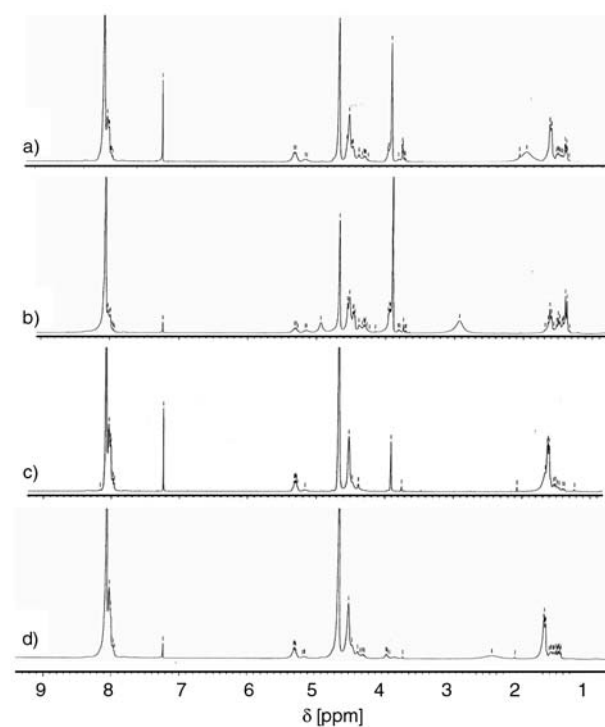
Figure 3. ^{1}H-NMR spectra of as-received copolyesters obtained from batches no.1 (a), no.2 (b), no.3 (c), and no.4 (d)

located between 3.7 and 4.0 ppm, especially the peak at ~3.9 ppm. These signals originate from the CH_2 proton in E end-groups and CH_3 proton in DMT and T end-groups (~3.93 ppm). The intensities of these peaks decrease from spectrum 3a to 3d, indicating a decrease in the number of chain-ends. This agrees with results obtained from GPC experiments that the average molecular weight of the copolymers increase as a result of increasing reaction temperature and time and the addition of excess amounts of ethylene glycol. It should be noted that a drop in intensity of the signal at 3.93 ppm is also possibly related to the decrease of residue DMT in the mixture, which also indicates a higher extent of polymerization.

The chemical structures of copolymers synthesized as a function of reaction conditions are unveiled by the degree of randomness (B) and the number-average sequential length of ET and L ($L_{n,ET}$ and $L_{n,L}$), as shown in Table 1. The B values of copolymers obtained from batches no.1, 2 and 4 are approaching the value of 1, indicating a production of random copolymers regardless of the polymerization conditions. The corresponding values of $X_{(ET)}$, $L_{n,ET}$, $Y_{(L)}$ and $L_{n,L}$ imply that the chain structure of these copolyesters consists of a longer ET sequence, compared to LL sequence. Also, the values indicate that the sequential length of ET in the copolymers is much more sensitive to the synthesis conditions than that of its LL counterpart. In addition, the results suggest that a longer block of ET can be obtained by employing more severe reaction conditions.

The $Y_{(L)}$ and $L_{n,L}$ values, which indicate the probability of finding L next to another L unit, of copolyesters obtained from batches no.1–4 (as also shown in Table 1) are close to the minimum value of 1, indicating a low probability of finding L to L linkage. This implies that almost all L units are separately linked to ET units or ET blocks (various lengths) in the copolymer chains. It should be noted that the addition of excess EG, which results in an increase in average molecular weight of the copolymer, has no significant effect on the sequential length of ET, as evidenced from the results of batches no.3 and 4.

Results on glass transition temperature (T_g) and melting temperature (T_m) of the copolymers from batches no.1–4 are also presented in Table 1. Single T_g, whose position is predominantly influenced by

the molecular weight of copolyesters, is observed in all samples, i.e., higher T_g is observed in samples with a lower number of end-groups (higher M_n). Melting peaks located at unusually low temperature and low values of ΔH_m were observed in samples from batches no.1 and 2. This is probably due to the melting of domain consisting of short-chain oligomers that possess chemical structures resembling BHET (T_m~106–109°C), and DMT residue (T_m~145°C). Although T_m of samples from batches no.3 and 4 is much higher, it is not comparable to that of neat PET (~255°C). This is probably because crystallizable portions of the copolymer chain are largely due to ET sequence. An inclusion of L units therefore interrupts the chain's ET sequence, which in turn leads to the lowering of T_m of the copolyesters.

3.2. Effect of thermo-stabilizers

As mentioned earlier, a higher extent of polymerization can be achieved by increasing the synthesis temperature. However, degradation also competes strongly at higher temperature, noticeable by the yellowish color of the samples. It is speculated that a thermo-stabilizer is able to minimize degradation at the high reaction temperature. Therefore, this hypothesis is investigated by employing various types of thermo-stabilizers, i.e., Irganox-1076, Zn-stearate, and Triphenyl phosphate (TPP), as the first two compounds are common antioxidants in polymer processing, while TPP is usually employed as thermal stabilizer in the synthesis of commercial PET. A typical Tin(II) octoate was also used as a catalyst. Efficiency of these stabilizers in enhancing the synthesis reaction is examined by comparing the results with those obtained from copolymer of batch no.4, where no stabilizer is added.

Table 2 summarizes properties of the copolymers synthesized from reactions conducted by similar conditions without and with the use of various thermo-stabilizers. We first discuss the effects of thermo-stabilizers on the copolymers molecular weight. As copolymers obtained from these batches of reactions are hardly soluble in any common solvents, GPC cannot be employed as a primary technique in measuring the molecular weight. Alternately, relative molecular weights are examined by comparing the copolymers reduced viscosity in trichloroacetic acid/chloroform mixed solvent. It

Table 2. Effects of thermo-stabilizers on reaction yield [%], chemical structure and physical properties of the copolymers synthesized using tin(II) octoate as a catalyst

Batch No.	Thermo-stabilizer	Yield [%]	Reduced viscosity [dl/g]	Solu-bility	M_n (10^{-3})	Sequential length		Number-average sequential length		T/L ratio	B	Transition temperatures [°C]	
						$Y_{(L)}$	$X_{(ET)}$	$L_{n,L}$	$L_{n,ET}$			T_g	T_m $(\Delta H_m$ [J/g])
4	–	58	0.16	+++	3.5	1.2	2.9	1.3	5.2	1.9	0.94	48.1	176.6 (2)
5	Irganox	50	0.17	++	2.3	1.2	3.2	1.5	6.3	2.1	0.84	53.2	174.9 (20)
6	Zn-stearate	50	0.13	+	1.2	1.4	2.6	1.7	5.1	1.5	0.78	44.2	169.0 (18)
7	TPP	56	0.17	+	1.6	1.3	3.4	1.4	7.0	2.6	0.87	41.9	182.4 (20)
8[a]	TPP	58	0.13	+	3.6	1.2	3.2	1.2	5.9	2.4	0.99	50.3	190.9 (24)

[a]Thermo-stabilizer was added into the reaction prior to raising the temperature to 200°C. In other batches, thermo-stabilizer was introduced after a completion of the reaction step at 200°C.

should be noted that the employment of strong acid such as trichloroacetic acid or trifluoroacetic acid as a mixed solvent for ET-based (co)polymers may result in end-groups modification, as reported by Kenwright and coworkers [22] that these strong acids slowly reacted with hydroxyl end-groups by esterification. The authors, however, observed no polymers degradation when the strong acids were employed. Given this finding, our measurement of reduced viscosity was carefully conducted by using freshly-prepared solutions with minimum amount of the acids (~7%). The reduced viscosity, however, shows no correlation between the molecular weight and the thermo-stabilizers efficiency, as opposed to that observed in NMR results. This is probably because of the low sensitivity of the technique. Molecular weight calculated from NMR spectra shows that samples from batches no.5–7 had significantly lower M_n than that of batch no.4, implying that the addition of these additives impedes the polymerization reaction. Besides inhibiting the reaction, the addition of these thermo-stabilizer also affect the copolymer microstructure. This is evidenced from the degree of randomness (B) values of lower than 1 of copolymer from batches no.5–7, indicating block structure and a much longer (average) sequential length of ET and L, compared to other batches (see Table 2). Interestingly, the M_n value of copolymer from batch no.8, where TPP was applied as thermo-stabilizer prior to raising the temperature to 200°C, is higher than that of batch no.7, where the stabilizer was added after completion of a reaction step at 200°C, and that of batch no.4, where no stabilizer was added. T_g and T_m values of copolymer obtained form batch no.8 are also higher than those of no.4,

indicating larger molecules. The appearance of the resulting copolymers (lighter color) also reflects the inhibition of the competing degradation during the polymerization. Given similar reaction conditions used in these reactions, the results indicate that TPP acts efficiently as a thermo-stabilizer for poly(lactic acid-co-ethylene terephthalate) when the reagent is added at an early stage of reaction at low temperature.

3.3. Effect of catalysts

To further improve the efficiency of the synthesis reaction, various types of catalysts were employed in the reaction batches no.9–11, i.e. Tin chloride with PTSA, $Ti(OBu)_4$ and Sb_2O_3. These catalysts were selected because the first two are commonly used in polycondensation of PLA, and Sb_2O_3 is a common catalyst for the synthesis of commercial PET. The results are then compared with that of batch no.4, where the typical Tin(II) octoate was used. The properties of the resulting copolymers are summarized in Table 3. The results on M_n, chemical structure, and transition temperatures of all copolymers from batches no.4, 9–11 are strongly dependent on catalytic systems. The reduced viscosity results, however, are significantly comparable, which is not correlated with M_n values calculated from NMR spectra, as a result of the low sensitivity of the technique. Nonetheless, it can be interpreted from the degree of randomness that random structure (B~1) is obtained when copolymers are synthesized beyond a moderate value of M_n (~2000) regardless of the types of catalysts. It can be concluded that among the three types of novel catalysts employed in this study,

Table 3. Effects of catalyst systems on reaction yield [%], chemical structure and physical properties of the copolymers

Batch No.	Catalyst	Yield [%]	Reduced viscosity [dl/g]	Solu-bility	M_n (10^{-3})	Sequential length		Number-average sequential length		T/L ratio	B	Transition temperatures [°C]	
						$Y_{(L)}$	$X_{(ET)}$	$L_{n,L}$	$L_{n,ET}$			T_g	T_m $(\Delta H_m$ [J/g])
4	Tin (II) octoate	58	0.16	+++	3.5	1.2	2.9	1.3	5.2	1.9	0.94	48.1	176.6 (2)
9	PTSA, Tin chloride	56	0.16	+++	2.1	1.2	2.3	1.1	7.7	3.4	1.01	35.3	–
10	Ti(OBu)$_4$	58	0.14	+	1.6	1.3	2.8	1.7	5.2	1.5	0.78	24.9	163.9 (13)
11	Sb$_2$O$_3$	60	0.13	+	4.5	1.2	3.2	1.2	5.8	2.6	1.03	52.4	185.1 (17)

Sb$_2$O$_3$ provides higher efficiency in producing copolymers with higher M_n and T_m, compared to the commonly-used Tin(II) octoate catalyst.

3.4. Chemical structure, thermal properties, and solubility

Grzebieniak reported that physicochemical properties of ethylene terephthalate/lactic acid copolyesters are dependent on the length of ET and L sequences [17]. The authors concluded that the length of ET and L sequence in the copolymers was dependent on the synthesis approach, in which the values increased in ascending order when synthesis reaction were changed from melt-polycondensation (approach I) to trans-esterification of PET and L-lactide (approach II) and to trans-esterification of PET and PLA (approach III), respectively. As a consequence, copolymers from approach I and II can dissolve easier in organic solvents, such as chloroform. The authors also reported that samples synthesized from approach I showed lower T_m and lower heat of melting (ΔH_m), compared to those of crystallized samples from approach II. Additionally, the authors observed that samples obtained from approach III exhibited a longer sequence of ET and L, which therefore resulted in a lowering of solubility of the materials in chloroform, but an increase in their crystallisability and T_m.

In this study, a similar synthesis procedure to that of approach I was employed, and copolymers obtained from batches no.3–4 show nearly identical $X_{(ET)}$ and $Y_{(L)}$ values to those reported by Grzebieniak [17]. Similar T_m and solubility in chloroform are also observed in these samples. Our copolymers synthesized from the novel synthesis procedure, however, showed an intriguing solubility property. The materials from batches no.5–8, synthesized in the presence of thermo-stabilizers, are now hardly

dissolved in chloroform (see Table 2), despite having comparable lengths of ET and L to the copolymers from approach I [17]. This reflects that the differences in the copolymer solubility cannot be simply explained by the difference in $X_{(ET)}$ and $Y_{(L)}$ values, but other factors may also play an important role in controlling the physicochemical properties of these copolymers. By carefully examining further results on T/L ratio, B, $L_{n,ET}$, and $L_{n,L}$, it is also unlikely to consistently correlate these individual parameters to the copolymer solubility. This non-correlation is also observed when different catalysts were employed in batches no.9–11 (as summarized in Table 3).

The T_g of samples from batches no.4–8 is observed at the temperature ranging from 42 to 53°C. This is significantly lower than the 62–67°C values reported by Grzebieniak [17], which is not surprising as the copolymers obtained here have lower molecular weight. Nonetheless, T_m of these samples is in the same range and depends strongly on the average length of ET ($X_{(ET)}$ and $L_{n,ET}$). These findings demonstrate that crystallization of the copolymers is possible when a suitable length of ET sequence is met. Moreover, the molecular weight imposes much smaller influence on the T_m than the chemical structure when the molecular weight is beyond a certain value. Interestingly, ΔH_m of copolymers from batches no.5–8 is remarkably higher than that of batch no.1–4 and that of approach I's samples [17]. It is speculated that this higher amount of crystalline phase is because the thermo-stabilizers act as a nucleating agent in the nucleation step of crystallization. Differences in crystalline content of these two groups of materials, therefore, results in the difference in their solubility.

As mentioned previously, solubility of the copolyester cannot be easily predicted from the parame-

ters collected from NMR spectra. It should be noted that this property is, however, correlated to or in good agreement with ΔH_m of the copolymers. A good solubility in chloroform is only observed in copolymers incapable of crystallization. This implies that information on $X_{(ET)}$ and $L_{n,ET}$ values is insufficient to provide in-depth information on crystallization behavior of the copolymers, but is satisfactory to use for interpreting or predicting their T_m.

3.5. Thermal stability of as-synthesized copolyesters

The effects of synthesis conditions, thermo-stabilizers, and catalysts on the thermal stability of the copolymers were investigated by employing TGA experiments. The thermograms of corresponding copolymers reported in Tables 1–3 are demonstrated in Figures 4–6, respectively. The thermograms are presented in comparison with those of commercial PET (acquired from the Nestle® drinking water bottle) and Cargil Dows' PLLA ($M_n \sim$ 100 K). From the insets of Figures 4–6, it is clearly shown that most of the copolymers synthesized in this work have lower on-set decomposition temperature than that of the commercial polymers. This is probably due to thermal degradation of the low molecular weight fraction of the copolymers. Intriguingly, more than 90% composition of the synthesized copolyesters has greater thermal stability than the high MW aliphatic PLLA. At a temperature near 415°C, PLLA is completely decomposed, while the relative mass of the copolyesters from batches no.2–11 and the commercial PET remains at about 65%. This implies that at least 65% composition of the copolyesters exhibits thermal stability comparable to PET.

Figures 5–6 show TGA thermographs of samples from batches no.4–11. Details on the initial stage of thermal degradation, as shown in the insets, indicate that only the samples from batches no.8 and 11 have better thermal stability than material from batch no.4. This is in good accord with M_n results obtained from NMR spectra. It is therefore concluded that M_n results are better representations for relative molecular weight of copolymers than the reduced viscosity. This also proves that the method used to calculate M_n reported by Olewnik *et al.* [19] is suitable for application in this copolymer system.
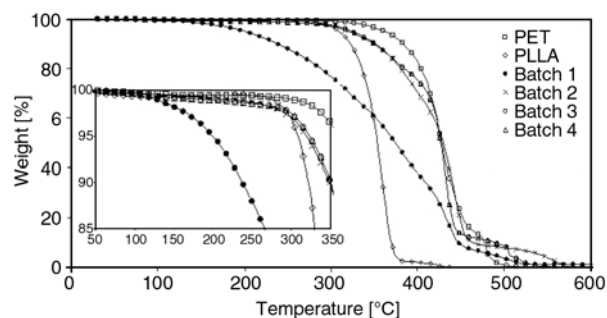

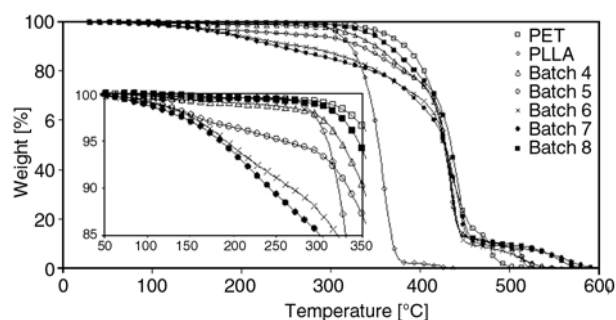**Figure 4.** TGA thermograms of copolymers batches no.1–4, PET, and PLLA

Figure 5. TGA thermograms of copolymers batches no.4–8, PET, and PLLA
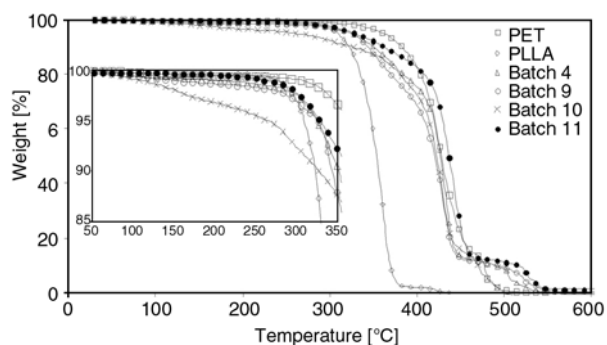

Figure 6. TGA thermograms of copolymers batches no.4, 9–11, PET, and PLLA

4. Conclusions

Lactic acid/ethylene terephthalate copolymers are synthesized by polycondensation of lactic acid, DMT, and EG. Effects of reaction conditions on the molecular weight of the copolymers, or the extent of polymerization were first investigated. In the synthesis reactions using Tin(II) octoate as a catalyst, low molecular weight copolymer was obtained when the reaction was carried out at 180°C. The molecular weight of copolymers can be enhanced by increasing reaction temperatures and employing excess amounts of EG to DMT. However, degradation was observed at 220°C. This can be avoided when TPP is applied as a thermo-stabilizer at an early stage of polymerization. The results on effects

of catalysts on the efficiency of the reaction indicated that among 4 types of catalysts employed in this study, Sb_2O_3 and Tin(II) octoate are potentially suitable for this reaction, as these yield copolymers with the highest molecular weight.

Reaction conditions also have remarkable effect on chain structure and properties of the copolyesters. This is evidenced by T/L ratio, degree of randomness, and the average length of ET and L sequence ($X_{(ET)}$, $L_{n,ET}$, $Y_{(L)}$ and $L_{n,L}$) results. All resulting copolymers show T/L ratio values of higher than 1, regardless of the initial equimolar of DMT/lactic acid. Additionally, random-structure characteristic (B~1) was observed in copolymers with moderate molecular weight (~2000 M_n).

Differences in physical properties of the resulting copolyesters are revealed by solubility results, T_g, T_m, ΔH_m, and TGA thermograms. It is found that the average length of ET sequence imposes considerable influence on T_m of the copolymers. The T_g value of the copolymers is, however, not only in relation with the average ET length, but also the molecular weight of the copolymers. This is probably due to the moderate molecular mass of the samples. Although the dissimilarity of the copolyesters solubility is significantly not correlated to any chemical-structure related parameters, the results at hand show good connection with the sample crystalline content. Essentially, copolymers with high ΔH_m are unlikely to dissolve in chloroform. In addition, TGA thermograms reveal that thermal stability of the copolymers is greater than that of high molecular weight PLA, reflecting the enhancement of this property when aromatic constituents are incorporated into the structure.

Acknowledgements

References

[1] Gerald S., Scott G.: Degradable polymers: Principles and applications. Kluwer Academic Publishers, London (2002).

[2] Albertsson A-C., Barnstedt C., Karlsson S.: Degradation of enhanced environmentally degradable polyethylene in biological aqueous media: Mechanisms during the first stages. Journal of Applied Polymer Science, **51**, 1097–1105 (1994).
DOI: 10.1002/app.1994.070510616

[3] Ki H. C., Park O. O.: Synthesis, characterization and biodegradability of the biodegradable aliphatic-aromatic random copolyesters. Polymer, **42**, 1849–1861 (2001).
DOI: 10.1016/S0032-3861(00)00466-3

[4] Gilding D. K., Reed A. M.: Biodegradation polymers for use in surgery – poly(ethylene oxide) poly(ethylene terephthalate) (PEO/PET) copolymers: 1. Polymer, **20**, 1454–1458 (1979).
DOI: 10.1016/0032-3861(79)90008-9

[5] Reed A. M., Gilding D. K.: Biodegradable polymers for use in surgery – poly(ethylene oxide) poly(ethylene terephthalate) (PEO/PET) copolymers: 2. Polymer, **22**, 499–504 (1981).
DOI: 10.1016/0032-3861(81)90169-5

[6] Kitotsukuri T., Masuda T., Tsutsumi N., Sakai W., Nagata M.: Poly(ethylene terephthalate copolymer)s with smaller amounts of poly(ethylene glycol)s and poly(butylene glycol)s. Polymer, **36**, 2629–2635 (1995).
DOI: 10.1016/0032-3861(95)91211-O

[7] Heidary S., Gordon B.: Hydrodegradable polyethylene terephthalate. Polymeric Materials Science and Engineering, **67**, 190–191 (1992).

[8] Heidary S., Gordon B.: Hydrolyzable poly(ethylene terephthalate). Journal of Environmental Polymer Degradation, **2**, 19–26 (1994).
DOI: 10.1007/BF02073483

[9] Nagata M., Kitotsukuri T., Minami S., Tsutsumi N., Sakai W.: Enzymatic degradation of poly(ethylene terephthalate) copolymers with aliphatic dicarboxylic acids and/or poly(ethylene glycol). European Polymer Journal, **33**, 1701–1705 (1997).
DOI: 10.1016/S0014-3057(97)00063-3

[10] Witt U., Müller R-J., Deckwer W-D.: Biodegradation behavior and material properties of aliphatic/aromatic polyesters of commercial importance. Journal of Environmental Polymer Degradation, **5**, 81–89 (1997).

[11] Witt U., Müller R-J., Augusta J., Widdecke H., Deckwer W-D.: Synthesis and biodegadability of polyesters based on 1,3-propanediol. Macromolecular Chemistry and Physics, **195**, 793–802 (1994).
DOI: 10.1002/macp.1994.021950235

[12] Witt U., Müller R-J., Deckwer W-D.: Biodegradation of polyester copolymers containing aromatic compounds. Journal of Macromolecular Science Part A: Pure and Applied Chemistry, **32**, 851–856 (1995).
DOI: 10.1080/10601329508010296

[13] Witt U., Müller R-J., Deckwer W-D.: New biodegradable polyester-copolymers from commodity chemicals with favorable use properties. Journal of Environmental Polymer Degradation, **3**, 215–223 (1995).
DOI: 10.1007/BF02068676

[14] Marten E., Müller R-J., Deckwer W-D.: Studies on the enzymatic hydrolysis of polyesters: II. Aliphatic - aromatic copolyesters. Polymer Degradation and Stability, **88**, 371–381 (2005).
DOI: 10.1016/j.polymdegradstab.2004.12.001

[15] Valiente N., Lalot T., Brigodiot M., Maréchal E.: Enzymatic hydrolysis of phthalic unit containing copolyesters as a potential tool for block length determination. Polymer Degradation and Stability, **61**, 409–415 (1998).
DOI: 10.1016/S0141-3910(97)00226-7

[16] Witt U., Einig T., Yamamoto M., Kleeberg I., Deckwer W-D., Müller R-J.: Biodegradation of aliphatic-aromatic copolyesters: Evaluation of the final biodegradability and ecotoxicological impact of degradation intermediates. Chemosphere, **44**, 289–299 (2001).
DOI: 10.1016/S0045-6535(00)00162-4

[17] Grzebieniak K.: Copolyesters of ethylene terephthalate and lactic acid susceptible to hydrolytic degradation. Fibres and Textiles in Eastern Europe, **4**, 34–37 (1996).

[18] Grzebieniak K., Ratajska M., Strobin G.: Estimation of hydrolysis and biodegradation processes in ethylene terephthalate and lactic acid copolymers. Fibres and Textiles in Eastern Europe, **9**, 61–65 (2001).

[19] Olewnik E., Czerwiński W., Nowaczyk J., Sepulchre M. O., Tessier M., Salhi S., Fradet A.: Synthesis and structural study of copolymers of L-lactic acid and bis(2-hydroxyethyl terephthalate). European Polymer Journal, **43**, 1009–1019 (2007).
DOI: 10.1016/j.eurpolymj.2006.11.025

[20] Olewnik E., Czerwiński W., Nowaczyk J.: Hydrolytic degradation of copolymers based on L-lactic acid and bis-2-hydroxyethyl terephthalate. Polymer Degradation and Stability, **92**, 24–31 (2007).
DOI: 10.1016/j.polymdegradstab.2006.10.003

[21] Tessier M., Fradet A.: Determination of the degree of randomness in condensation copolymers containing both symmetrical and unsymmetrical monomer units: A theoretical study. e-Polymers, no. 30 (2003).

[22] Kenwright A. M., Peace S. K., Richards R. W., Bunn A., MacDonald W. A.: End group modification in poly(ethylene terephthalate). Polymer, **40**, 2035–2040 (1999).
DOI: 10.1016/S0032-3861(98)00433-9